HYDRODYNAMICS LABORATORY

KÁRMÁN LABORATORY OF FLUID MECHANICS AND JET PROPULSION

CALIFORNIA INSTITUTE OF TECHNOLOGY

PASADENA, CALIFORNIA

EXPERIMENTAL STUDY OF CAVITATING HYDROFOILS IN CASCADE

National Aeronautics and Space Administration
Contract NGR 05-002-059

A. J. Acosta and R. B. Wade

FINAL REPORT

California Institute of Technology
Division of Engineering and Applied Science
February 1968

EXPERIMENTAL STUDY OF CAVITATING HYDROFOILS IN CASCADE

by

A. J. Acosta
and
R. B. Wade

Contract NASA NGR 05-002-059

FINAL REPORT

1. INTRODUCTION

Liquid filled hydraulic systems often operate in such a way that cavitation may take place in one or more of the components of the system. Most often the cavitation will take place in a pump or a turbine as the liquid velocity there is usually greatest in these devices. However, cavitation can also occur in bends or elbows or constrictions in the system, such as a venturi tube. When cavitation does take place, the region occupied by the cavitation process displaces liquid that was formerly there, creating in a sense a "reservoir", the volume of which depends upon the extent of the cavitation. In every case the amount of cavitation in any type of hydraulic device will increase as the system pressure is lowered. The liquid that has been displaced causes changes in the motion of the fluid throughout the system causing or requiring time-varying pressure gradients to occur. In most practical hydraulic systems in which cavitation can occur, these transient pressure changes die away and the liquid flow system operates about some steady mean value. Indeed, for some applications cavitation is deliberately introduced into the system in such a way as to cause the flowing system to operate at a steady, stable condition.

The basic cavitation process is itself an inherently unsteady phenomenon. For example, observations made on the cavitating flow past hydrofoils in a water tunnel (Ref. 1) reveal that when the length of the cavity formed on the hydrofoil is somewhat less than the chord of the hydrofoil itself, the flow is not steady but has a more or less periodic behavior in which the length of the cavitating region grows and collapses periodically with a corresponding change in force on the hydrofoil. On the other hand, when the cavities are much longer than the chord of the hydrofoil, the so-called supercavitating state, the flow is steady in the mean. Similar observations have been made on cavitating inducers (Ref. 2). In both of these examples a characteristic feature of interest is the inherent unstable behavior of flow and pressure fields due to the presence of cavitation.

The unsteady phenomenon mentioned above for the hydrofoil is thought to be associated with the intrinsic nature of cavitation on a body in an infinite fluid medium. As previously suggested this situation is somewhat different from that of a complete hydraulic system subject to cavitation. There, because of the dynamics of the liquid motion in the piping of the system, it may be possible for a system instability to occur. The inherently unsteady behavior of cavitation observed on single hydrofoils may or may not play a direct role in causing such a system instability. In any event, system instabilities do occur in applications. A good example of this phenomenon is the thrust instability sometimes observed in liquid rocket engines. This type of instability is due to a coupling between the feed pump, the thrust of the engine, the supporting structure and the motion of the propellant in the feed lines to the pump. It is described aptly by the name "POGO" instability and has been the subject of considerable study (Refs. 3, 4, 5). Typically in these works, the dynamics of the system

consisting of the motion of the fluid in the liquid-filled lines, the associated structure and certain assumed characteristics of the turbo-pump assembly are analyzed to determine under what conditions dynamic instability can take place. Various types of approximations are made for the motion within the liquid filled portions of the system; for example, incompressible mass oscillations of the liquid can sometimes be assumed (as is the case in hydro-electric surge towers) or more accurate acoustic approximations may be made for this liquid flow (Ref. 6). In any case, several important simplifying assumptions in these analyses have been made regarding the dynamic behavior of the cavitating pump itself during the non-steady motions. Typically, the two types of assumptions made are the following. Firstly, a passive "compliance" is attributed to the presence of cavitation in the pump, that is, the presence of cavitation is visualized as acting like a pressurized reservoir. Secondly, the behavior of the pump during the unsteady motions of the transient flows is assumed to be quasi-steady, that is, the change in pump performance parameters with flow rate and inlet pressure are assumed to be those which occur for steady state operation. Numerical values for pump cavitation compliance are determined from dynamic experiments to make the observed frequencies match the theoretical ones.

This type of analysis is certainly the correct one for a first step and if the frequencies of oscillation are sufficiently low, it seems reasonable that the quasi-steady representation of the pump is satisfactory. On the other hand, it should be pointed out that the aforementioned inherent instability of cavitating flows is not taken into account. But beyond that lies the question — when is it permissible or when is it suitable to treat the pump behavior in the cavitating condition in the steady state manner? At the present time only partial answers to this question are available. The

work of Rubin (Ref. 3 and 4) indicates that the quasi-steady compliance and other steady state characteristics of the pump do, in fact, depend upon frequency. A somewhat different approach was taken by Sack (Ref. 7) in which a more complicated model of the dynamic behavior of a cavitating inducer is proposed; yet it is still one in which the basic performance of the machine is treated on a quasi-steady basis. The work of References 6 and 8 is in essence similar to that of Rubin in that a quasi-steady description of pump dynamics is made. Only recently have direct attempts been made to measure these transient characteristics. Work still in progress at the National Aeronautics and Space Administration Flight Propulsion Laboratory* is intended to provide such direct information by operating a pump in a state of cavitation and perturbing the inlet pressure to the pump. The subsequent fluctuations in mass flow into and out of the pump and pressure rise across the pump are to be measured. This work is, however, not yet finished.

The present study is not concerned with a complete pumping system but rather an element of the pump, namely, a cascade which simulates the action of the vanes of the inducer portion of the pump. The role of cascade analysis and experimentation in turbomachinery is too well-known to be elaborated upon here. Suffice it to say, that in many important respects a properly arranged cascade can in fact simulate the action of the vanes of a pump rotor. In the present context we wish to examine experimentally the characteristics of a cavitating cascade in the hope that it will shed some light upon the behavior of a cavitating pump or turbine.

As in the preceding comments above, we will be interested in the fully wetted behavior of the cascade, and the performance of the cascade

---

* Private communication, M. Hartman.

under various degrees of cavitation. As previously mentioned, the cavitation process itself is inherently unsteady. We wish to examine the characteristics of this unsteady motion as it takes place on a cascade of stationary blades. The quantities of interest, as in a regular pump test, will consist of the time average values of the forces on the blades of the cascade, the angular change of the flow as it passes through the cascade, and also the existence of any "naturally-occurring" unsteady phenomena of the cavitation process. In addition it would be very desirable to be able to perturb the cavitating cascade system and in this way observe the output quantities that would be associated with this perturbation. This latter type of experiment is exceedingly difficult to carry out properly and has not been attempted in the present work. The main value, we feel, of the present experiments will be to provide information as to the kind of phenomena that can occur in a cavitating system and to provide definite quantitatitive information on this type of flow which would serve as the experimental basis for any subsequent theory of nonsteady cavitating flow through a machine. It is not expected that these results will be directly applicable to a cavitating pump such as that mentioned in the POGO problem described above. On the other hand, this type of information is, we feel, essential to have before a full understanding of the basic phenomena of cavitation in machines can be achieved.

At this point it will be useful to outline here the organization of the text to follow: Firstly, the experimental set-up and apparatus used for the cascade test is described. This has an important bearing on the outcome of the experiments because, as is generally known, there are very few liquid cascade tunnels in the world. The present experiments were carried out in a large, but otherwise conventional, closed circuit-water tunnel.

This first section of the text describes the modifications to this tunnel to permit the cascade tests to be made. Next is a description of the actual operation of the tunnel with the cascade installed, including the fully wetted, partially cavitating and fully cavitating flow regimes. The instruments used to measure the steady and fluctuating quantities measured in the tests are then described together with their calibration procedures. The results of these measurements are then presented. They include a full description of the steady, or time averaged measurements for fully wetted flow in a compressor and in a turbine cascade, together with comparisons from relevant cascade theory. The same is done also for the cavitating steady, or time averaged, performance. It will be seen there that the present experiments do in fact reasonably simulate the operation of a true cascade. Next, the types of unsteady measurement and their results are summarized. It may be mentioned here that the unsteady measurements made on the cascade consisted of the fluctuating lift force on the blades of the cascade, the fluctuating velocity upstream and downstream of the cascade, the fluctuating static pressure upstream and downstream of the cascade, and the fluctuating static pressure in the nozzle of the tunnel. In addition, high-speed motion pictures of the cavitating process were taken for various operating conditions. These steady measurements and unsteady measurements are then subsequently discussed at length and an attempt is made to determine the relevance of the phenomena observed to the turbomachine application. Finally, some suggestions for further work in this field are presented. The data reduction procedures used are outlined in appendices at the end of the report.

It should also be mentioned here that the basic experimental apparatus and procedure follow rather closely the work reported in Ref. 9, which

was a similar but more limited investigation of cavitating cascades on a different hydrofoil profile. The reasons for the different set-up and different hydrofoil profile will be brought out in the following sections.

2. EXPERIMENTAL SET-UP AND APPARATUS

2.1 Description of basic tunnel.

The water tunnel used for the present cascade tests is the same as that in Ref. 9 and the basic design of the water tunnel is discussed at length in Ref. 10. In brief, the tunnel is a closed circuit recirculating water tunnel having an available pump power of approximately 350 hp to drive water through the working section at various controlled pressures. The speed of the water flow in the working section of the basic tunnel can be varied from a very low value of a foot or so per second up to approximately 80 ft/sec. Originally this tunnel was equipped with only a circular working section of one square foot cross-sectional area. A new working section (Ref. 11) having a rectangular working section six inches wide and thirty inches high, and four feet in length was later provided for cavitating two-dimensional hydrofoil tests. It was the installation of this new working section that made it possible to conceive of doing cascade tests. The feasibility of carrying out such experiments is discussed in Ref. 9. There it was concluded that for a limited range of stagger angles, less than about 45°, cascade tests in either the compressor or the turbine mode could be carried out for fully wetted flow, for partially cavitating flow, and fully cavitating flow. The modifications needed to be made to the basic two-dimensional working section to permit cascade tests are described in the following section.

2.2 Tunnel modifications for cascade test set-up.

The significant feature distinguishing cascade tests from experiments on isolated hydrofoils is that the basic flow is turned as it passes through the cascade. It is, therefore, necessary to make provision for the turning of this flow in the test facility. In the past this has been done in one of several ways: air cascade test facilities often discharge the flow from the cascade into the surrounding atmosphere. Then the leaving flow adjusts itself automatically to the proper angle required. It is not usually possible to do this for a liquid flow because of the necessity of containing the large volume of liquid under low pressure as is required for cavitation studies. Instead, the flow leaving the cascade is guided by adjustable walls and it is thence discharged into the return portion of the liquid circuit. The mechanism required for completely guiding the discharge flow in the above manner is quite complex and expensive. Accordingly, for the present text a somewhat simpler scheme was adopted; namely, that the leaving flow, downstream of the cascade, is guided by two adjustable walls which subsequently discharge the flow into the existing tunnel diffuser through an abrupt expansion.

In any event it is necessary to obtain the physical space required for the turning of the flow. This necessitates reducing the height of the working section approaching the cascade. The adjustable walls then have room to guide the flow either for a diffusing or compressor cascade, or an accelerating or turbine cascade. The reduction in height of the working section is accomplished by inserting into the tunnel nozzle a symmetric pair of faired inserts. In the present case, these inserts were made solid being a cast of epoxy resin so that no voids in the nozzle region upstream of the cascade would be present in the flow.

These modifications are reasonably straightforward and can be carried out on any similar type of water tunnel. The principle disadvantage of the present scheme is that the rapid expansion of the flow downstream of the adjustable walls into the tunnel diffuser causes a large loss of energy which limits the maximum speed of the tunnel; the free jet so formed may also lead to eddying motion which may disturb the steadiness of the flow in the tunnel.

In a compressor cascade the main flow, being diffused, experiences a pressure rise which in turn causes a thickening of the side wall boundary layers. A more elaborate tunnel configuration would have provision for removing these side wall boundary layers upstream of and through the cascade itself. It was not possible to incorporate this feature in the present tunnel modification.

It would also be desirable to vary independently the stagger angle and angle of incidence to the oncoming flow of the blades of the cascade. To incorporate these features would require extensive modification of the basic water tunnel structure and would be extremely costly. For these reasons a nominal stagger angle was chosen. Bearing in mind that the objective of the present work was to observe phenomena typical of cavitating cascades, this latter restriction does not seem to be objectionable. In order to insure that the flow through the cascade test set-up reasonably well simulates that of a proper cascade, it is necessary that the flow remain essentially two-dimensional. For this reason the pressure rise across the cascade or the flow turning through the cascade was limited to rather low values. This, together with the desirability of having an adequate view of the cavitating process throughout the cascade more or less dictated the cascade geometry discussed in the next section.

2.3 Cascade Geometry and Physical Arrangements.

The inserts mentioned in the above paragraph were sized to provide a clear opening of 13.58 inches approaching the cascade test section. The blades of the cascade were arranged on a nominal stagger angle of 45°. The spacing between the blades was set at 3.2 inches, thereby permitting five blades to be installed in the working section. Adjustable walls were then attached to the ends of the insert pieces at either end of the cascade section. These walls were sealed along the top and bottom edges and terminated at the end of the two-dimensional portion of the working section. These walls were adjusted by means of external jacks. The blades themselves were cantilevered from the lucite window; the central foil of the cascade, however, was mounted to the force measuring dynamometer which is a part of the basic tunnel facility. The hinge points connecting the movable walls to the stationary insert pieces were also sealed to prevent, insofar as possible, leakage from the working section to the space behind the movable walls. These details and the general laboratory arrangements are shown in Figures 1 through 4.

Figure 1 is a photograph of the laboratory floor area showing the instrumentation and the cascade section of the water tunnel. While not apparent from this photograph, the cascade is arranged to be in a horizontal plane so as to minimize the effects of the hydrostatic pressure gradient. The cascade may be seen in the mirror mounted above the working section in Figure 1. Figure 2 shows four of the adjustable blades of the cascade mounted into the transparent lucite working section. Close inspection of this photograph shows that each of the blades has a small pin at its free end. This pin fits into a recessed hole on the opposite side of the tunnel when the window assembly is mounted into the working section to prevent

deflection of the foils under load. A view of the working section before installation of the window is shown in Figure 3. This figure shows the central foil attached to the mounting plate which in turn is fastened to the force balance. Also visible are the two movable walls and the hinge points of the cascade. Figure 4 is a photograph of the adjusting mechanism for the movable walls.

The incidence angle of the four foils mounted to the transparent window were adjusted externally. Each of the foils had attached to it a carefully indexed lever and these levers were in turn ganged together so that only one adjustment had to be made for all of these blades. The incidence of the central foil was adjusted through an angle-changing mechanism provided for in the force balance. Great care was taken to see to it that the indicated angular adjustment of each of the blades was the same.

2.4 Model geometry.

The experimental work reported in Ref. 9 was carried out on a very similar cascade of plano-convex hydrofoils. The solidity of these hydrofoils was 1.25 and the maximum thickness was 8 percent. In certain respects these parameters did not lend themselves readily to experimentation of the type desired for cavitating flows. There are essentially two reasons for this: the relatively large camber of the plano-convex foils give rise to a significant turning of the flow through the cascade at low angles of attack. It may be mentioned here that the movable walls can be adjusted to plus or minus ten degrees only. For this reason large lift coefficients on the blades of the hydrofoils cannot be accommodated. As a result, the tests of Ref. 9 had to be conducted at relatively small incidence angles. Consequently when cavitation was made to occur, it was found that over a wide

range of the operating parameters, cavitation did not occur at the leading edge of the hydrofoil. Instead, it would sometimes occur near the point of maximum camber on the normal suction surface of the foil; or in other cases it would occur, even when the lift was positive, on a portion of the pressure face of the hydrofoil. In the present work we were particularly interested in cavitation originating at sharp leading edges as it occurs in inducer pumps. We were also anxious to be able to operate at higher incidence angles than proved possible for the test in Ref. 9. For these reasons it was decided to adopt for the purposes of these tests a profile with zero camber and solidity of 1.0. The chord of the hydrofoil was therefore fixed at 3.2 inches; in order to insure adequate strength of the hydrofoil sections, a nominal thickness of 1/4 inch was used, or in other words, a thickness ratio of 8 percent. The construction details of the model foils can be seen in Figure 5. The actual thickness distribution for these profiles is not thought to be crucial, and for manufacturing simplicity the actual shape of the profile consisted of flat cuts so arranged as to simulate that of a bi-convex hydrofoil having a leading and trailing edge radius of approximately 1.7 percent of the chord.

Before leaving this section it is perhaps worthwhile to mention again that the details of the profile shape will have an important bearing on the cavitation performance of the foil with different degrees of cavitation. For example in the fully wetted and partially cavitating conditions, the thickness distribution of the foil is relatively unimportant and the camber distribution is the more important feature. However, in the so-called fully cavitating condition when the cavity extends many chord lengths behind the foil, and when the cavity originates at a sharp leading edge, the flow is then in contact with the foil only on the wetted surface. The

characteristics with this type of cavitation are then determined solely by the shape of the wetted surface and not by the distribution of camber line and thickness. It can then be seen that if one wishes to study fully cavitating hydrofoils in cascade one should be concerned only with the shape of the wetted surface and, except for reasons of strength, not with the thickness or camber distribution. It was for this reason that the plano-convex profile shape was chosen for the work of Ref. 9 because in a fully cavitated flow a flat wetted surface was in contact with the liquid.

Wedge profiles have also been used for the study of supercavitating flows. However, a wedge profile is not suitable for investigating the condition of partial cavitation. From these remarks it may be seen that no single type of profile is fully suitable for a wide range of angle of attack and additionally from fully wetted to fully cavitating flow — especially if one is interested in cavitation which starts at a sharp leading edge. We will find, accordingly, that the present profile, having zero camber, will properly simulate the behavior of a flat plate foil with some thickness under conditions of partial cavitation and that cavitation will originate at the leading edge under small angles of attack. On the other hand, for the fully cavitating condition the wetted surface of the present foil presents a negative camber and a positive incidence to the oncoming flow. Under these conditions, the liquid flow may not remain attached at all times to the pressure face of the foil, and, depending upon the cavitation number, it is even possible that a negative lift force may be developed even with a normally positive incidence.

2.5 Desired measurements.

Two types of measurements are desired for the present work; the first are the steady or time-averaged measurements of the forces on the

blades of the cascade and the flow turning produced by the cascade as a function of incidence angle and blade Reynolds number for various conditions of cavitation. These are the normal cascade characteristics that would be used in a design of a pump, for example. In addition to these, we desire to measure the fluctuating quantities associated with the periodic flow observed through the cascade under the conditions of partial cavitation. These measurements would include the fluctuating forces on the cascade, the fluctuating velocity approaching the cascade, the fluctuating velocity leaving the cascade, and the associated fluctuating pressures that would be observed upstream and downstream of the cascade. Also, it would be desirable to be able to correlate the geometry of the cavity formed with these quantities. The instruments and apparatus used for these purposes are discussed in the following sections.

2.5.1 Instruments for measuring the steady quantities.

Steady or time average force measurements on the central blade of the cascade were made with the force balance of the tunnel. This instrument described in Ref. 9 measures lift force, pitching moment, and drag force by means of a mechanical-hydraulic load cell and readout system. The time response of this apparatus is very slow, on the order of one to two seconds but it is quite accurate having a least count in lift and drag force of 0.01 lbs. Angular adjustment of the hydrofoil is provided by a direct adjustment on the balance proper. As mentioned previously, the angular adjustment of the remaining blades in the cascade is carried out by a separate external actuator. The wall angles are set by the two jack screws seen in Fig. 4. The position of these screws is calibrated as a function of the wall angle and they are individually adjusted. The tunnel

flow speed and ambient pressure are determined by measuring the static pressure at the working section upstream of the cascade, midway through the contracting nozzle, and in the settling chamber upstream of the contracting nozzle. The pressure differences across the nozzle are measured on a mechanical-hydraulic balance similar to the force readout elements which gives a least count of 0.01psi. The static pressure at the working section is measured with an absolute manometer. These pressure tap positions are indicated schematically in Figure 6. There, pressure p_2 is the pressure in the working section some twelve inches upstream of the central foil of the cascade. Pressure p_N is the pressure more-or-less midway between the plenum pressure p_H and the working section. For the purpose of carrying out these tests, it was convenient to measure the absolute pressure at the location p_N and the dynamic pressure in terms of the difference between pressure p_H and p_N. This necessitated calibration of the clear tunnel in order to express this difference in terms of the dynamic pressure and absolute pressure at the working section. This procedure is explained in Appendix II. The reason this procedure was adopted is that the static pressure p_2 is only some four chords upstream of the central foil of the model; this close proximity during the cavitating tests may have some influence on the average static pressure values measured at that point, whereas at the point further up the nozzle this influence, if any, will have been diminished.

Provision was also made for measuring the absolute pressure of the cavity formed on the central blade of the hydrofoil.

For reference at this point, the cascade geometry and notation is indicated in Figure 7. In this figure, V_1 is the velocity measured in the

tunnel approaching the cascade. The angle α_1 is the angle between the chord line and the oncoming velocity. The velocity leaving the cascade is indicated by V_2. The lift force L and the drag force D measured by the balance are perpendicular to and parallel to the oncoming tunnel velocity V_1 respectively. The quantities L_m and D_m represent the lift and drag forces referenced to the vector mean of the incoming and outgoing velocities; these are the quantities usually calculated in a cascade theory.

2.5.2 Apparatus for measuring fluctuating quantities.

From the work carried out in Ref. 9 it was anticipated that with the range of tunnel speeds to be used the frequency of the oscillations to be encountered in force, pressure, etc. would vary from about 10 to 20 cycles per second. Consequently, instrumentation to measure and record fluctuations of these frequencies had to be developed. Fortunately, this is a moderately low frequency and frequency response, as such, did not pose a particular problem.

To obtain a measure of the fluctuating force on the hydrofoil, a solid-state strain gage was fitted into a recess machined in the root of the central foil. The particular gage used was a half-bridge consisting of a "p" element and an "n" element connected to form a half bridge. The bridge was completed externally. The bridge element was manufactured and potted into place with an epoxy resin by Micro-Systems, Inc. The recess into which the bridge was mounted was then closed with a cover plate which was also cemented into position. By this means, variations in hydrostatic pressure on the foil would not cause an output from the bridge. The output of the bridge was conditioned with typical strain gage patch work and the output could be read either directly or recorded on a

recording oscillograph. Calibration of this strain gage was achieved by measuring the output signal against the observed lift force as measured by the water tunnel force balance. The resulting signals were on the order of 20 millivolts for an applied lift force of 40 lbs.

Fluctuating pressures were measured at points p_1 in the plenum upstream of the nozzle, points p_2 upstream of the cascade, and point p_3 an equal distance downstream of the cascade. The pressure at point p_1 was measured with a Statham ±15 psi differential pressure strain gage transducer. Pressures p_2 and p_3 were measured with 0 to 100 psia flush mounted pressure transducers. These were excited by constant current generators and were also supplied by Micro-Systems, Inc. The output voltage of these latter devices was on the order of 5 millivolts per psi. Again these outputs could be recorded directly or put onto a recording oscillograph.

By far the most difficult measurement to make was that of the fluctuating velocity both upstream and downstream of the cascade. First of all it is clear that it would be desirable to measure the oncoming velocity distribution as it approaches the cascade row from one end of the cascade to the other to determine if the flow is sufficiently uniform. This was not possible in the present arrangement nor was it possible to make a similar arrangement downstream of the cascade. Instead, because of tunnel limitations, only two sites were readily available for the insertion of velocity measuring probes. These are indicated on Figure 6 as V_2 upstream of the cascade and V_3 downstream of the cascade. It will be seen that position V_3 is on the centerline of the cascade axis. The practical result of having one downstream location is that, depending upon the flow

leaving angle, V_3 may or may not be in the wake of an upstream blade. While this may not be too important in fully wetted flow, it has an important bearing on the fluctuating measurements in cavitating flow.

It had been decided at the outset to use, as fluctuating velocity sensors, hot film anemometers. Indeed, in a nonuniform flow such as a cascade flow it would be difficult to do anything else. It may be mentioned here that no other single aspect of this experimental program experienced as much difficulty as did the work with this type of equipment, and it would be safe to say that to this day hot film anemometry for service in liquid flow has not yet reached a desirable state of perfection, particularly at fluid velocities greater than 5 ft/sec. In our preliminary experiments using hot film anemometry, three different hot film amplifiers were used with three different types of sensors made by different manufacturers. It was found that the most sensitive sensor was that of the plated-cylinder type manufactured by Thermo-Systems, Inc. However, this type of sensor catches the small debris in the tunnel, such as hairs, bits of paint, etc., which lodge on the sensor and change its reading. This debris is very difficult to dislodge. Furthermore, these sensors are not sufficiently rugged to withstand the high operating velocities in the water tunnel. It may be mentioned here that the range of velocities used was from 20 to 40 ft/sec approximately. It was also desirable that they be able to survive the possibility of small amounts of cavitation in the oncoming flow. Two additional types of sensing elements were, however, tried which did fulfill our principle objectives. These were a conical sensor again produced by Thermo-Systems and a very rugged wedge-type sensor produced by Disa Corp. Neither of these sensors is as sensitive as the cylindrical sensor

but debris does not seem to be caught by them. It was found, however, that at flow speeds of 30 ft/sec and with the chance of incidental cavitation, that the conical sensor did not have an adequate service life. On the other hand, the wedge sensor could withstand many hours of operation (up to 100 hours) and could even survive a cavitating flow. The amplifiers finally selected for use consisted of a Shapiro & Edwards constant temperature amplifier already on hand and an additional battery-powered constant temperature amplifier (Model Type D5505) obtained from Disa Corp.

Although the outputs of these amplifiers could be read directly on conventional equipment, it was decided to record these fluctuating outputs together with those for the pressures and fluctuating lift force simultaneously on a recording oscillograph. In order to do this, it was necessary to incorporate two isolation amplifiers on each of the hot film outputs. Furthermore, because of the large zero velocity signal coming from the amplifiers, additional biasing and padding was necessary before these signals could be recorded with adequate sensitivity.

Block diagrams illustrating the hookup of the solid state strain gage pressure transducers and velocity probes are shown in Figures 8a, 8b, 8c.

In closing this section, we may mention that all of the fluctuating quantities, i.e. force, pressure and velocity, were recorded on a Consolidated recording oscillograph. The galvanometers of the oscillograph had a flat response in each case up to a minimum of 90 cycles per second. Each of the outputs could be biased and adjusted so that the excursion on the oscillograph would be convenient for subsequent analysis. In addition, each of the transducers for the experimental variables could be calibrated on the oscillograph paper either by varying tunnel speed, tunnel pressure, or force on the central hydrofoil.

2.6 Operational procedures — the cascade condition.

Cascade testing differs from its counterpart in isolated hydrofoil testing in that the basic flow through the cascade is turned. The amount of the turning is not arbitrary depending upon the geometry of the cascade and the angle of incidence to the oncoming flow. Furthermore, the proper cascade condition requires that each of the blades experiences the same force. If in addition the flow is two dimensional, the component of velocity normal to the cascade axis in incompressible flow is then constant in the absence of side wall boundary layer growth. There then exists a unique relationship between the lift and drag force on the blades of the cascade, the stagger angle of the cascade, and the amount of turning experienced by the flow in passing through the cascade. As this relationship cannot be determined beforehand, it has to be determined experimentally. Hence in the present work the foils were set at a given angle of inclination to the oncoming stream and with a given wall setting the forces were measured. The aforementioned cascade condition was then checked to see if the observed forces and the given wall angle were in agreement as determined by the two dimensional cascade momentum relation. In general, of course, they did not and the wall angle was systematically changed by trial and error to find a condition under which the observed force and the observed turning angle were in agreement with each other as determined from said cascade momentum equation. This procedure is elaborated more fully in Appendix III.

This type of iterative procedure was carried out for all the conditions of cascade testing, both fully wetted and cavitating. It turned out to be especially important to do this during conditions of partial cavitation as

under these circumstances the forces experienced by the cascade varied significantly with the degree of cavitation on the hydrofoil. However, it was found that when the cavities were very long the observed force on the central hydrofoil became insensitive to the exact downstream wall angle.

When the wall angle had been adjusted as described above, the steady force data were entered upon a data log and then a run was taken on the recording oscillograph to record the fluctuating quantities. In addition a photograph was taken of each of the cavitating runs.

3. DISCUSSION OF RESULTS

3.1 Description of the operation of the cascade tunnel.

Before launching into a discussion of the experimental results, it may be helpful to record here some visual observations of the behavior of the cascade as the pressure is gradually lowered in the tunnel from a condition where there is no cavitation to a point where the cascade is fully cavitating. The nominal flow velocity in most of these experiments was 30 ft/sec. When the pressure is sufficiently high so that there is no cavitation, the tunnel is very quiet and, except for the forces on the blades of the hydrofoil measured by the instruments, it is difficult for an observer to detect that there is flow in the working section. There is, however, a very slight vibration of the working section structure in this fully wetted flow originating from the eddies in the mixing region of the diffuser. As the ambient pressure is slowly decreased, no change in the sounds emanating from the working section occurs until cavitation commences. If the angle of incidence is two or three degrees or larger, the cavitation forms first at the sharp leading edges of the foils. Then there is an abrupt rise in the apparent sound level which has a characteristic hiss or a high pitched

squeal commonly associated with cavitation inception. When the pressure is further decreased, the extent of the cavitation from the leading edge increases and a white frothy band of cavitation is easily seen on the suction surface of the blades. This band appears to be stable but it is in fact an opaque frothy mixture of vapor bubbles. As the pressure is lowered and this cavitation zone becomes enlarged, the pitch of the sound gradually lowers and appears to become more intense to the ear. Such cavitation, since it is less than the length of the chord, is termed 'partial' or partially cavitating flow. When the length of this partially cavitating zone is approximately one-half the chord, the flow appears to become unstable in the sense that the length of the cavity commences to fluctuate and these fluctuations soon develop into a strong oscillation with the length of the cavity growing and collapsing in a periodic manner. At the same time a definite audible "chugging" sound can be heard from the cascade. By this time definite fluctuations in the force on the hydrofoil and the pressures and velocities upstream and downstream of the cascade can be observed on the instrumentation. This oscillating or chugging mode of cavitation persists and grows more intense as the pressure is lowered until the maximum length of the cavity bubble formed during the oscillation cycle is approximately 15 to 20 percent longer than the chord of the hydrofoil. At this time the fluctuations in lift and pressure throughout the cascade are greatest. Then with a slight, but still further decrease in pressure, the cavities become considerably longer than the chord and the oscillations cease entirely and the audible noise coming from the cavitation is greatly diminished. The length of the cavity 'wake' then formed is extremely sensitive to ambient pressure, so that it is difficult to

maintain the cavity at a definite length for any period of time. Nevertheless, the resulting velocity and forces on the hydrofoil are reasonably steady in time. A further but slight decrease in pressure is still possible at which condition the cavities extend throughout the working section of the cascade and disappear into the diffuser. Then for all practical purposes the minimum operating pressure level of the tunnel for the particular geometry has been achieved. The tunnel is essentially "choked". The cavities, of course, collapse in the diffuser in a highly unsteady fashion. This gives rise to considerable noise, sometimes practically of an explosive type, and may cause considerable vibration of the entire tunnel leg. It is, however, possible to operate in this "choked" condition for extended periods of time during which the velocity and pressure change only very slightly. The force changes experienced by the cavitating hydrofoils during this sequence of cavitation depends greatly upon the type of profile used and angle of incidence. When the cavitation commences at a sharp leading edge and nowhere else there is almost always an increase in drag and lift force over the fully wetted values. This increase persists until the length of the cavitating bubble is approximately equal to the chord. Thereafter with further decrease in pressure and increase in cavity length, the lift and drag on the hydrofoil decrease. The magnitude of this decrease depends, as suggested earlier, greatly upon the specific shape of the wetted surface of the hydrofoil.

3.2 Steady measurements.

3.2.1 Fully wetted flow.

The steady state measurements for the operation of the cascade and fully wetted flow for both the compressor and turbine arrangements

are given in Figures 9 through 12. The method of reducing the data for these tests is indicated in Appendix IV. It should be mentioned, however, that in these graphs no account of the tare force on the foil mounting plate has been taken. These tare forces are small and are summarized in Appendix I. The chief effect of these tare forces is on the drag.

Figure 9 shows the force coefficients versus the mean angle of attack, the angle between the chord and the vector mean of the inlet-outlet velocities across the cascade. Also shown are two theoretical comparisons, one from the work of Schlichting (Ref. 12) and the other from the work of Mellor (Ref. 13). It should be pointed out that with the present test set-up, as the incidence angle α_1 is changed , the stagger angle of the cascade is changed also. The theoretical line taken from Ref. 13 incorporates this variable stagger angle whereas the results of Ref. 12 are calculated with a constant stagger angle equal to 45°. It can be seen that the zero lift angle agrees with the theory within a third of a degree and that in general the slope of the lift versus mean angle of attack curve agrees reasonably well with that predicted from two-dimensional theory. There is a definite Reynolds number effect; it can be seen that the lower Reynolds number, about 440, 000 based on chord gives rise to a bump in the lift curve typical of a leading edge separation bubble. At the higher Reynolds number 840, 000 this bump has disappeared. The observed drag coefficients are rather high. However, we see from the tare forces of Appendix I that the tare drag coefficient (based on the same reference area used for Figure 9) is approximately half the observed drag shown in Figure 9 which is a level to be expected for this type of profile. From these results, it is concluded that the test set-up simulates in a satisfactory manner true cascade behavior. The results of Figure 9 are plotted in different form in

Figure 10 where the turning angle of the flow, the lift drag ratio, and the deviation angle of the leading flow are given as functions of the incidence angle α_1 to the cascade. Again, there is a pronounced Reynolds number effect and it can be seen that the deviation angle α_2 in the present notation is only slightly dependent upon the angle of incidence α_1.

It was also possible in these fully wetted tests to carry out similar measurements on a turbine cascade. The reason for this is that the foils are symmetric fore and aft. Because of this fact, what would normally correspond to negative incidence angles are in reality positive incidence angles for a turbine cascade having a stagger angle of nominally minus 45°. The results of these measurements are shown in Figures 11 and 12. In Figure 11 the force coefficients based on the vector mean velocity are presented versus the mean angle of attack just as in Figure 9. It can be seen that the lift coefficient is a nonlinear function of the angle of attack, α_m, owing to the varying stagger angle. The dashed lines of this graph are the expectations from cascade theory for a fixed stagger angle of 45°. In the vicinity of zero angle of attack the observed values agree closely with the theoretical values. The results of Figure 11 are also presented in Figure 12 in the same manner as in Figure 10, namely deviation angle, turning angle, and lift drag ratio versus the incidence angle, α_1.

3.2.2 Cavitating results.

Force information during cavitation of the compressor arrangement is given as a function of the cavitation parameter K_v for various angles of incidence α_1 in Figure 13a through e. Several points command attention in these graphs. First, in Figure 13a it is seen that the advent of cavitation causes a gradual reduction in lift force with decreasing cavitation

parameter until the length of the cavity is about equal to the chord. Thereafter the lift decreases very rapidly and becomes strongly negative at the minimum cavitation number of about 0.22. The drag, on the other hand, rises slowly from its fully wetted value and the moment like the lift force decreases with decreasing cavitation number but not as much. Also shown on Figures 13a and b is a dashed line. This line gives the predictions that would be obtained in a zero thickness cascade of flat plates with cavitation from the leading edge. It can be seen that for the four degree incidence angle this theory (Ref. 14) has no bearing on the observed outcome. The situation changes somewhat with an incidence angle of six degrees. Here the cavitation definitely starts at the leading edge and, like the theoretical predictions of Ref. 14, the experiments show a marked increase in lift coefficient with decreasing cavitation parameter until the cavity bubble becomes as long as the chord. Thereafter the lift force sharply decreases with decreasing cavitation parameter and again assumes a negative value at the lowest cavitation parameter. The drag coefficient shows a gradual rise and the moment coefficient a decrease with cavitation. The results at higher angles of attack are similar except for the ten and twelve degree incidence angles where the peak lift force occurs before the cavity becomes as long as the chord.

At these two higher angles of attack a new phenomenon appears, the results of which can be seen perhaps more clearly in Figure 13e. There we see that at the lowest cavitation numbers the lift can either be positive or negative -- indicated by the dashed line. There is a similar effect on both the moment and the drag. Visual observations of the flow about the foil revealed that these two sets of data corresponded to two different cavity flow

configurations about the hydrofoil. The case of negative lift corresponded to the flow fully wetting the pressure surface of the hydrofoil. It was observed, however, that sometimes the liquid flow separated from the normal pressure surface at a point upstream of the trailing edge. These points have the lower drag but positive lift coefficient. The remarks made earlier concerning this type of cavity flow configuration may now be recalled. At these low cavitation numbers only the normal pressure face of the hydrofoil is in contact with the liquid; in this instance and with this type of foil the hydrofoil presents a negative camber to the flow. It is this negative camber that is responsible for the negative lift found at the lowest cavitation numbers for practically all of the angles tested. However, when the cavity separation point moves forward from the trailing edge, the extent of this negative camber is decreased and the apparent incidence angle to the oncoming flow is increased. Both effects give rise to increasing the lift and decreasing the drag of hydrofoil.

The length of the cavity expressed in chords was measured from photographs of the cavitating cascade and plotted against the cavitation parameter K_v for one angle of incidence, namely six degrees, and it is shown in Figure 15. There it can be seen that cavitation commences at a value of $K_v \approx 1.0$. The cavity grows slowly at first and then reaches an asymptote at about $K_v = 0.3$. Then very small changes in cavitation number cause large changes in the length of the cavity.

To gain a visual appreciation of the cavitating process, several of the data photographs are assembled in Figure 14a through e. The letters underneath each of these photographs correspond to the marked points on the graphs of Figure 13. In these photographs the four foils mounted in the

plastic window can be seen, together with their actuating mechanism. The central foil attached to the opposite side of the tunnel is also visible. The cavitation on the blade surfaces is not too apparent in these photographs until it extends beyond the length of the chord. It is observed that the cavities on each of the foils are not precisely the same, and that there is a definite influence from the corner of the adjustable wall. At this point there is inevitably some leakage and influence from the pressure gradient there that is not the same as that of the blades themselves. It should be mentioned, however, that each of the hydrofoils has an end gap or tip clearance. The gap clearance on the four foils mounted to the window is about 0.005 inches on the window side and 0.015 on the free end. The tip clearance of the central foil against the window surface is about 0.015 inches. Much of the cavity pattern seen in these photographs taken directly from above is due to cavitation in the tip and boundary layer region of the flow adjacent to the wall and it does not persist across the entire depth of the foil. For this reason these photographs cannot be taken as being too representative of the actual cavity shape behind the foils, except possibly for the one on the central foil. It is interesting to observe in Figures 14a and b that the downstream hot film anemometer shown just to the right of center is cavitating at these pressures. The cavitation shown occurs on the stem of the sensor and not on the active face which was undamaged by this flow.

A further word of explanation as to how the wall angles were adjusted is in order here. The wall angle was continuously adjusted so that it agreed with the measured lift force as previously discussed up to the point where the cavity was about as long as the chord. It was then

left fixed in position as the cavitation parameter was further decreased. For this reason and for the larger angles of incidence the cascade was "unbalanced" for the longer cavities. This can be seen in Figure 14e for example where the lengths of the longest cavities are not all the same on the various hydrofoils but increase running from the topmost foil seen to the bottommost. Apparently for fully cavitating flow this has a negligible effect on the lift of the central foil. However, at smaller angles, such as shown in Figure 14b this unbalancing effect is not so important in altering cavity lengths across the cascade.

We now turn to the unsteady measurements.

3.3 Unsteady measurements.

3.3.1 Recorded Data.

The principal means of acquiring the unsteady data was by recording all of the quantities on a recording oscillograph. Some typical oscillograph traces are taken from the data and are presented in Figures 16 through 20. In these the fluctuating pressures, velocities, and lift are given for various cavitation parameters and at various incidence angles. For each of these angles three or four traces are shown for different cavitation parameters. Generally they start at the left with a relatively high cavitation number but one at which the unsteady nature of the flow has already been achieved. For example, in Figure 17 on the far left is shown sample traces for an angle of incidence equal to six degrees and for a cavitation parameter of 0.42. There it is seen that the pressures on either side of the cascade are oscillating in synchronism with a period of approximately 0.07 sec. There is also a fluctuation in the lift force though not of an appreciable magnitude. The pressure p_1 in the upstream plenum is relatively constant

and neither of the velocities sensors indicate a sensible fluctuation. Incidentally the smallest divisions on the tracing represent a time scale of 0.01 sec. As the pressure is lowered we see from the traces of Figure 17 that the period of the oscillations increases as well as their amplitudes. In fact, it is difficult at times to separate the various traces. On this figure for the cavitation number 0.36 the oscillation is at about its greatest intensity. Then, even the pressure p_1 in the upstream plenum shows a small periodic variation. However, it is much less than the pressures p_2 and p_3 on either side of the cascade. The lift force shows a tremendous excursion and there is evidence on this trace of "ringing" of the foil at one of its structural vibration modes (approximately 100 cps). At the lowest pressure shown in Figure 17 the oscillations have nearly died away and only the lift force shows an occasional perturbation. The traces for the other angles of attack are similar to the one described except that for the larger angles of attack the fluctuations in lift force and velocity downstream of the cascade are so great that they become very confusing. However, all of these traces have several recurring features in common. The period of the fluctuations increase as the cavitation number decreases until they die away. Secondly, the pressures on either side of the cascade, the velocity fluctuations and the lift fluctuations tend to be in phase.

3.3.2 High speed motion pictures.

In addition to the fluctuating pressures and velocities, it would be highly desirable to be able to correlate the observed cavity motion with the forces and pressures observed on the cascade during the fluctuations. For this purpose a high-speed motion picture camera, an Eastman Kodak, capable of taking pictures up to about 2000 frames per second was

mounted over the working section of the tunnel to photograph the cavities on the suction side of the central hydrofoil. To provide a reference with the other fluctuating data, it was decided to incorporate on the frames of this motion picture film one of the fluctuating quantities. The parameter chosen for this purpose was the fluctuating lift; this was accomplished in the following way. A "visicorder" was mounted on the tunnel working section just upstream of the blade in question. This particular recording oscillograph has an intense source of light for exposing the paper of the recorder. In the present case this beam of light was made to impinge on a mirror which was in the field of view of the motion picture camera. In this way a bright dot whose position is proportional to the lift force appeared on each frame of these high speed motion pictures and, by this means, it was possible to correlate the instantaneous lift with the appearance of the cavity. Because of disturbances to the alignment of this equipment during the subsequent operation of the tunnel, these data did not turn out to be as good as desired and only a few film strips had an identifiable lift signal on them.

3.3.3 Data tabulation.

A great many traces of the type described above were analyzed in the course of this work. The central features of interest were the amplitudes, frequencies and phases of these fluctuation quantities. For future reference these results are tabulated in Table I. Listed there is the run number of each of the oscillograph traces together with the derived quantities. Three sets of experiments are given; these are summarized as the fully wetted runs in which there is no cavitation, the cavitating runs in which there are various degrees of cavitation corresponding to the

various cavitation numbers, and finally a set of data for those conditions in which the oscillation was a maximum. For reference a set of conversion factors for the oscillograph traces of Figures 16 through 20 are tabulated in Table II.

3.3.4 Hot film sensor dynamic calibration.

The hot film anemometer provides the means of measuring the steady velocities as well as the fluctuating velocities provided that the frequency response of the system is sufficient. In practice this is usually accomplished by having an amplifier and feedback system with sufficient gain to overcome the inherent thermo-inertia of the hot film. If it is known that the frequency response of the entire sensor-amplifier system is adequate, calibration of the output signal with velocity can be done on a steady state basis. Indeed this is the procedure already mentioned. However, because the phase of these velocity signals are important in the present work, it was thought desirable to insure that the dynamic frequency response of the system used was adequate for the present purpose. To accomplish this end, the hot film sensor and its mounting device were installed in a specially constructed mechanical oscillator. This oscillator assembly was installed in the Free Surface Water Tunnel of the Laboratory and was so arranged that the sensor was moved to and fro longitudinally in the direction of the water flow. The position of minimum or maximum oscillation velocity could be measured and compared to the hot film output. The object of this test was to measure any possible phase lag that might exist between the output of the sensor and the known mechanical velocity of the oscillating assembly. The flow speed for these tests was 22 feet per sec and the oscillating frequency was 10 cps. The amplitude of the

imposed velocity fluctuations was approximately 1 ft per second. Typical results of this type of experiment are shown in Figure 21. Several pairs of traces are shown in this figure, the upper one in each case is the output of the hot film and the lower trace shows a spike at the position of minimum velocity. It can be seen that for both overheat ratios shown (these are typical of the ones used in the test) there is no appreciable phase lag between the velocity signal and the imposed motion.

4. DISCUSSION

4.1 Steady results.

We have seen that the fully wetted performance of the compressor and turbine cascade arrangements compare reasonably well with relevant cascade theory even though end wall boundary layer removal was not used. In this respect the results are similar to those of Ref. 9. The steady cavitation performance is in some respect similar also to that of Ref. 9 except that the rise in lift coefficient associated with leading edge cavitation is more pronounced in the present tests. In addition the subsequent behavior of lift coefficient for fully cavitating flow is different because of the different profile shapes as already indicated.

4.2 Frequency of oscillation.

We now examine the frequencies of the oscillations recorded in traces such as Figure 16. It is evident from these traces that practically all of the fluctuating quantities that can vary with time do so. It is interesting to note, however, that pressure fluctuations in the working section of the cascade are evident even when there is no cavitation (a trace of this is not given). These observations are summarized in Table I under "fully wetted flow". Upon reference to this table, it may be seen that the

static pressure downstream of the cascade and near the end of the cascade working section does exhibit a fairly regular fluctuation which is no doubt due to the eddying nature of the flow in the diffuser. However, in fully wetted flow no pressure oscillations are observed at point p_1 or at point p_2 just upstream of the cascade. Also neither the lift nor the velocities show any appreciable perturbations in fully wetted flow. The frequencies of these pressure oscillations in fully wetted flow are presented against angle of incidence α_1 in Figure 22 for the nominal flow speed for these tests, about 31 ft per second. These frequencies range from about 10 to 14 cps. It should be mentioned that for each of these incidence angles in fully wetted flow the cascade is operating as a proper cascade. Therefore, the geometry of the diffuser section is being continuously varied as the flow turning is varied. It is natural to present this type of data in the form of a Strouhal number except that the characteristic dimension required for this latter parameter is not known.

Similar information is presented in Figure 23 for various incidence angles α_1 as a function of cavitation parameter K_v. There we see that at the lowest incidence angle 4^o the frequencies range from about 14 cycles per second to nearly 20 cycles per second. The lower frequency corresponding to the lower cavitation number. The trend is similar for the other incidence angles except that as a general rule the higher the incidence angle the lower the observed oscillation frequency. There appears to be a connection between the observed frequency for the fully wetted flow, again these are all determined by the fluctuation of pressure p_3, and the frequencies observed during cavitation at the lower cavitation numbers for each angle of incidence. From these figures it appears that the oscillations commence at frequencies higher than that for the fully wetted flow and as

the length of the cavity becomes larger the frequency tends toward the value for the fully wetted flow. This raises the possibility that these "maximum" oscillations observed near the lower cavitation parameters may be coupled to, or driven by, the pressure fluctuations taking place in the diffuser. On the other hand, this coupling does not seem to occur when the cavity oscillations first begin.

It is, however, an assumption that the diffuser is controlling the frequency of the oscillations in pressure p_3; these oscillations may well be controlled by the blades themselves, especially at the higher incidence angles when stall is approached. For the purpose of being definite, a Strouhal number was defined for these frequencies based upon the approach tunnel speed and the chord of the foil. These are plotted as a function of incidence angle α_1 in Figure 24, both for the fully wetted case and for the case of maximum cavity oscillation. We see that for the 4^o case even for the maximum oscillation there is a distinct separation in the Strouhal number for the fully wetted flow and the maximum oscillation cavity flow. It will be recalled that generally speaking the onset of the cavity oscillations occurs at the distinctly higher frequency than that for the fully wetted flow.

Perhaps too much is being made of the coincidence in frequency of the fully wetted pressure oscillations and those for the maximum intensity cavitation oscillations. It should be pointed out that the present cavitation oscillations in the cascade set-up are very similar to those observed on a single hydrofoil with a sharp leading edge in the tunnel without the cascade modifications (and hence the abrupt expansion diffuser) and also to the observations on a single hydrofoil of Ref. 1 in which the diffuser was of a completely different type. This suggests that the

phenomenon being observed is in fact a characteristic of the cavitating cascade itself and not of the particular experimental apparatus.

The effect of tunnel speed upon the Strouhal number for the maximum intensity of oscillation was investigated for a given angle of incidence equal to 6° and is shown in Figure 25. There it is seen that the Strouhal number is on the whole rather constant as the velocity increases from 24 to 38 feet per second. This finding suggests that the frequency in this cavitating process is controlled by the flow and not by some resonant characteristic of the tunnel itself.

4.3 Velocity and pressure fluctuations through the tunnel nozzle.

The velocity fluctuations upstream of the cascade, V_2, are typically one percent of the approaching velocity. The amplitude of pressure fluctuations and the steady pressure at this point are on the order of 5 percent of the dynamic pressure. The fluctuations in the pressure p_1 are usually smaller than this. The distance between the measuring points for pressures p_1 and p_2 is on the order of 5 feet; the nozzle through which the water flows consists of a rigid steel casting and, as mentioned before, the nozzle inserts are made of solid epoxy resin. It should be possible, therefore, to correlate the difference in pressure upstream of the nozzle and downstream of the nozzle with the observed velocity fluctuations measured by the hot film anemometer. To do this, the difference between pressure p_1 and pressure p_2 is formed as a function of time and the non-steady Bernoulli equation is used to calculate the resulting fluctuating velocity. Plots of this pressure difference and the associated observed velocity are given in Figures 26a through d. As a rule the velocity trace tends to be rather ragged yet they show clearly that the fundamental period

of the velocity fluctuation is the same as that of the pressure difference fluctuation. There is a pronounced phase difference between the velocity and pressure difference traces; generally, the peak of the velocity occurs near the valley of the pressure difference trace.

The pressure difference traces of Figure 26 were then used to calculate velocity fluctuations at point 2. The actual details of this calculation are contained in Appendix V. The basis of the calculation is this: it is assumed that there is no compliance of the fluid or the working section between points 1 and 2 (owing to the rigidity of the nozzle wall and to the short length of fluid path, approximately 5 feet). Then with the continuity relation between these points and the Bernoulli equation, fluctuations in velocity V_2 can then be calculated. Because the observed velocity trace is rather ragged and has high harmonic content, it was decided to compare the amplitude and phases of the fundamental of the pressure fluctuation with the fundamental of the observed velocity fluctuation. In this way the harmonic content of both traces would not influence the "eye". Accordingly, a Fourier analysis of these two traces was carried out to determine the fundamentals of each and the phase relations between them. (A twelve ordinate scheme was used for each cycle.) These results were at first quite encouraging. The measured amplitude of the velocity fluctuations was within about 10 percent of the calculated value as seen in Figure 27. The phase angles, however, were a different story. The observed phase angle of the velocity fluctuation relative to the pressure difference was approximately 120°; however, the calculated phase angle for the same conditions was about minus 80°. This large difference remains to be explained. It was in fact, because of this result, that the dynamic

calibration of the velocity probe was undertaken. It can be seen from Figure 21 that an instrumental phase lag of this magnitude is not possible nor is it possible to ascribe the results to a sign error either in the instrumentation or in the resulting analysis. A number of schemes and effects were suggested which might account for the phase discrepancy. But none of these would seem to account for the change in phase without disturbing the agreement in amplitude.

4.4 General features of the fluctuating flow across the cascade.

4.4.1 Relationships between the fluctuating components across the cascade.

A rather unexpected outcome of these measurements is that on the whole the fluctuating pressures and the fluctuating velocities tend to oscillate together, that is, the maximum pressures occur with the maximum velocity. Indeed, this is particularly true for the "maximum intensity" oscillations in which not only do the pressures and velocities oscillate together in phase, but the lift does also. There is a distinct phase change between the lift and pressures for the various degrees of cavitation, however. Unfortunately this point was not sufficiently explored experimentally but it can be seen from Table II that for an incidence angle of $\alpha = 8^{\circ}$ that the pressure tends to lead the lift oscillation at the higher cavitation numbers when the fluctuating lift percentage is small. On the other hand, for the lower cavitation numbers and the stronger oscillations the pressure tends to lag the lift fluctuation. In any case the pressures upstream and downstream of the cascade tend to track together. This latter observation can also be seen for an angle of attack of 6°; there for a wide range of cavitation number there is little difference in phase between the fluctuating

lift and the fluctuating pressures. The fluctuating velocities on either side of the cascade on the whole track together, although at the higher cavitation numbers, the velocity V_3 tends to lag that of V_2.

The magnitudes of these various fluctuating quantities are in themselves of interest. Again, with reference to Table I, we see for example for an angle of incidence equal to 6° (maximum oscillation) that the fluctuating lift can actually exceed the mean lift. The amplitude of the pressure fluctuations themselves range from about 3 percent to 7 percent of the dynamic pressure but the amplitude of the fluctuating velocity, V_2, is about 2 percent or less of the tunnel speed. However, the fluctuating velocity downstream of the cascade, V_3, shows a much greater amplitude. In some cases it is at least twice that or more of the upstream velocity of perturbation. We should mention again at this point that the downstream velocity is much "spikier" than the upstream velocity. This is easy to understand since it lies in the wake of the upstream cavitating foils. The large fluctuations in lift (from lifting surface theory) should give rise to similar changes in the circulation around each of the foils. This shed circulation should be responsible for some of the perturbations seen on velocity V_3. The spikiness of the lift trace is thought to be real. The high frequency oscillations seen on this trace correspond closely to its natural frequency of oscillation. It is interesting that the downstream velocity sensor seems to reflect even these rapid variations. Another feature worth mentioning is that the pressure in the upstream settling chamber, p_1, also varied during the cavitation oscillations showing that the tunnel did participate in this process. However, there was usually considerable phase lag between this pressure and that of the lift or the

other pressure fluctuations; generally it lagged these other fluctuations by about 130° and was usually smaller in magnitude than the other pressures.

To obtain some insight on the significance of these variations, cavity lengths measured from the high speed motion pictures were plotted together with the fluctuating lift. The three best examples of this correlation are shown in Figures 29 a, b, c. They are all for the maximum oscillation and not the onset. They all tell the same story. For angles of incidence equal to 4, 6 and 8° we see that generally the lift is at its lowest value when the cavity is longest, indicating that for this condition of cavitation there is a direct connection between cavity length and lift force. We have already seen that there is a more or less direct correlation between the pressure just upstream of the cascade and the lift force, certainly for the maximum oscillations.

These findings suggest that at least for the maximum oscillations and the larger blade angles, the effects of inertia on the dynamics of the cavity oscillations are not too important. For example, with reference to data point 5674 of Table II for an angle of incidence equal to 6° near the maximum oscillation intensity, the pressure change across the cascade due to acceleration of the mean flow may be compared to the fluctuating pressure just upstream of the cascade. Knowledge of the frequency and magnitude of the fluctuating velocity component V_2 enables this ratio to be determined; it is found that the ratio of the acceleration pressure difference across the cascade using the chord of the cascade as the relevant length to the upstream pressure fluctuation is approximately 0.2. This figure is not negligible, yet on the other hand, it is not large either.

This suggests then that for the condition of maximum oscillation, the instantaneous flow across the cascade may be taking place in a quasi-steady fashion. Now the measured lift as a function of cavitation number as shown in Figures 13 is actually the time averaged lift at each data point. If it is assumed that this curve also applies at each instant during the cavitating process, estimations of fluctuating lift can be made from a knowledge of the fluctuating pressure and hence cavitation parameter just upstream of the cascade. Again with reference to the data point 5674, we see from Figure 13b and with the data of Table II that the average lift coefficient is about 0.1; swings in the cavitation number of an amount equal to the fluctuating upstream pressure would on Figure 13b drive the lift force to a negative value of about minus 0.08 to a maximum of approximately 0.2. Fluctuations in lift force of this magnitude are indeed recorded dynamically as shown in Table II.

From the above point of view, the cavitating cascade for the condition of maximum oscillations may be thought of to first order as operating in a quasi-steady fashion. It must be remembered though that the instantaneous lift versus angle of attack characteristic of the cavitating cascade is not really known for reasons which will be subsequently discussed.

4.4.2 Continuity check across cascade.

It is readily observed from the tabulations of Table II that the velocities V_2 and V_3 on either side of the cascade are different. Conservation of mass requires that this difference be made up by a change in the density or, for an incompressible flow, a change in the volume of the region between the two velocity measurements. Such a check was carried out for the present tests by measuring the length and estimating the

volume of the cavities that grow and collapse on the blades of the cascade. These measurements are then converted into volume changes with respect to time and these were then compared with a similar calculation made with the velocities determined by the sensors. It must be appreciated that it is difficult to estimate the volume of the growing and collapsing cavities, especially for the cavitation taking place in the tip clearance regions of the foils. The results of this calculation are presented in Table III where this continuity check is presented for angles of incidence equal to 4, 6 and 8 degrees. The largest angle gives a difference in these two quantities of only 11.3 percent. This difference increases to 35 percent for the lowest angle of 4 degrees; it is then, however, much more difficult to estimate cavity volumes and in any case an equally great uncertainty is how well the downstream velocity sensor, V_3, represents the average flow leaving the cascade.

An additional factor which would contribute to the lack of a continuity check across the cascade would be compliance of the side walls of the tunnel. The deflection of the tunnel side walls has been measured in a separate experiment as a function of ambient pressure. Summary calculations of the effect of this compliance upon the continuity check indicate that it would be less than about 2 percent of the values indicated in Table III.

4.4.3 Total pressure loss across the cascade.

The total pressure loss across the cascade was computed as a function of time from a knowledge of the instantaneous velocities and pressure levels upstream and downstream of the cascade. In this calculation the effect of the accelerating main stream from the point of measurement of the pressures was taken into account. Graphs of the total

pressure loss normalized by the dynamic pressure are given for two angles of incidence in Figure 30. Also, plotted for reference is the static pressure at point p_2. This is a difficult calculation to make because of the spikiness of the velocity traces; these in turn caused large changes in the pressure between the cascade and the reference point due to the large acceleration of the main stream. Nevertheless, it does appear that the total pressure loss is least when the static pressure upstream of the cascade is greatest; this is more clear for the 6 degree case than the 8 degree case. In any event, the amplitude of the total pressure loss fluctuation is approximately 10 percent of the dynamic pressure. The amplitude of the pressure fluctuation is approximately one-half psi which corresponds to approximately 8 percent of the dynamic pressure at a nominal tunnel speed of 30 feet per second. Thus the total pressure loss is on the order of the static pressure fluctuation.

4.5 Remarks on the unsteady flow through the cascade.

Why does the partially cavitating flow in the cascade oscillate? Unfortunately we cannot give a rigorous answer to this question. The following remarks bear on various aspects of this question and on the possible influence of the tunnel on the phenomenon observed.

We begin these remarks by noting that in Ref. 1 oscillations of a partially cavitating isolated hydrofoil were observed which bear a resemblance to those of the present work. In the discussion of this paper it is suggested that these oscillations are connected with the time-varying circulation around the hydrofoil. For either an isolated hydrofoil or cascade of hydrofoils the effect of time-varying circulation is to cause a perturbation in the upstream incidence angle approaching each of the

blades. Under some conditions, for cascade flows, it is known that these perturbations lead to a major disturbance of the flow that propagates from one blade to the next; this is the well known "propagating stall" or disturbance which progresses from one blade to another at a definite speed depending upon the flow geometry. In fact, such a propagating disturbance due to cavitation is suggested in motion pictures of a cavitating pump taken by NASA*. So it was with special interest that we examined the high-speed motion pictures of the oscillating cavitation in the present cascade. In this instance, after many repeated viewings of these motion pictures, we could not conclude that there was a progressive disturbance across the cascade in the sense of a propagating stall which is responsible for the instability that is observed. This is not to say that in a cavitating cascade with a great many more blades that propagating stall will not occur. However, it should be pointed out that the present experimental setup does not properly simulate such oscillations because of the fact that the cascade axis is not perpendicular to the fluctuating pressure gradient. Thus it can be seen by reference to the diagram of Figure 6 that during the oscillation process the fluctuating pressures cannot all be the same across the face of the cascade. This, then, is an essential limitation of the present type of experimental cascade arrangement. It could be avoided if a different type of facility were available (or if the stagger angle was zero degrees).

The unsteady cavitation process observed in the working section of the tunnel is, of course, coupled to the fluid dynamics in the remainder of the tunnel circuit. Because of unknown conditions in the diffuser downstream of the cascade, it is not possible without extremely elaborate,

---

* Courtesy M. Hartman.

comprehensive instrumentation to determine these coupling effects. In particular, the effective "inertia" and "compliance" of this diffuser section is unknown because during operation there is generally some unknown amount of free air in the diffuser. Moreover, the flow field in the diffuser, even if fully wetted, is essentially unsteady. It is clear from the present experimental results that there is indeed a fluctuating mass flow or volume flow through the tunnel cascade section. Because of the structural compliance of the overall tunnel system and because of the possibility of free air bubbles occurring either upstream or downstream of the working section, it is unlikely that this same fluctuating flow rate occurs throughout the tunnel system. It would furthermore be very difficult to determine if it did.

For the purpose of the present experiments, we are mainly interested in the fluctuating quantities that occur across the cascade and in their mutual relationships. It is conceivable, however, that the instability observed during partial cavitation in the cascade is due to the coupling of the cascade flow to the entire tunnel circuit. While there is this possibility, we do not believe that it is the source or cause of the observed instability. The reasons for this statement stem primarily from the observed behavior of the tunnel when single bodies are subject to cavitation in the working section. There, as in Ref. 1, the unsteady cavitation observed on a single sharp-edged hydrofoil does not seem to be tunnel-dependent. Experiments on non-lifting bodies such as bluff flat plates or rounded torpedo-like shapes show that the cavitation, as it develops, does not lead to a periodic flow in the tunnel as is observed here. It should be mentioned that the presence of cavitation in a flow either on a

lifting surface or non-lifting surface causes a total pressure loss across the working section that continues to increase with increasing extent of cavity. Thus, as in the present work, there is an increase in total pressure loss with decrease in tunnel pressure much as is observed in Figure 30 of the present work. It is easy to show that the dynamic system consisting of the nozzle flow, the cavitating flow in the working section, plus some allowance for the inertia of the diffuser flow leads to a third order system which is inherently stable provided only that the total pressure loss due to cavitation in the working section increases as the ambient pressure decreases. This is in fact the reason why supercavitating flows are essentially stable in the tunnel, as indeed they are observed experimentally to be.

The present point of view is then that the oscillations observed during partial cavitation on the present cascade set-up are due to an inherent instability in the cavitating cascade flow itself and are not due to a coupled interaction with the tunnel. It may well be that the tunnel may modify these oscillations and may even determine in some sense their frequency or amplitude but it does not seem likely that the basic instability is due to a tunnel interaction.

4.6 Discussion continued.

In view of the preceding discussions, we may inquire as to the significance of the present experimental results to the phenomenon of unsteady cavitation observed in complete turbomachines. First, let us review the salient features observed during the nonsteady cavitation of the present cascade. The frequency of these oscillations seem to be cavitation number dependent; starting with small cavities the frequency is

relatively high and then it decreases as the cavitation number is lowered. It appears that the "hardest" oscillations occurring when the cavity is about as long as the chord may have their frequency controlled somewhat by the downstream effects in the diffuser. However, at the onset of cavitation instability the frequency is probably not controlled by the downstream diffuser flow. Indeed, as was mentioned we are not sure that the diffuser is in fact controlling these fluctuations. It was pointed out that during the nonsteady motions the cascade test set-up does not properly simulate the true cascade flow. Nevertheless, this fluctuating cavitation process is so similar to the "oscillating cavitation" observed in Ref. 1 and elsewhere that it cannot be mere coincidence. It seems very likely that they are both the same process. In the present cascade tests the magnitude of the fluctuating lift force during the cavitation instability is undoubtedly controlled to a great extent by the type of blade profile used.

At the present time a self-consistent mechanism which would explain the origin and frequency of both the instabilities observed in the cascade and in complete inducers does not exist. In the case of the cascade, experiments and theory both show that as the cavity approaches the chord length the lift and circulation about each of the blades rises to a maximum. With further increase in cavity length or decrease in cavitation parameter the circulation and lift both decrease. The changes in lift force during the cavitation cycle thus give rise to changes in circulation and hence to an upwash of the flow approaching the cascade. At the present time for cavitating flow it is not known if the interaction between the upwash, the circulation on the hydrofoil, and the associated vortex wake could give rise to the instability — much in the same manner as for propagating stall. In addition, there are inherent total pressure losses associated

with the cavity flow. These are not known from theory; the results of the present work suggest that they are directly related to the fluctuating pressure upstream to the cascade but we do not know how general these results might be. In any event, it would seem possible that interactions of this type could lead either to the cavitation instability observed in a cascade or in a complete turbomachine. Our knowledge of these processes is so meager at the present time that we cannot say whether a cavitating propagating stall or a mere nonsteady surging oscillation of the sort observed herein will take place.

These comments are foscused on the naturally "occurring" cavitation instability observed in the present cascade tests and in cavitating inducers. We may next ask if there is a relationship between this type of cavitation instability and the "POGO" oscillations? In analyzing the nonsteady behavior of a cavitating pump during the system oscillations one would like to know the output quantities, head, mass flow, etc. as a function of the fluctuating upstream flow. It would seem inevitable that this "forced" type of periodic behavior would be related to the naturally occurring cavitation instability perhaps rather like that of a forced oscillation of a mechanical system. This analogy cannot be pushed very far because of our great uncertainty of the actual physical processes taking place during the unsteady motions of the cavitating cascade. It does, however, lead us to consider the relevant time scales of the various dynamic phenomena that can take place in a machine. There is first of all the period of the naturally occurring cavitation instability; if the transient accelerations experienced by the cavity flow associated with this period give rise to pressure differences in the vicinity of the cascade comparable

to those (suitably normalized) of the cavitation parameter, it would seem reasonable that the naturally occurring cavitation instability is dynamically controlled. On the other hand, if these pressure fluctuations are "small" it would seem reasonable that the naturally occurring cavitation instability can be explained on a "quasi-steady" approach. Similar comments may be made in respect to the behavior of a cavitating pump subject to inlet pressure perturbations as occurs in the POGO effect; namely, if the period of the fluctuation is sufficiently long the cavitation process can be treated on a quasi-steady basis. If the reverse is true the dynamics of the growing and collapsing cavities within the pump have to be treated in detail.

4.7 Further remarks.

The essential problem for the "POGO" oscillations is to determine for a particular system how the non-steady behavior of the pump, with cavitation, is to be represented. As a useful, practical result one would like to know when it is possible to treat the pump under these conditions in a quasi-steady manner as this is, in fact, the basis of the treatment in Refs. 3, 4, 5, for example. It appears to us that further work of both an experimental nature and theoretical nature must still be carried out before even this question can be answered adequately. It is certainly a complex question because the phenomenon of cavitation in machines cannot be fully explained in terms of ideal fluid mechanics by reason of the inherent dissipation that takes place at the terminus of the cavity wake. Because of this fact, further experimental work preferably on complete machines such as a cavitating inducer should be carried out to provide the output quantities for given inlet pressure perturbations.

This is in fact already underway, as mentioned, at the NASA Flight Propulsion Laboratory. There is an additional aspect of cavitating flows in turbomachines different from that of the cascade of the present work that does bear mention. Namely, under some conditions of operation a frothy cavitating region stemming from the tip clearance flow of the rotor can occur for many diameters upstream of the pump impeller. This two-phase flow is often an integral aspect of the cavitating machine and will clearly participate in any nonsteady flow phenomena. On the other hand, there are those situations also in which this upstream tip clearance flow does not exist and for these situations the results of such an inlet perturbation would be easier to identify and analyze. In passing over this point we may note as a separate comment that the analysis of two-phase flows — liquid and vapor bubbles — is still in an unsatisfactory state and needs further attention in its own right.

The theoretical complexities attendant upon the analysis of unsteady cavitating flows are clearly outlined in the work of Ref. 15 in which a time-dependent analysis of the unsteady free streamline flow past simple objects such as bluff bodies in two dimensions is formulated. From this work we see that to carry out a full analysis of such a cavitating flow in a cascade would be very formidable indeed. As a simpler alternative the linearized free streamline theory of Ref. 14 and Ref. 16 can in principle be adapted to non-steady cavitating cascade flows (see for example Ref. 17). It should be pointed out, however, as study of Refs. 16, 17 will show that even the linearized theory leads to analyses of considerable complexity.

5. SUMMARY

An experimental program on a cavitating cascade of flat plate hydrofoils having a mean stagger angle of 45° and a solidity of one has been carried out. The blade profile was in essence that of a biconvex airfoil having a thickness percentage of 8 percent. It was found that when cavitation commenced at the leading edge the cavitation process became unstable and fluctuated with a frequency dependent on the angle of attack and the mean cavity length. The cavities had to be about one-half the chord length before the oscillations would commence; the initial frequency of oscillation was relatively high and it decreased with increase in cavity length. When the cavities were sufficiently long, a quarter chord or so greater than the hydrofoil, these oscillations ceased and the flow became essentially steady. The condition of maximum lift on the hydrofoil occurred when the mean cavity length was about one chord in length; this corresponded to the fluctuations of maximum intensity. Here, depending upon the angle of attack, the fluctuations in lift force were on the order of the mean lift. It was pointed out, however, that these fluctuating amplitudes will depend upon the type of profile thickness chosen for the cascade. Fluctuations of tunnel speeds approaching the cascade and of ambient pressure approaching the cascade were also observed; these were on the order of one percent of the tunnel speed and five percent of the dynamic pressure, respectively. For these experiments, the fluctuating static pressure upstream of the cascade and lift force on the blades of the cascade were essentially in phase. This was explained on a quasi-steady basis for the present profile section at the lower frequencies. The cavitation instability observed in these experiments is believed to be an inherent

phenomenon of lifting cavitating surfaces for those situations in which cavitation occurs from a sharp leading edge. It is suggested that a similar type of naturally occurring cavitation fluctuations takes place in a cavitating turbomachine. Insufficient evidence and understanding of this complex phenomenon prevents us, however, from interpreting these results either as a propagating cavitating stall or as a uniform oscillation of the entire cascade row. The real flow in a turbomachine is often complicated by the presence of an upstream cavitating tip clearance flow which is not present in these cavitating cascade tests. Some suggestions are included for further analysis and research.

ACKNOWLEDGMENT

We would like to record here our appreciation for the efforts of the staff of the Hydrodynamics Laboratory: C. Eastvedt, photography, H. Hamaguchi, J. Kingan, G. Lundgren for assistance on the water tunnel, Mrs. Phyllis Henderson for secretarial work, and to Mrs. Madeline Fagergren for preparing the manuscript. Appreciation for the efforts of H. Petrie in helping to reduce the considerable volume of data is also acknowledged.

References

1. R. B. Wade and A. J. Acosta, "Experimental Observations on the Flow Past a Plano Convex Hydrofoil", Journ. Basic Engineering, Trans. ASME, Series D, Vol. 88, 1966, p. 273.

2. A. J. Acosta, "An Experimental Study of Cavitating Inducers", Second Symposium on Naval Hydrodynamics, August, 1958, Wash., D.C., sponsored by Office of Naval Research, Dept. of the Navy, ACR-38.

3. S. Rubin, "Instability Model of Missile Longitudinal Oscillation Due to Propulsion Feedback", Report No. TOR-269(4126)-28, Aerospace Corp., September 1964.

4. S. Rubin, "Longitudinal Instability of Liquid Rockets Due to Propulsion Feedback (POGO)", Journ. of Spacecraft and Rockets, Vol. 3, No. 8, August 1966, pp. 1188-1195.

5. F. E. Bikle, L. E. Fidler, and J. B. Rohrs, "A Study of System Coupled Instability Analysis Techniques, Final Report, Parts I and II", Technical Report AFRPL-TR-66-143, July 1966, Air Force Rocket Propulsion Laboratory, Research and Technology Division, Edwards Air Force Base, California.

6. R. H. Fashbaugh and V. L. Streeter, "Resonance in Liquid Rocket Engine Systems", Trans. ASME, Series D, Vol. 87, No. 4, 1965, p. 1011.

7. L. E. Sack and H. B. Nottage, "System Oscillations Associated with Cavitating Inducers", Trans. ASME, Vol. 87, Series D, No. 4, 1965, p. 917.

8. R. G. Dorsh, D. J. Wood, and C. Lightner, "Distributed Parameter Analysis of Pressure and Flow Disturbances in Rocket Propellant Feed Systems", National Aeronautics and Space Administration Technical Note TND 3529, 1966.

9. R. B. Wade and A. J. Acosta, "Investigation of Cavitating Cascades", Trans. ASME, Vol. 89, Series D, No. 4, 1967, p. 693.

10. R. T. Knapp, J. Levy, J. P. O'Neill, and F. B. Brown, "The Hydrodynamics Laboratory of the California Institute of Technology", Trans. ASME, Vol. 70, 1948.

11. T. Kiceniuk, "A Two-Dimensional Working Section for the High Speed Water Tunnel at the California Institute of Technology", Cavitation Research Facilities and Techniques, ASME, 1964.

12. H. Schlichting, "Berechnung der reibungslesen inkompressiblen Stromung fur ein vergegebenes ebenes Shaufelgitter", VDI forschungscheft 447, 1955.

13. G. L. Mellor, "An Analysis of Axial Compressor Cascade Aerodynamics, Pt. I", Journ. Basic Engineering, Trans. ASME, Vol. 81, 1959.

14. R. B. Wade, "Linearized Theory of a Partially Cavitating Cascade of Flat Plate Hydrofoils", Applied Science Research, Vol. 17, p. 169, 1967.

15. D. P. Wang and T-Y Wu, "Small-Time Behavior of Unsteady Cavity Flows", Archive IV, Rational Mechanics and Analysis, Vol. 14, No. 2, 1963, p. 127.

16. J. A. Geurst, "Linearized Theory of Two Dimensional Cavity Flows", Thesis from the Technische Hogeschool Delft, Netherlands, 1961 (supported by U. S. Office of Naval Research, Contract N62558-2269).

17. F. Sisto, "Nonstationary Cascade at Fully Stalled or Supercavitated Conditions. I - Linearized Theory", Proceedings 5th Nat. Congress of Applied Mechanics, ASME, 1966.

LIST OF FIGURE CAPTIONS

Fig. 1. General view of working area showing the tunnel and readout equipment.

2. View of foils mounted to lucite window.

3. Working section of tunnel showing movable walls and center foil mounted to force balance.

4. View illustrating actuating mechanism for setting movable walls.

5. Drawing of model.

6. Definition sketch showing location of pressure taps and velocity probes.

7. Definition of cascade parameters.

8a Block diagram illustrating strain gage hookup.

8b Block diagram illustrating pressure transducer hookup.

8c Block diagram illustrating velocity probe hookup.

9. Force coefficients based on mean flow velocity as a function of the vector mean angle of incidence for compressor cascade of solidity $\sigma = 1.00$ for two Reynolds numbers.

10. Lift-to-drag ratio, turning angle and leaving angle as a function of the angle of incidence α_1 for compressor cascade of solidity $\sigma = 1.00$ for two Reynolds numbers.

11. Force coefficients based on mean flow velocity as a function of the vector mean angle of incidence for turbine cascade of solidity $\sigma = 1.00$ for two Reynolds numbers.

12. Lift-to-drag ratio, turning angle and leaving angle as a function of the angle of incidence α_1 for turbine cascade of solidity $\sigma = 1.00$ for two Reynolds numbers.

13a Variation of the force coefficients based on upstream velocity with the cavitation parameter K_v for an angle of incidence of 4° in a compressor cascade of solidity $\sigma = 1.00$.

13b Variation of the force coeffecients based on upstream velocity with the cavitation parameter K_v for an angle of incidence of 6° in a compressor cascade of solidity $\sigma = 1.00$.

13c Variation of the force coefficients based on upstream velocity with the cavitation parameter K_v for an angle of incidence of 8° in a compressor cascade of solidity $\sigma = 1.00$.

Fig. 13d Variation of the force coefficients based on upstream velocity with the cavitation parameter K_v for an angle of incidence of 10° in a compressor cascade of solidity $\sigma = 1.00$

13e Variation of the force coefficients based on upstream velocity with the cavitation parameter K_v for an angle of incidence of 12° in a compressor cascade of solidity $\sigma = 1.00$.

14a Photograph of cavitation occurring in the compressor cascade, solidity $\sigma = 1.00$, for various cavitation parameters K_v at an angle of incidence α_1 equal to 4°.

14b Photograph of cavitation occurring in the compressor cascade, solidity $\sigma = 1.00$, for various cavitation parameters K_v at an angle of incidence α_1 equal to 6°.

14c Photograph of cavitation occurring in the compressor cascade, solidity $\sigma = 1.00$, for various cavitation parameters K_v at an angle of incidence α_1 equal to 8°.

14d Photograph of cavitation occurring in the compressor cascade, solidity $\sigma = 1.00$, for various cavitation parameters K_v at an angle of incidence α_1 equal to 10°.

14e Photograph of cavitation occurring in the compressor cascade, solidity $\sigma = 1.00$, for various cavitation parameters K_v at an angle of incidence α_1 equal to 12°.

15. Cavity-to-chord ratio as a function of the cavitation parameter K_v for an angle of incidence of 6° in a compressor cascade of solidity $\sigma = 1.00$.

16. Traces of the fluctuating pressures, velocities and lift measured at various points in the tunnel for various cavitation parameters K_v in a compressor cascade of solidity $\sigma = 1.00$ at an angle of incidence of 4°.

17. Traces of the fluctuating pressures, velocities and lift measured at various points in the tunnel for various cavitation parameters K_v in a compressor cascade of solidity $\sigma = 1.00$ at an angle of incidence of 6°.

18. Traces of the fluctuating pressures, velocities and lift measured at various points in the tunnel for various cavitation parameters K_v in a compressor cascade of solidity $\sigma = 1.00$ at an angle of incidence of 8°.

Fig. 19. Traces of the fluctuating pressures, velocities and lift measured at various points in the tunnel for various cavitation parameters K_v in a compressor cascade of solidity $\sigma = 1.00$ at an angle of incidence of 10°.

20. Traces of the fluctuating pressures, velocities and lift measured at various points in the tunnel for various cavitation parameters K_v in a compressor cascade of solidity $\sigma = 1.00$ at an angle of incidence of 12°.

21. Comparison of the output of the hot film probe with oscillating sinusiodal input. The top trace is the hot film probe output and the spikes on the lower trace indicate points of maximum velocity input.

22. Frequency of pressure fluctuations (p_3) versus angle of incidence for fully wetted flow in a compressor cascade of solidity $\sigma = 1.00$.

23. Frequency of oscillations versus cavitation parameter K_v spanning the region of maximum oscillations for various angles of incidence in a compressor cascade of solidity $\sigma = 1.00$. The nominal tunnel speed is 30 ft./sec.

24. Strouhal number versus angle of incidence for fully wetted and maximum oscillation conditions.

25. Dependence of Strouhal number on velocity at maximum oscillation conditions at an angle of incidence of 6°.

26a Fluctuation differential pressure across main tunnel nozzle and fluctuating velocity approaching the cascade for an angle of incidence of 6° in a compressor cascade of solidity $\sigma = 1.00$.

26b Fluctuation differential pressure across main tunnel nozzle and fluctuating velocity approaching the cascade for an angle of incidence of 8° in a compressor cascade of solidity $\sigma = 1.00$.

26c Fluctuation differential pressure across main tunnel nozzle and fluctuating velocity approaching the cascade for an angle of incidence of 8° in a compressor cascade of solidity $\sigma = 1.00$.

26d Fluctuation differential pressure across main tunnel nozzle and fluctuating velocity approaching the cascade for an angle of incidence of 8° in a compressor cascade of solidity $\sigma = 1.00$.

27. Comparison of calculated velocity amplitude ratio $(V_2/\overline{V})$ using Bernoulli's Equation with measured velocity amplitude ratio $(V_2/\overline{V})$ for angles of incidence of 6° and 8° in a compressor

LIST OF TABLES

APPENDICES

NOMENCLATURE

The following notation is generally used except for changes across the cascade itself. There the notation of Figure 7 is used to be in accord with the usual notation of cascade flows.

A, B, C	constants
A	plan form area = (s x c)
c	chord length
C_D	drag coefficient = $\frac{D}{A\rho V^2/2}$
C_L	lift coefficient = $\frac{L}{A\rho V^2/2}$
C_M	moment coefficient = $\frac{M}{Ac\rho V^2/2}$
C_P	pressure coefficient = $\frac{\Delta p}{\rho V^2/2}$
D	drag force on model
f	frequency of oscillations
i	$\sqrt{-1}$
K	corrected cavitation number $\frac{p - p_k}{\rho V^2/2}$
K_v	cavitation number based on vapor pressure $\frac{p - p_v}{\rho V^2/2}$
ℓ	cavity length
L	lift force on model
M	moment on model about center of section
p	tunnel static pressure
p_k	measured cavity pressure
p_v	vapor pressure of water

R	radius of circular surface of model
R_e	Reynolds number = $\frac{Vc}{\nu}$
S	Strouhal number fc/V
t	thickness of hydrofoil
V	tunnel velocity
α	angle of incidence measured from chord line
β	stagger angle, angle between normal to chord line and cascade axis
γ	cascade angle, angle between axis of cascade and normal to upstream velocity
δ	deviation angle, angle between exit flow direction and tangent to circular surface at the trailing edge
ν	kinematic viscosity of water
θ	turning angle measured between upstream flow and downstream flow directions
ρ	density of water
σ	solidity, ratio of chord to spacing

In reference to Figure 7:

$( )_1$	denotes upstream of cascade
$( )_2$	downstream of cascade
$( )_m$	based on vector mean of upstream and downstream velocities across cascade
$( )_h$	homogeneous solution
$( )'$	perturbation components
$\overline{( )}$	complex conjugate quantity

Generally, however, (in reference to Figure 6):

$( )_1$	inlet to nozzle
$( )_2$	denotes the tunnel velocity upstream of cascade
$( )_3$	denotes the tunnel velocity downstream of the cascade.

APPENDIX I

TARE FORCE CORRECTIONS FOR CASCADE EXPERIMENTS

The tare forces acting on the fairing plate were obtained by remounting the center foil of the cascade from the lucite window and inserting a blank disk on the balance spindle. An extra model had been manufactured for this purpose. The procedure used was then to measure the lift, drag and moment on this disk for various angles of attack of the model. It was found that these forces were relatively small and in the case of the moment negligible.

The results of this test are presented in graphical form in Figs. A-1 and A-2 for the compressor of 1.00 solidity.

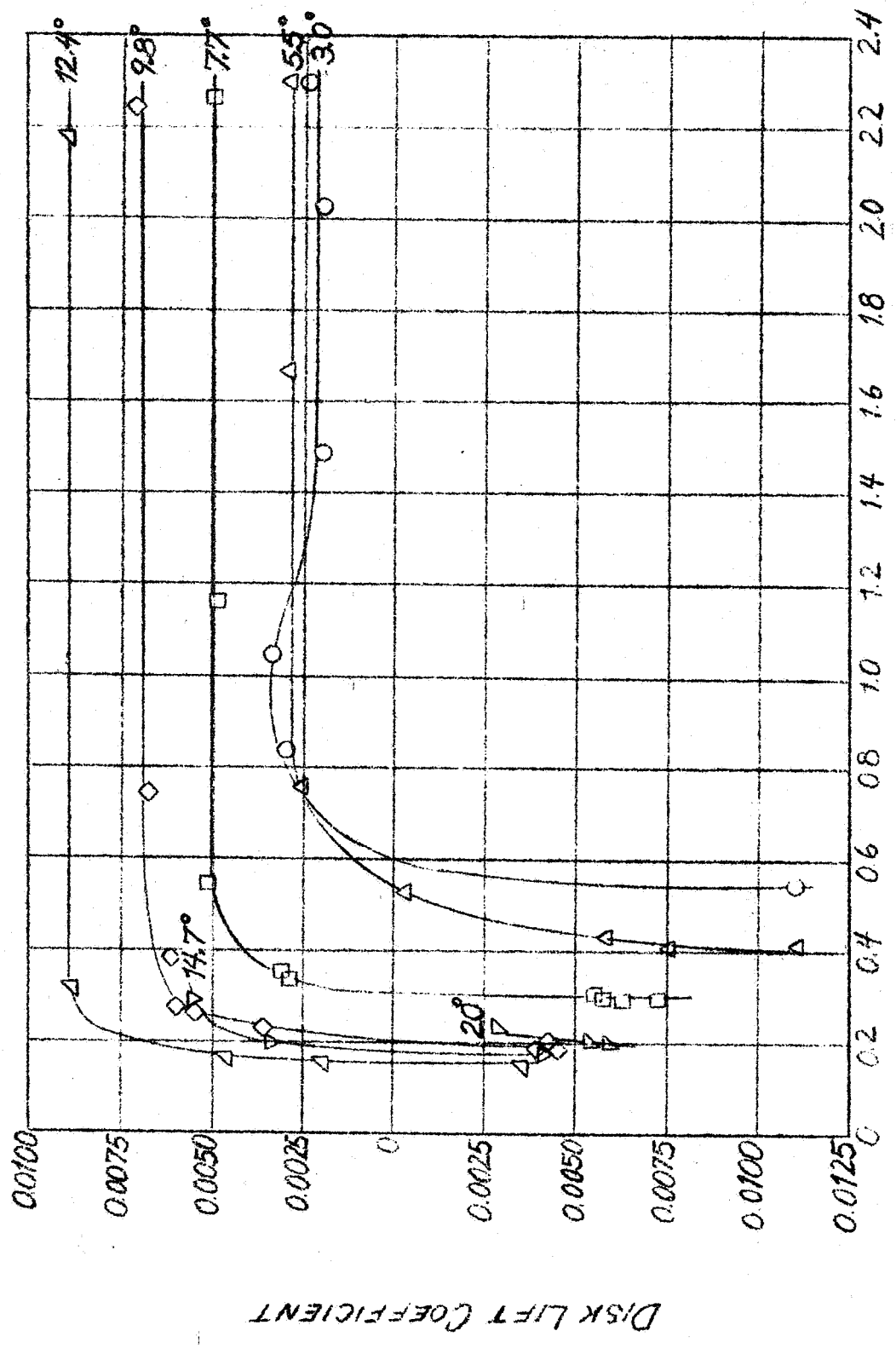
12.4°
9.8°
7.7°
5.5°
3.0°
14.7°
20°
0.0100
0.0075
0.0050
0.0025
0
0.0025
0.0050
0.0075
0.0100
0.0125
0
0.2
0.4
0.6
0.8
1.0
1.2
1.4
1.6
1.8
2.0
2.2
2.4
Disk Lift Coefficient
Cavitation Parameter Kv

Fig. A-1

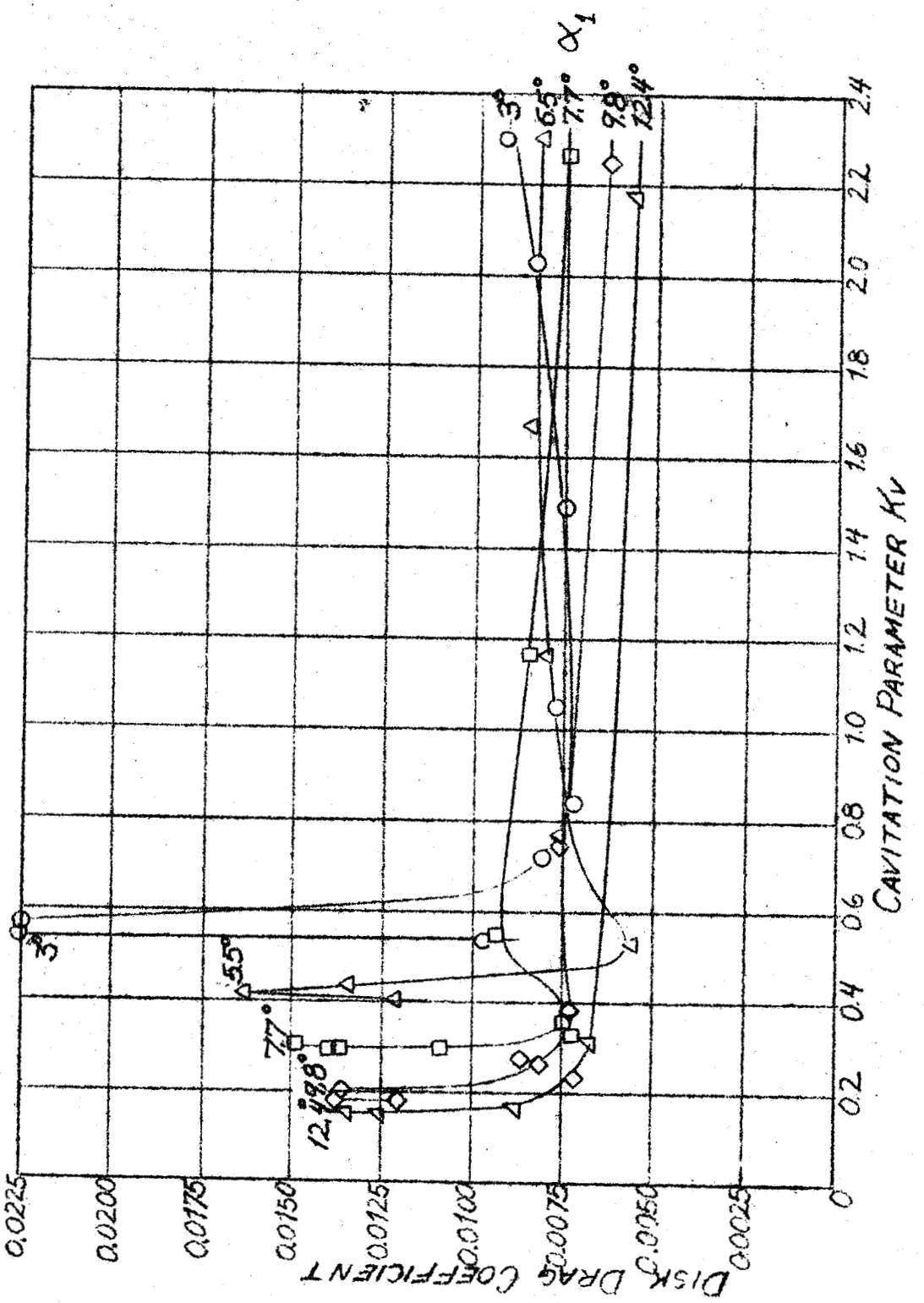
α_1
3°
5.5°
7.7°
9.9°
12.4°
3°
5.5°
7.7°
9.8°
12.4°
0.0225
0.0200
0.0175
0.0150
0.0125
0.0100
0.0075
0.0050
0.0025
0
DISK DRAG COEFFICIENT
0.2
0.4
0.6
0.8
1.0
1.2
1.4
1.6
1.8
2.0
2.2
2.4
CAVITATION PARAMETER K_v

FIG. A-2

APPENDIX II

CALIBRATION OF MODIFIED TWO-DIMENSIONAL WORKING SECTION

The calibration of the modified working section was undertaken with several aims in view. Since this particular arrangement had never been run before it was of interest to determine whether the design was performing as anticipated and to obtain some idea of the flow characteristics and boundary layer effects. The influence of the movable walls on the pressure distribution in the tunnel was also investigated. The main purpose of the calibration, however, was to correlate the readings of static pressure and differential pressure obtained at the measuring orifice in the nozzle with those measured at a pressure tap located 6 inches upstream of the balance center line. This correlation would enable all static pressures and differential pressures during the tests to be taken at the nozzle orifice, thus obviating any model influences on these readings. The nozzle orifice was deemed to be sufficiently far upstream from the cascade that effects due to circulation and drag would be of negligible importance.

The tests were conducted in the following manner: For constant tunnel speed, static pressure readings were taken at 6 inch intervals along the center line of the tunnel over the entire length of the working section. These readings were recorded with respect to the pressure in the settling chamber with the multi-tube mercury manometer. The static pressure at the nozzle orifice was recorded on a well-type mercury manometer and the differential pressure across the nozzle to this point

was recorded on the oil manometer. From these readings the static pressure distribution along the tunnel center line was found. These readings were repeated for several tunnel speeds.

At each tunnel speed the tunnel ambient pressure was changed and the tests repeated for various pressures to determine if any effect was discernable on the correlation function between the nozzle orifice and the working section orifice. These runs were all carried out with the walls parallel.

It was found that the pressure coefficient at the pressure point p_N used as the calibration tap was little affected by change in wall angle. Furthermore, little pressure undershoot at the nozzle throat existed confirming the expectations of the insert design. Thus little chance exists for cavitation to occur here. This was further confirmed by running the clear tunnel at very low pressures.

Fig. B-1 gives the correlation function, f, essentially as a function of tunnel speed represented here by the differential pressure H_1, across the nozzle to the nozzle orifice. The results shown represent the averages of many readings. However, extremely little scatter occurred in these readings. The function f is defined as the ratio of the differential pressure, H_2, across the tunnel nozzle to the working section to the differential pressure, H_1. It will be seen that this ratio can be represented as two straight lines over the range of velocities examined.

The evaluation of this function enables the true dynamic head and the tunnel static pressure in the working section to be determined from readings of these quantities at the nozzle orifice. These are obtained simply as follows. Since

$$H_1 = p_H - p_N \quad \text{and} \quad H_2 = p_H - p_T$$

and since

$$f = \frac{H_2}{H_1}$$

we thus have

$$H_2 = H_1 \, f(H_1) \qquad \text{B-1}$$

and

$$p_T = p_N - \left[f(H_1) - 1\right] H_1 \qquad \text{B-2}$$

Therefore, knowing f, H_1, and p_N, one can determine H_2 and p_T.

Under test conditions therefore we obtain from equations B-1 and B-2 the dynamic head and tunnel static pressure that would exist in the clear working section.

CALIBRATION FUNCTION $f = h_2/h_1$
$h_1 = (P_H - P_M)$ psi
$h_2 = (P_M - P_L)$ psi
0
10
20
30
40
0.5
1.0
1.5

APPENDIX III

METHOD OF SETTING THE DOWNSTREAM WALL ANGLES

The iteration procedure used for setting the wall angles in the fully wetted and partially cavitating regions is presented here. Before describing the method the relevant formulae used will be derived for both the compressor and turbine configurations. The notation is that of Fig. 7.

Compressor Configuration - With reference to Fig. 7, we have

$$L_m = L\cos\theta_m + D\sin\theta_m$$

where L and D are the measured lift and drag on the force balance. Defining the force coefficients in the following way

$$C_{Lm} = \frac{L_m}{\rho V_m^2 c/2}; \quad C_L = \frac{L}{\rho V_1^2 c/2}; \quad C_D = \frac{D}{\rho V_1^2 c/2}$$

we obtain

$$C_{Lm} = (C_L\cos\theta_m + C_D\sin\theta_m)\, V_1^2/V_m^2 .$$

However, from the velocity triangles in Fig. 41 we have the following relationship

$$V_m^2 = V_1^2 + u^2 - 2V_1 u\cos\left(\frac{\pi}{2} - \gamma\right)$$

i.e.,
$$\frac{V_m^2}{V_1^2} = 1 + \frac{u^2}{V_1^2} - 2\frac{u}{V_1}\cos\left(\frac{\pi}{2} - \gamma\right)$$

but
$$V_1\sin\theta = 2u\sin\left(\frac{\pi}{2} - \gamma + \theta\right)$$

or
$$\frac{u}{V_1} = \frac{\sin\theta}{2\cos(\gamma - \theta)} = \chi \text{, say}$$

From this equation we have $\chi = \chi(\gamma, \theta)$, hence this quantity is only a function of the turning angle θ once the cascade geometry is known. We therefore have that

$$\frac{V_m^2}{V_1^2} = 1 + \chi^2 - 2\chi \sin \gamma$$

which in turn is only a function of θ.

As an initial approximation we neglect the drag term in the expression for the lift coefficient above. This is certainly justifiable since under most circumstances $C_D \sin \theta_m << C_L \cos \theta_m$. Doing this we obtain

$$C_{Lm} = C_L \cos \theta_m V_1^2 / V_m^2$$

or

$$C_L = \frac{C_{Lm}}{\cos \theta_m} \frac{V_m^2}{V_1^2} .$$

Now, from the Kutta-Joukowski law for the cascade, we have that

$$L_m = \rho V_m \Gamma = \rho V_m (2us)$$

hence

$$C_{Lm} = \frac{4u}{\sigma V_m}$$

where $\sigma = \frac{c}{s}$, the solidity ratio.

Therefore

$$C_{Lm} = \frac{4}{\sigma \cos \theta_m} \cdot \frac{u}{V_m} \cdot \frac{V_m}{V_1}$$

Again, from the velocity triangles, we find that

$$V_1 - u \cos (\tfrac{\pi}{2} - \gamma) = V_m \cos \theta_m$$

or

$$\cos \theta_m = \frac{V_1}{V_m} \left[1 - \frac{u}{V_1} \sin \gamma \right]$$

$$\cos \theta_m = \frac{1}{(1 + \chi^2 - 2\chi \sin \gamma)^{\frac{1}{2}}} \left[1 - \chi \sin \gamma \right] .$$

We can therefore finally write

$$C_L = \frac{4}{\sigma} \chi \cdot \frac{(1 + \chi^2 - 2\chi \sin \gamma)}{(1 - \chi \sin \gamma)}$$

This expression is purely a function of the turning angle, θ for any given cascade geometry.

In the above fomulation the approximation made was in neglecting the drag term. If this term is considered as a correction term to the above expression, we have as error the term $-C_D \tan \theta_m$ which can be written as

$$- C_D \cdot \frac{\chi \cos \gamma}{(1 - \chi \sin \gamma)}$$

This error term is known as a function of θ provided the drag coefficient is known for the particular lift conditions.

Based on the above formulae the following iteration for setting the walls is adopted.

Step 1 - For any given angle of attack α the walls are adjusted while monitoring the lift balance until a rough setting is obtained.

Step 2 - The lift coefficient is then obtained from the balance and differential pressure reading and the corresponding turning is read off the C_L versus θ curve in Fig. C-1, obtained from the above equations. The walls are then readjusted to this value.

Step 3 - The new lift is calculated and the procedure repeated, if necessary. When the values are in close agreement the drag is also determined and from the $\tan \theta_m$ versus θ curve a value of $\tan \theta_m$ is read off and the correction term is thus obtainable. This gives a new value for C_L from which a more accurate value of θ can be found.

Step 4 - This last process may be repeated until no further change occurs.

Usually the method converges very rapidly. After two iterations,

in fact, a fairly accurate angle is obtained. One correction for drag is all that is necessary to achieve final convergence to within experimental values.

Turbine Configuration: The procedure used here is identical with the preceding one. The relevant formulae are

$$C_L = \frac{4}{\sigma} \chi \cdot \frac{(1 + \chi^2 + 2 \chi \sin \gamma)}{(1 + \chi \sin \gamma)}$$

and for the correction term we obtain

$$- C_D \tan \theta_m = - C_D \frac{\chi \cos \gamma}{(1 + \chi \sin \gamma)}$$

These formulae are simply obtained by replacing γ by $- \gamma$ in the previous formulae. These functions are plotted in Fig. C-2.

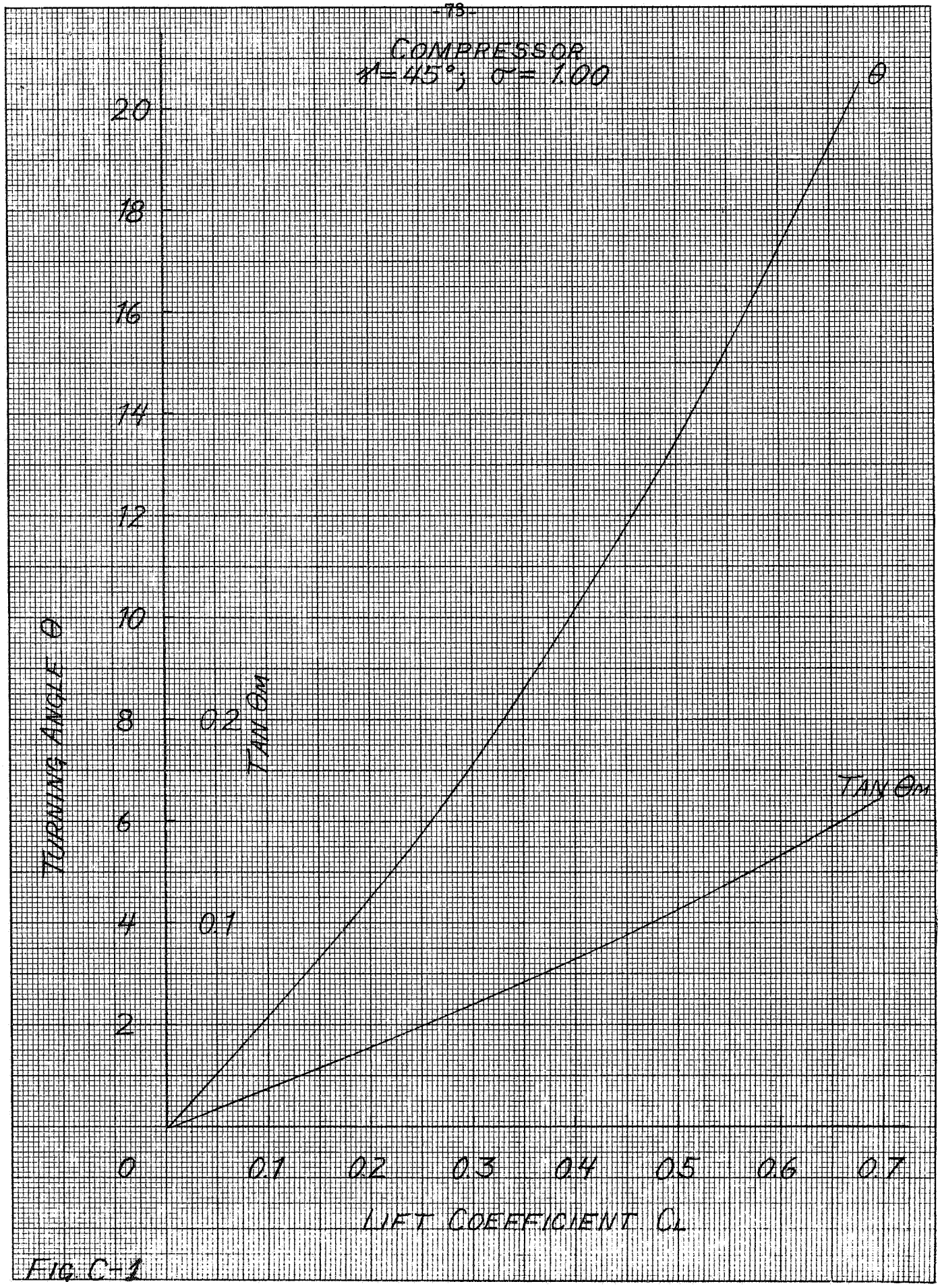
COMPRESSOR
$\beta^1 = 45°$; $\sigma = 1.00$
20
18
16
14
12
10
8
6
4
2
0
TURNING ANGLE θ
0.2 TAN θm
0.1
θ
TAN θm
0
0.1
0.2
0.3
0.4
0.5
0.6
0.7
LIFT COEFFICIENT C_L

Fig C-1

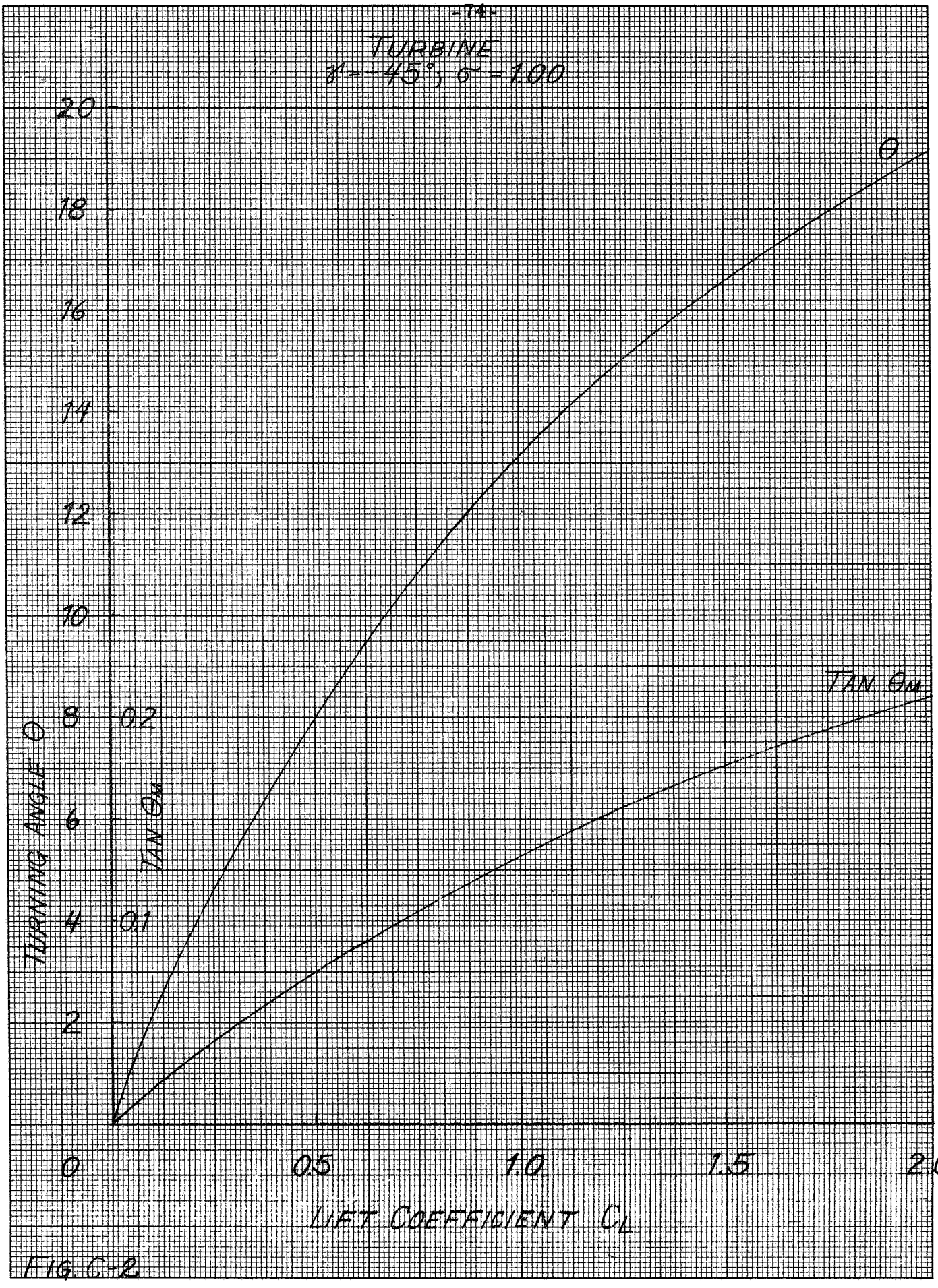
TURBINE
$\gamma' = -45°$; $\sigma = 1.00$
20
18
16
14
12
10
8
6
4
2
0
0
0.2
0.1
TAN θ_M
TURNING ANGLE θ
0
0.5
1.0
1.5
2.0
LIFT COEFFICIENT C_L

FIG. C-2

APPENDIX IV

DATA REDUCTION FOR CASCADE TESTS

1. Calculation of Force Coefficients

Two systems of representation are used in the fully wetted data — the force coefficients based on upstream flow velocity and those based on the mean conditions. These two systems are interrelated. The notation is that of Fig. 7. From Fig. 7 we obtain the following equations

$$L_m = L \cos \theta_m + D \sin \theta_m$$

$$D_m = - L \sin \theta_m + D \cos \theta_m$$

defining the lift and drag coefficient as

$$C_{Lm} = \frac{Lm}{\rho V_m^2 A/2} \quad \cdot \quad C_{Dm} = \frac{Dm}{\rho V_m^2 A/2}$$

$$C_L = \frac{L}{\rho V_1^2 A/2} \quad \cdot \quad C_D = \frac{D}{\rho V_1^2 A/2}$$

we obtain from above

$$C_{Lm} = \left[C_L \cos \theta_m + C_D \sin \theta_m \right] \frac{V_1^2}{V_m^2}$$

$$C_{Dm} = \left[- C_L \sin \theta_m + C_D \cos \theta_m \right] \frac{V_1^2}{V_m^2}$$

where L and D are the measured lift and drag from the force balance. The moment coefficient is defined as

$$C_M = \frac{M}{\rho V_1^2 Ac/2} \quad , \quad C_{Mm} = \frac{M}{\rho V_m^2 Ac/2} \quad .$$

The mean force coefficients can therefore be obtained from the measured ones provided θ_m and V_1/V_m can be determined experimentally.

2. Calculation of Flow Angles

From Fig. 7 we see that

$$V_1 \cos \gamma = V_2 \cos (\gamma - \theta) = V_m \cos (\gamma - \theta_m) \qquad \text{D-1}$$

Further

$$V_1 \sin \gamma = 2 \left[V_m \sin (\gamma - \theta_m) - V_2 \sin (\gamma - \theta) \right] + V_2 \sin (\gamma - \theta)$$

or

$$V_m \sin (\gamma - \theta_m) = \frac{1}{2} \left[V_1 \sin \gamma + V_2 \sin (\gamma - \theta) \right]$$

hence we obtain

$$\tan (\gamma - \theta_m) = \frac{1}{2} \left[\tan \gamma + \tan (\gamma - \theta) \right] \qquad \text{D-2}$$

If we compare these equations with those usually used in cascade work using the angles α, α_2, α_m, and β as defined in Fig. 7, then we obtain

$$\gamma - \theta_m = \alpha_m + \beta$$

$$\gamma = \alpha + \beta$$

$$\gamma - \theta = \alpha_2 + \beta$$

or

$$\beta = (\gamma - \alpha); \quad \alpha_m = (\alpha - \theta_m); \quad \alpha_2 = (\alpha - \theta)$$

where α is the angle of attack. Furthermore from equation (D-2), θ_m can be determined from the measured value of θ which is the wall angle. Hence α_m and α_2 are also determined.

3. Velocity Ratios

The velocity ratios can be obtained from equation (D-1). They are given by

$$\frac{V_1}{V_m} = \frac{\cos(\gamma - \theta_m)}{\cos \gamma}$$

and

$$\frac{V_1}{V_2} = \frac{\cos(\gamma - \theta)}{\cos \gamma} .$$

4. Cavitation Parameter

The cavitation parameter used in all of the cascade tests is based on vapor pressure and upstream velocity, i.e.,

$$K_v = \frac{p - p_v}{\rho V_1^2/2}$$

APPENDIX V

PRESSURE AND VELOCITY FLUCTUATIONS ACROSS THE NOZZLE

In this appendix the connection between the fluctuating component of velocity V_2 (see Figure 6) and the fluctuating pressures p_1 in the nozzle and p_2 in the working section are established.

The non-steady Bernoulli equation is

$$\int_1^2 \frac{\partial V}{\partial t}\, dx + \frac{V_2^2}{2} + \frac{p_2}{\rho} = \frac{V_1^2}{2} + \frac{p_1}{\rho} \qquad \text{E-1}$$

where V is the flow velocity and dx is an increment of length between points 1, 2. It is now assumed the nozzle is perfectly rigid so that

$$V = V_2 A_2/A \qquad \text{E-2}$$

where A(x) is the cross sectional area of the tunnel. Velocity V_1 is much less than that of V_2 and is neglected. The working section velocity V_2 is split into a mean value $\overline{V}$ and a time varying value v(t); i.e.,

$$V_2 = \overline{V} + v \ .$$

Then

$$L_e \frac{dv}{dt} + \overline{V}v + \frac{\overline{V}^2 + v^2}{2} = \frac{p_1 - p_2}{\rho}$$

where

$$L_e = \int_1^2 (A_2/A)\, dx \ .$$

The square of v is neglected compared to $\overline{V}v$ and $\overline{V}^2$ and on putting

$$(p_1 - p_2) = \Delta p + a_o \sin \omega t$$

where Δp is the mean pressure difference, we have

$$\overline{V} = \sqrt{\frac{2\Delta p}{\rho}}$$

and

$$L_e \frac{dv}{dt} + \overline{V}v = \frac{a_o}{\rho} \sin \omega t \quad . \qquad \text{E-3}$$

From this

$$v(t) = A \sin (\omega t + \varphi) \qquad \text{E-4}$$

where

$$\varphi = \tan^{-1} \left(\frac{L_e \omega}{\overline{V}} \right) \qquad \text{E-5}$$

$$A = \frac{a_o}{\rho \overline{V}} \cdot \frac{1}{\sqrt{1 + (L_e \omega / \overline{V})^2}} \qquad \text{E-6}$$

TABLE I

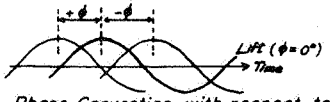

Phase Convention with respect to max and min of Lift

FULLY WETTED RUNS

Run No.		Freq (cps)	P_1/q	P_1 Phase Max	P_1 Phase Min	P_2/q	P_2 Phase Max	P_2 Phase Min	P_3/q	P_3 Phase Max	P_3 Phase Min	V_2/V	V_2 Phase Max	V_2 Phase Min	V_3/V	V_3 Phase Max	V_3 Phase Min	Lift L/L	Lift Phase	S^*	K_V
5017	(4°)	11.6	0			Not measured			0.035	0°	0°	Not measured			Not measured			0		0.099	
18	(5°)	11.3							.042											.096	
19	(7°)	13.8							.044											.114	
20	(8°)	14.9							.031											.121	
25	(10°)	11.2							.059											.091	
26	(12°)	9.3							.036											.076	
27	(14°)	10.8							.043											.087	
29	(6°)	10.9							.043											.100	
31	(4°)	10.6							.036											.092	
32	(2°)	11.2	0.020	180°	180°				.059											.099	
43	(0°)	10.3	0						.045											.100	

CAVITATING RUNS

$\alpha = 4°$																					
5300		14.4				0.056	−30°	−30°	0.049	−30°	−30°							0.346	0°	0.131	0.323
02		15.2				.066	−30	−30	.046	−30	−30							.262		.139	.328
28		16.3				.059	−30	−30	.047	−30	−30							.274		.146	.363
$\alpha = 6°$																					
5216		17.3	0	—	—	0.042	—	—	0.035	—	—							0	0°	0.151	0.485
23		11.6	0.052	−105°	−165°	.092	30°	15°	.077	30°	−30							0.830		.103	.372
28		11.6	.036	−105	−165	.027	30	15	.050	30°	−30							1.017		.104	.348
67		16.8	0	—		.041	0	30	.031	0	0							0		.153	.509
70		16.3	0	—		.087	−90	−90	.040	−90	−90							.307		.148	.396
71		12.5	.049	−135	−120	.061	0	15	.057	0	−30							.881		.115	.379
75		11.2	.051	−90	−120	.048	0	15	.042	0	−30							.949		.106	.350

TABLE I

CAVITATING RUNS

Run No.	Freq. (cps)	A/g	P_1 Phase Max	P_1 Phase Min	P_2/g	P_2 Phase Max	P_2 Phase Min	P_3/g	P_3 Phase Max	P_3 Phase Min	V_2/V	V_2 Phase Max	V_2 Phase Min	V_3/V	V_3 Phase Max	V_3 Phase Min	L/L	Lift Phase	S	K_V
$\alpha = 8°$																				
5386	13.3	0			0.046	—	—	0.034	—	—	Not measured			Not measured			0.133	0°	0.123	0.586
88	13.9				.051	135°	165°	.047	135°	135°							.077		.129	.587
90	13.7				.039	−90	−90	.039	−90	−90							.284		.126	.447
5400	13.2				.036	−90	−90	.035	−90	−90							.255		.121	.446
29	12.7				.035	−90	−90	.035	−90	−90							.252		.117	.496
35	11.5				.059	0	0	.059	0	−30							.724		.107	.385
37	10.8				.064	0	15	.065	20	−30							.750		.101	.401
$\alpha = 10°$																				
5471	14.5	0.019	−45°	−45°	0.034	90°	90°	0.027	90°	90°							0.073	0°	0.136	0.639
75	12.4	.026	−120	−90	.047	0	50	.042	0	30							.289		.116	.490
77	23.6	.019	—	—	.026	—	—	.026	—	—							.350		.220	.485
5515	14.6	0	—	—	.043	—	—	.035	—	—							.102		.137	.642
21	10.0	.028	−75	−165	.028	45	15	.086	45	−30							.546		.093	.470
27	10.8	.017	−90	−90	.057	0	30	.049	0	0							.622		.103	.446
$\alpha = 12°$																				
5598	8.9	0.029	−135°	−165°	0.069	0°	15°	0.065	0°	−30°							0.610	0°	0.081	0.443
5600	8.8	.022	−135	−135	.061	0	60	.060	0	0							.578		.081	.459
01	8.8	.022	−135	−135	.050	0	60	.046	0	0							.475		.080	.436
43	10.3	.018	—	—	.046	0	0	.044	0	0							.344		.099	.497
44	10.0	.026	−135	−135	.056	0	45	.054	0	0							.396		.096	.494
45	10.6	.018	−135	−135	.041	0	45	.039	0	0							.413		.101	.497

TABLE I

MAXIMUM OSCILLATION

Run No	Freq (cps)	P_L/q	P_L Phase Max	P_L Phase Min	P_2/q	P_2 Phase Max	P_2 Phase Min	P_3/q	P_3 Phase Max	P_3 Phase Min	V_2/V	V_2 Phase Max	V_2 Phase Min	V_3/V	V_3 Phase Max	V_3 Phase Min	L/L LIFT	Phase	Σ	K_V
$\alpha = 4°$																				
5809	16.2	0.012	No Period		0.039	−60°	−30°	0.036	−60°	−60°	0.011	−60°	−60°	0.012	−150°	−150°	0.262	0°	0.150	0.344
10	15.7	.017			.042	−60	−30	.033	−60	−60	.010	−60	−60	.020	−150	−150°	.202		.144	336
11	14.4	.014			.041	−60	−60	.034	−60	−60	.010	−60	−60	.018	−150		.294		.135	326
12	14.1	.012			.040	−40	−30	.037	−60	−30	.008	−60	−30	.017	−90	−60°	.256		.129	301
13	14.1	.023			.038	−60	0	.030	−60	−30	.008	−60	−30	.018	—	—	.382		.132	323
14	14.3	.021			.039	−60	0	.028	−60	−30	.008	−60	−30	.018	—	—	.296		.134	323
15	14.7	.019			.040	−60	−30	.040	−60	−30	.009	−60	−30	.018	—	—	.263		.137	326
16	15.8	.010			.055	−60	−30	.050	−60	−30	.008	−60	−30	.013	—	—	.284		.145	336
17	15.0	.038			.052	−40	−10	.041	−60	−30	.008	−60	−30	.022	—	—	.364		.140	356
18	15.0	.020			.042	−40	−10	.035	−60	−30	.008	−60	−30	.015	—	—	.217		.138	317
19	18.4	.010			.035	0	−30	.025	0	0	.004	—	—	.006	—	—	.051		.178	447
20	18.1	.010			.034	0	−30	.027	0	0	.003	0	0	.014	—	—	.064		.167	452
$\alpha = 6°$																				
5665	16.0	0.016	−90°	−90°	0.042	20°	20°	0.034	0°	0°	0.007	0°	0°	0.009	−60°	−60°	0.118	0°	0.144	0.458
66	16.8	.018	−90	−90°	.033	20	20	.032	0	0	.007	0	0	.013	−60	−60	.124		.154	.474
67	15.1	.021	−90	−90°	.040	20	20	.034	0	0	.008	0	0	.011	−60	−60	.223		.146	.396
68	14.2	.019	−90	−90°	.057	20	20	.050	0	0	.011	0	0	.019	−60	−60	.219		.128	.399
69	12.1	.028	−150	−150	.066	0	60	.061	0	0	.018	0	0	.038	0	0	.776		.110	.353
70	12.4	.026	−120	−120	.062	0	60	.062	0	0	.010	0	0	.033	0	0	.721		.112	.342
71	12.3	.018	−120	−120	.073	0	60	.044	0	0	.008	0	0	.031	0	0	.778		.111	.347
72	11.2	.032	−120	−120	.060	0	30	.058	0	0	.012	0	0	.030	—	—	1.003		.104	.354
73	11.0	.034	−120	−120	.078	10	45	.066	0	0	.014	0	0	.029	30	30	1.099		.102	.364
74	11.2	.029	−150	−150	.068	0	45	.072	0	−20	.012	0	0	.026	0	0	1.010		.104	.354
75	12.3	.025	−120	−120	.062	0	30	.059	0	0	.008	0	0	.023	0	0	.665		.112	.366
76	12.3	.023	−120	−120	.086	0	60	.066	0	0	.010	0	0	.036	0	0	.822		.112	.369
77	12.5	.025	−120	−120	.066	0	60	.064	0	0	.018	0	0	.033	0	0	.630		.114	.362
78	11.9	.023	−120	−120	.069	0	30	.061	0	0	.026	0	0	.065	0	0	.668		.108	.362
79	13.3	.021	−120	−120	.056	0	30	.048	0	0	.013	0	0	.021	−45	−45	.310		.120	.376
80	14.4	.027	—	—	.038	0	0	.032	0	0	.007	—	—	.012	−30	−30	.221		.129	.329
81	15.3	.016	−120	−120	.066	0	20	.048	0	0	.014	0	0	.023	−60	−60	.228		.140	.378
82	14.6	.024	−120	−120	.055	0	20	.060	0	0	.012	0	0	.020	−60	−60	.251		.134	.378
83	17.0	.019	−120	−120	.037	0	20	.034	0	0	.008	0	0	.008	−60	−60	.177		.163	.475
84	17.0	.018	—	—	.041	0	20	.039	0	0	.007	0	0	.008	—	—	.067		.155	.494
85	17.1	.008	—	—	.034	0	20	.031	0	0	.007	0	0	.010	—	—	.084		.166	.485

TABLE I

MAXIMUM OSCILLATION

Run No.	Freq (cps)	R_1/g	R_1 Phase Max	R_1 Phase Min	R_2/g	R_2 Phase Max	R_2 Phase Min	R_3/g	R_3 Phase Max	R_3 Phase Min	V_2/V	V_2 Phase Max	V_2 Phase Min	V_3/V	V_3 Phase Max	V_3 Phase Min	Lift L/T	Lift Phase	S	K_v
$\alpha = 8°$																				
5698	—	0.008	—	—	0.020	—	—	0.025	—	—	0.004	—	—	0.009	—	—	0.129	0°	—	0.480
5699	15.9	.018	—	—	.018	—	—	.020	—	—	.005	—	—	.008	—	—	.102	↓	0.145	.479
5700	16.0	.008	—	—	.025	—	—	.021	—	—	.004	—	—	.009	—	—	.165		.146	.479
01	11.6	.023	−105°	−165°	.054	30°	30°	.051	30°	−30°	.008	30°	−10°	.032	60°	0°	.446		.106	.407
02	11.5	.020	−105	−165	.061	30	30	.064	30	−30	.008	30	−10	.038	60	0	.547		.106	.397
03	12.6	.018	−105	−165	.083	30	30	.072	30	−30	.011	30	−10	.030	60	0	.559		.115	.402
04	11.7	.026	−105	−165	.110	30	30	.075	30	−30	.009	30	−10	.033	30	−30	.480		.107	.402
05	9.4	.049	−135	−135	.084	0	0	.089	0	−45	.011	0	−45	.032	90	45	.836		.090	.416
06	9.7	.029	−135	−135	.085	0	0	.092	0	−45	.011	0	−45	.048	90	45	.796		.094	.428
07	9.4	.027	−135	−135	.086	0	0	.088	0	−45	.023	0	−45	.046	90	45	.781		.086	.422
5718	10.2	.036	−135	−135	.064	0	0	.069	0	−45	.009	0	−45	.041	135	45	.766		.094	.435
19	10.2	.037	−135	−135	.074	0	0	.080	0	−45	.010	0	−45	.040	90	45	.649		.094	.425
20	10.2	.040	−135	−135	.069	0	0	.076	0	−45	.007	0	−45	.039	135	45	.746		.091	.430
21	2.5	.029	−20	−20	.034	30	30	.044	0	0	.007	0	0	.019	—	—	.492		.069	.397
22	7.7	.029	−45	−30	.042	0	60	.058	0	−30	.010	±45	−60	.042	135	60	.555		.071	.396
23	9.7	.034	−90	−135	.054	0	−25	.066	0	−45	.007	0	−45	—	—	—	.668		.088	.397
24	10.2	.028	−90	−135	.060	0	−25	.049	0	−45	.010	0	−45	.023	180	90	.628		.093	.376
25	9.8	.031	−90	−135	.049	0	15	.058	0	−45	.011	0	−45	.030	180	90	.691		.080	.384
26	8.6	.021	−90	−135	.061	0	15	.074	0	−45	.009	0	−45	.020	180	90	.601		.078	.380
27	11.4	.036	−135	−180	.060	0	45	.062	0	−45	.009	0	−45	.022	135	90	.525		.103	.414
28	11.3	.031	−90	−120	.069	20	15	.063	0	−30	.007	0	−30	.030	90	60	.436		.103	.429
29	11.1	.033	−90	−150	.052	20	15	.061	0	−30	.006	0	−30	.021	90	60	.521		.101	.421
30	11.8	.032	−90	−135	.056	0	0	.068	0	−45	.007	0	−45	.023	45	45	.463		.106	.441
31	11.8	.029	−90	−135	.064	0	0	.064	0	−45	.007	0	−45	.023	45	45	.500		.106	.421
32	14.8	.019	—	—	.025	—	—	.030	—	—	.004	—	—	.017	—	—	.181		.128	.439
33	—	.016	—	—	.031	—	—	.025	—	—	.004	—	—	.011	—	—	.112		—	.441

TABLE I

MAXIMUM OSCILLATION

Run No.	Freq (cps)	R/ℓ	R Phase Max	R Phase Min	B_2/ℓ	B_2 Phase Max	B_2 Phase Min	B_3/ℓ	B_3 Phase Max	B_3 Phase Min	$V_2/\bar{V}$	V_2 Phase Max	V_2 Phase Min	$V_3/\bar{V}$	V_3 Phase Max	V_3 Phase Min	L/ℓ	Lift Phase	S	K_V
$\alpha = 10°$																				
5754	11.2	0.026	−90°	−90°	0.046	0°	0°	0.049	0°	0°	0.008	0°	0°	0.036	30°	30°	0.325	0°	0.108	0.490
63	9.7	.042	−120	−135	.062	30	15	.067	0	−45	.007	0	−45	.026	90	46	.571	↓	.093	.446
64	10.8	.035	−135	−135	.044	30	15	.059	0	−45	.006	0	−45	.029	90	45	.655	↓	.099	.450
69	12.4	.016	−135	−90	.042	30	20	.048	0	0	.005	0	0	.033	90	90	.344	↓	.116	.469
$\alpha = 12°$																				
5785	10.4	0.013	−90°	−90°	0.056	0°	0°	0.046	0°	0°	0.008	0°	0°	0.052	90°	90°	0.183	0°	0.097	0.529
89	9.1	.021	−150	−150	.103	0	0	.084	0	−30	.008	0	−30	.051	90	60	.486	↓	.085	.528
91	9.2	.024	−150	−150	.077	20	0	.070	0	−30	.010	0	−30	.037	90	60	.407	↓	.086	.515
96	10.2	.012	−180	−180	.061	0	0	.039	0	0	.006	0	0	.038	90	90	.288	↓	.094	.528
VELOCITY RUNS																				
$\alpha = 6°$																			V	
5838	11.0	0.021	−90°	−120°	0.091	45°	30°	0.072	45°	−30°	0.012	45°	0°	0.024	−15°	−60°	0.586	0°	24.3	0.121	0.369
39	10.4	.019	−105	−120	.075	30	30	.073	30	−30	.011	30	0	.025	30	−30	.634	↓	24.5	.113	.359
40	10.5	.021	−105	−120	.087	30	30	.075	30	−30	.011	30	0	.029	0	−60	.605	↓	24.6	.114	.346
5845	12.6	.030	−105	−120	.071	30	30	.066	30	−30	.007	30	−30	.026	0	−30	.473	↓	29.3	.115	.369
46	13.8	.027	−105	−120	.048	30	30	.048	30	−30	.007	30	−30	.020	0	−30	.419	↓	29.7	.124	.350
47	13.0	.031	−105	−120	.046	30	30	.044	30	−30	.006	30	−30	.025	30	−0	.424	↓	29.4	.123	.368
5850	14.4	.033	−90	−60	.059	0	45	.062	0	0	.006	45	0	.016	0	0	.302	↓	32.5	.118	.484
51	15.3	.026	−90	−60	.040	30	45	.034	0	0	.005	0	0	.013	0	0	.204	↓	32.7	.125	.469
52	15.8	.036	−90	−60	.057	30	45	.047	0	0	.004	0	0	.019	0	0	.255	↓	32.5	.130	.486
5855	12.1	.053	−75	−90	.057	60	45	.042	60	0	.009	90	60	.017	60	0	.535	↓	38.3	.119	.473
56	12.0	.045	−105	−135	.061	30	0	.056	30	−45	.009	—	—	.019	0	−45	.458	↓	38.3	.118	.473
57	16.4	.048	−90	−135	.039	45	0	.042	45	−45	.007	135	45	.018	45	−45	.486	↓	38.3	.114	.473
HIGH SPEED MOVIES																				
5857 (4°)	12.3	0.027	−135°	−90°	0.068	0°	45°	0.056	0°	0°	0	—	—	0	—	—	No Trace —			
5865 (6°)	12.8	.019	−135	−90	.091	0	45	.065	↓	↓	0.006	0°	0°	0.032	−45°	0°	Phase Reference is P_3			
5866 (4°)	14.3	.024	—	—	.057	0	20	.045	↓	↓	.008	0	0	.019	−60	−45				
5874 (8°)	11.2	.047	−120	−120	.067	0	60	.060	↓	↓	.006	−20	0	.047	120	−45				

TABLE II

CONVERSION FACTORS FOR OSCILLOGRAPH TRACES

Run No.	P_1 psi/in	P_2 psi/in	P_3 psi/in	V_2 ft/sec/in	V_3 ft/sec/in	L lbs/in	q psi	V ft/sec	L lbs
$\alpha = 4°$									
5819	1.84	1.05	1.00	0.56	2.24	11.58	5.97	29.1	10.14
5812	1.84	1.05	1.00	0.76	2.41	11.58	6.02	29.2	11.77
5303	1.87	1.04	1.01	—	—	12.72	5.93	29.0	7.33
5306	1.87	1.04	1.01	—	—	12.72	5.92	29.0	−3.52
$\alpha = 6°$									
5219	1.87	0.94	0.97	—	—	11.09	6.74	30.8	23.36
5674	1.97	0.97	0.98	0.80	2.34	12.98	5.90	28.8	12.14
5670	1.97	0.97	0.98	0.80	2.28	12.98	6.22	29.5	14.26
5277	1.87	0.94	0.97	—	—	11.09	5.86	28.8	−7.32
$\alpha = 8°$									
5387	1.89	0.99	1.01	—	—	11.83	6.00	29.2	27.52
5730	1.91	0.99	1.00	0.82	2.27	11.15	6.24	29.7	21.92
5701	1.91	0.99	1.00	0.83	2.57	11.15	6.06	29.2	21.49
5403	1.89	0.99	1.01	—	—	11.83	5.53	27.8	3.14
$\alpha = 10°$									
5471	1.86	1.02	1.00	—	—	11.42	5.74	28.6	34.32
5763	1.85	0.94	1.05	0.74	2.33	10.63	5.50	27.9	22.80
5761	1.85	0.94	1.05	0.74	2.33	10.63	5.30	27.7	18.51
5532	1.86	1.02	1.00	—	—	11.42	5.49	27.7	−3.66
$\alpha = 12°$									
5578	1.86	0.98	0.97	—	—	11.67	5.74	28.6	41.12
5786	1.86	1.09	1.02	0.82	2.37	10.89	5.70	28.4	31.70
5790	1.86	1.09	1.02	0.82	2.37	10.89	5.79	28.6	29.73
5603	1.86	0.98	0.97	—	—	11.67	6.31	29.9	4.97

TABLE III

CONTINUITY CHECK

RUN NO	CALC VOL CHANGE FROM VELOCITY ft^3/sec.	MEASURED VOL CHANGE ft^3/sec
5865 $\alpha_1 = 6°$	0.66	1.01
5866 $\alpha_1 = 4°$	0.375	0.535
5874 $\alpha_1 = 8°$	1.41	1.26

Fig. 1

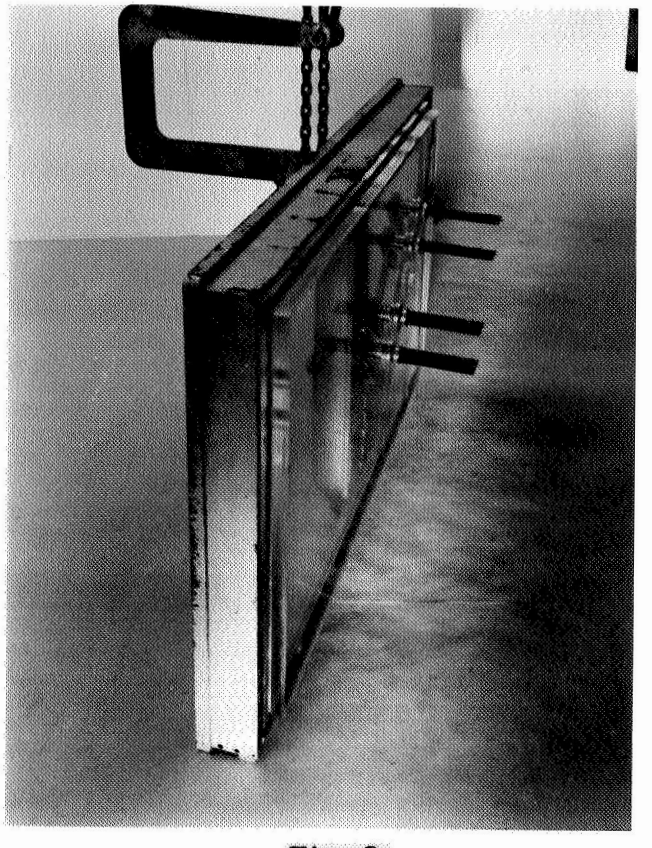

Fig. 2

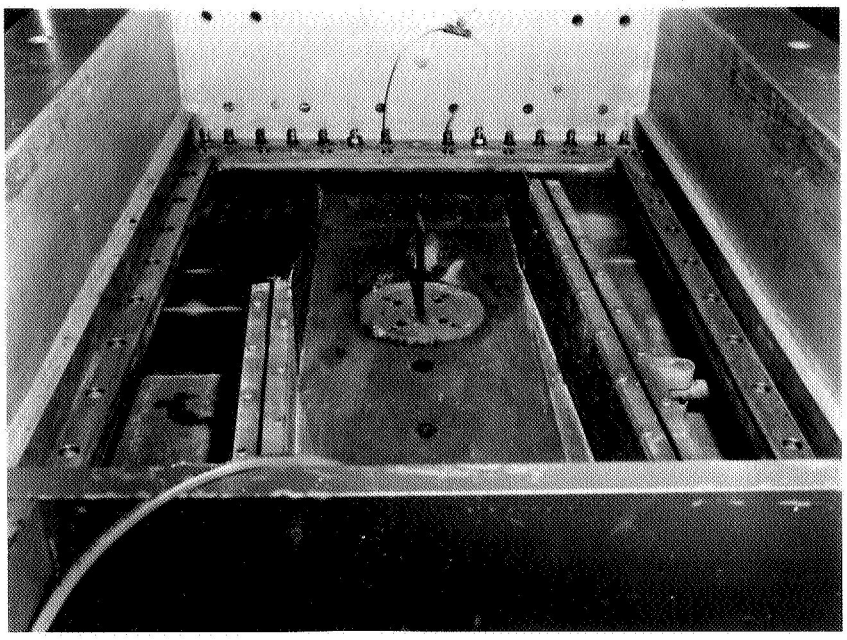

Fig. 3

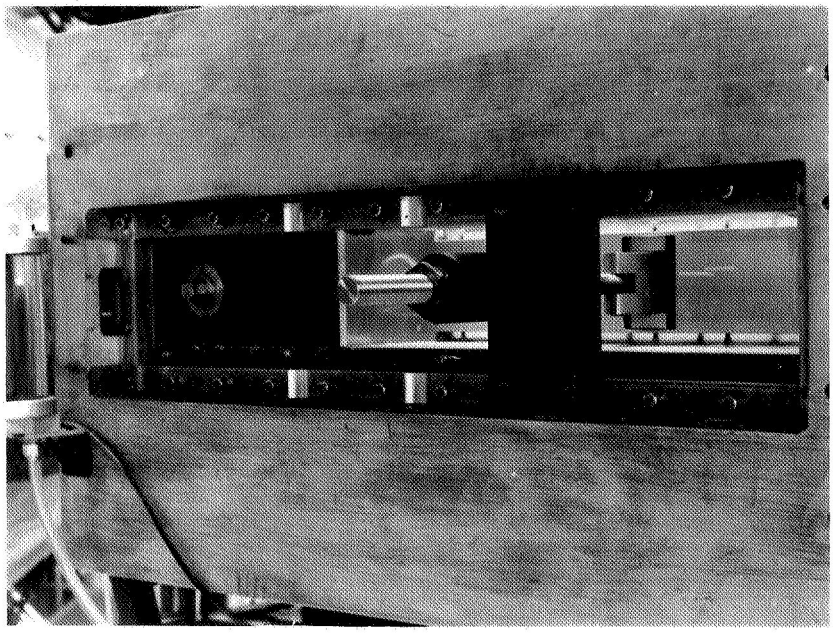

Fig. 4

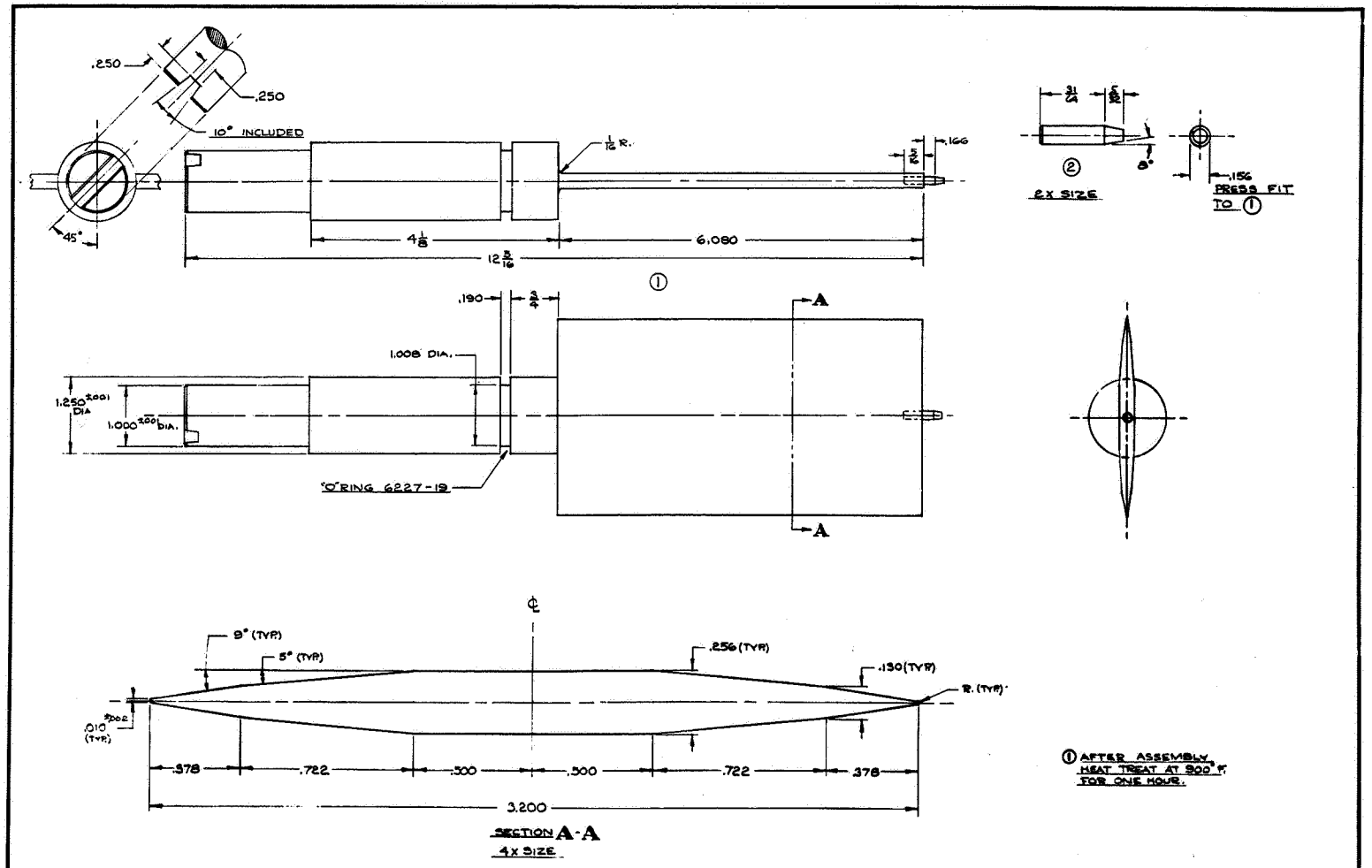

FIG 5

			2	4	17-4 PH S.S.
			1	4	17-4 PH S.S.

CALIFORNIA INSTITUTE OF TECHNOLOGY

CASCADED HYDROFOIL

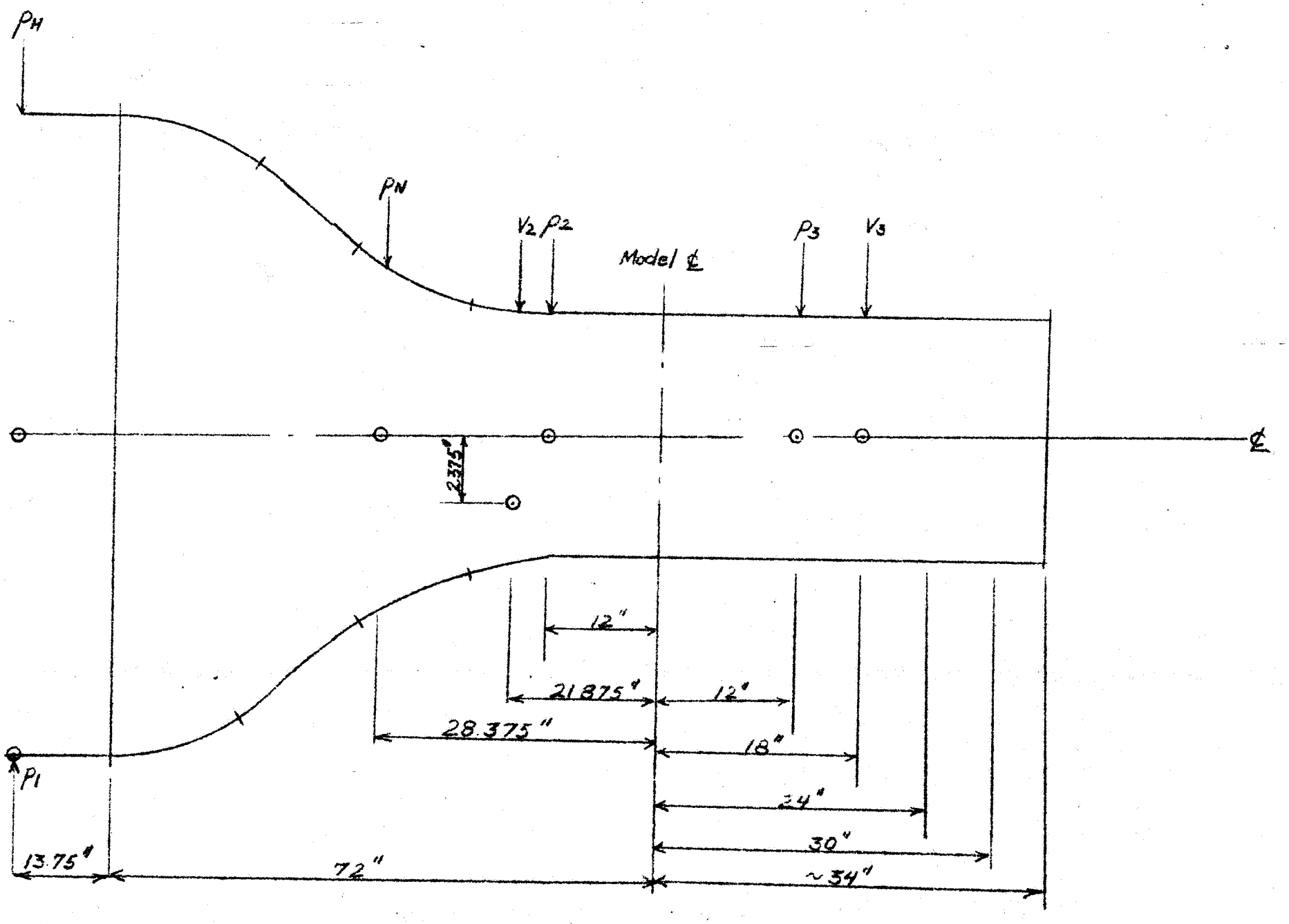
p_H
p_N
V_2 p_2
Model ℄
p_3
V_3
℄
2.375"
12"
21.875"
12"
28.375"
18"
24"
30"
~34"
p_1
13.75"
72"

FIG. 6

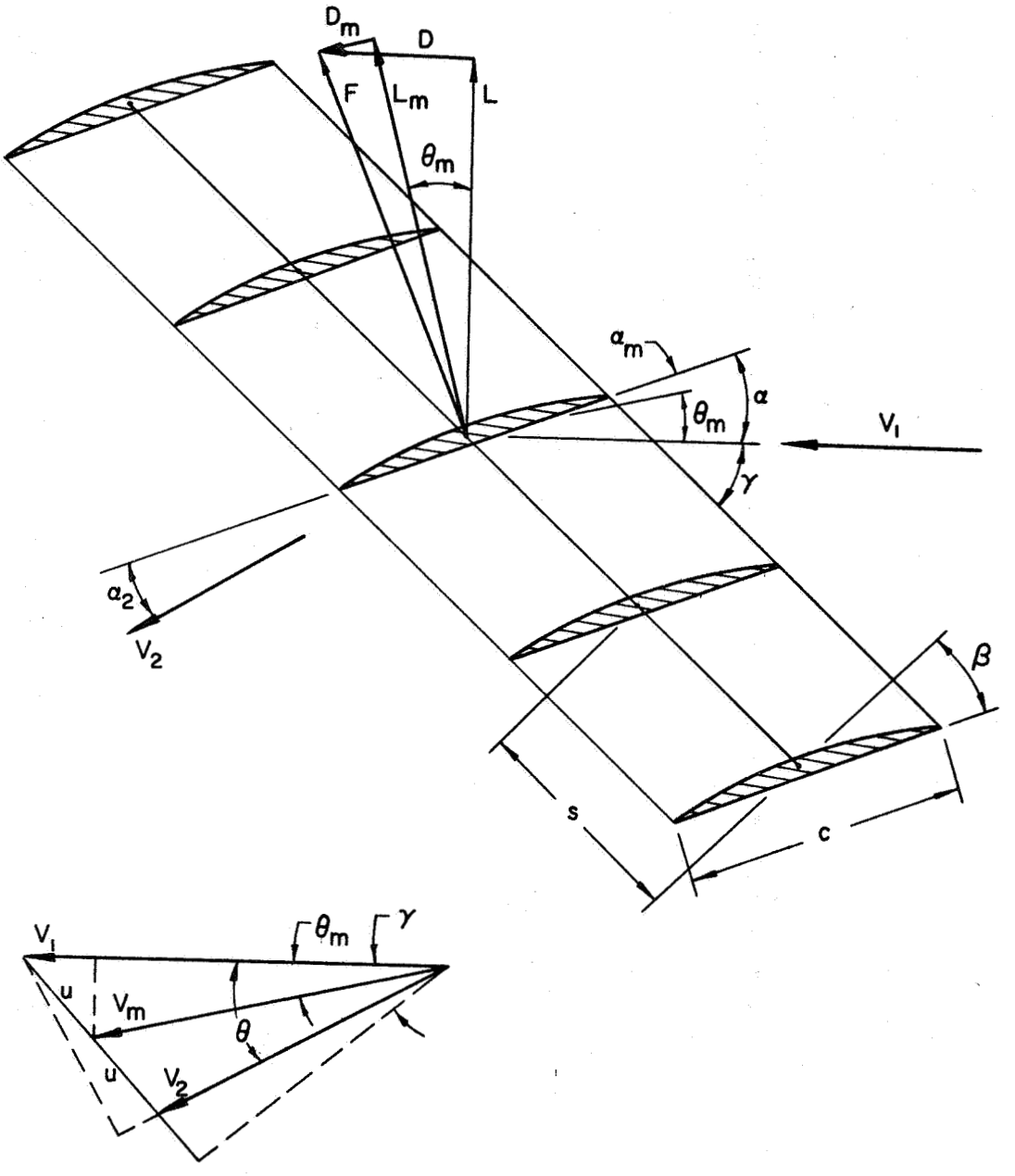
D_m
D
F
L_m
L
θ_m
α_m
α
θ_m
V_1
γ
α_2
V_2
β
s
c
V_1
θ_m
γ
u
V_m
θ
u
V_2

FIG. 7

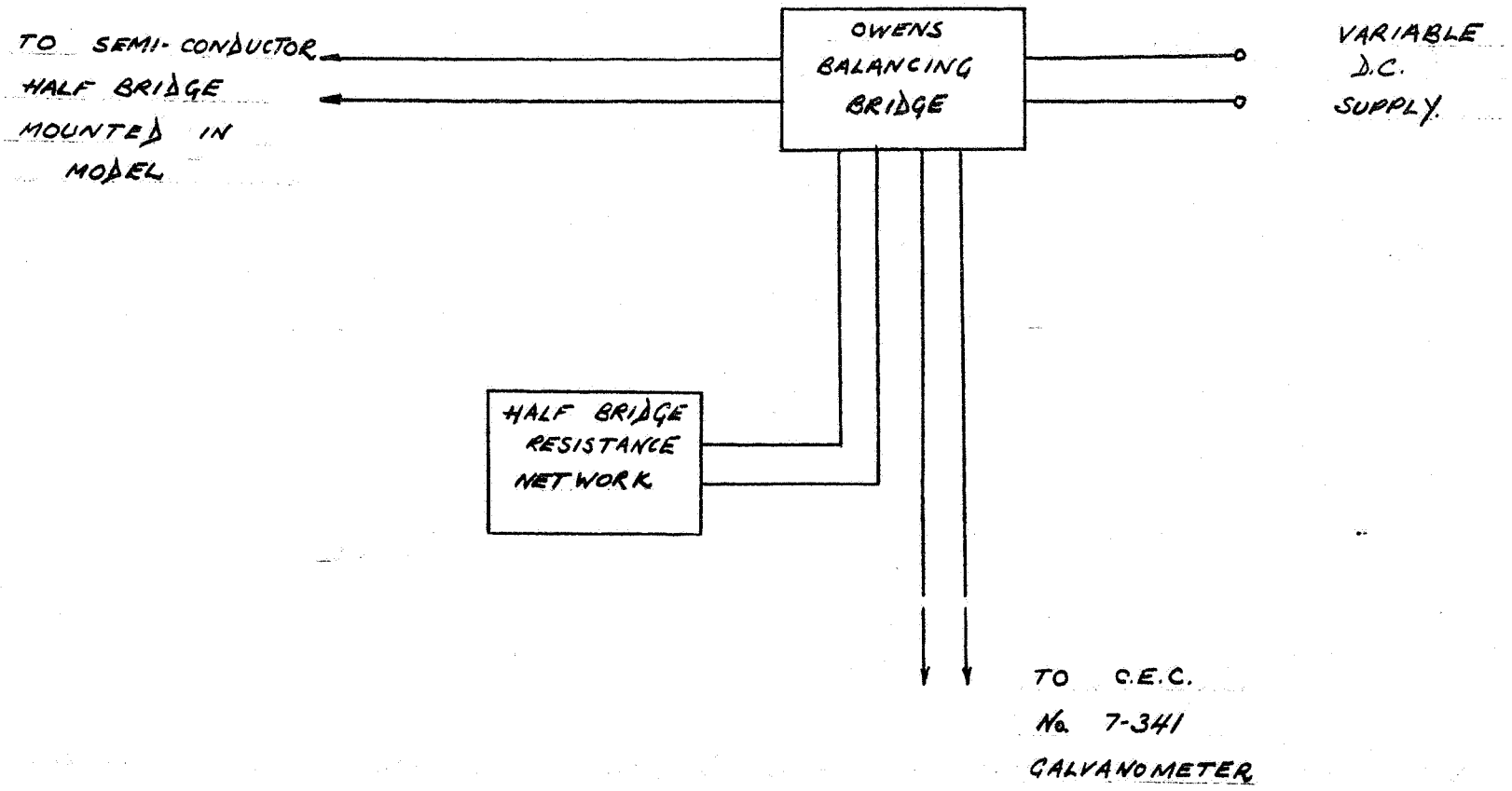
TO SEMI-CONDUCTOR HALF BRIDGE MOUNTED IN MODEL
OWENS BALANCING BRIDGE
VARIABLE D.C. SUPPLY
HALF BRIDGE RESISTANCE NETWORK
TO C.E.C. No. 7-341 GALVANOMETER

FIG. 8a

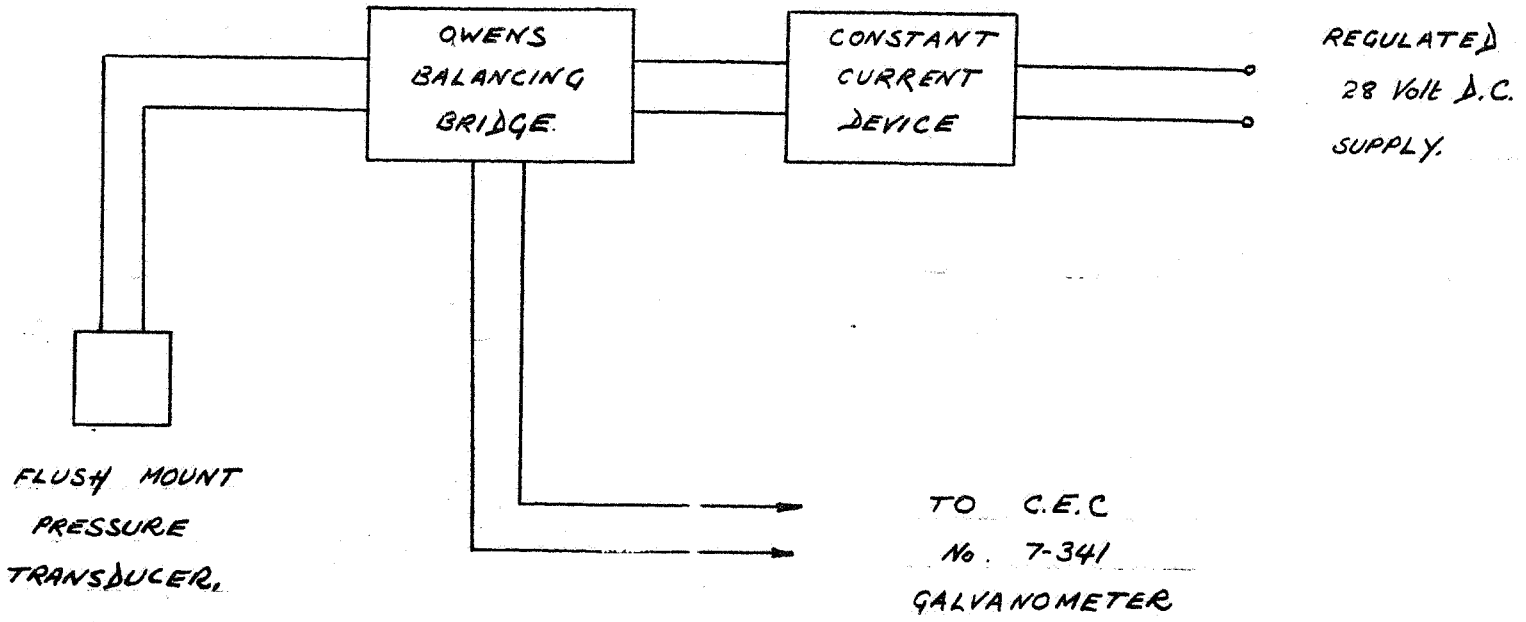
QWENS
BALANCING
BRIDGE
CONSTANT
CURRENT
DEVICE
REGULATED
28 Volt D.C.
SUPPLY.
FLUSH MOUNT
PRESSURE
TRANSDUCER.
TO C.E.C
No. 7-341
GALVANOMETER

FIG. 8b

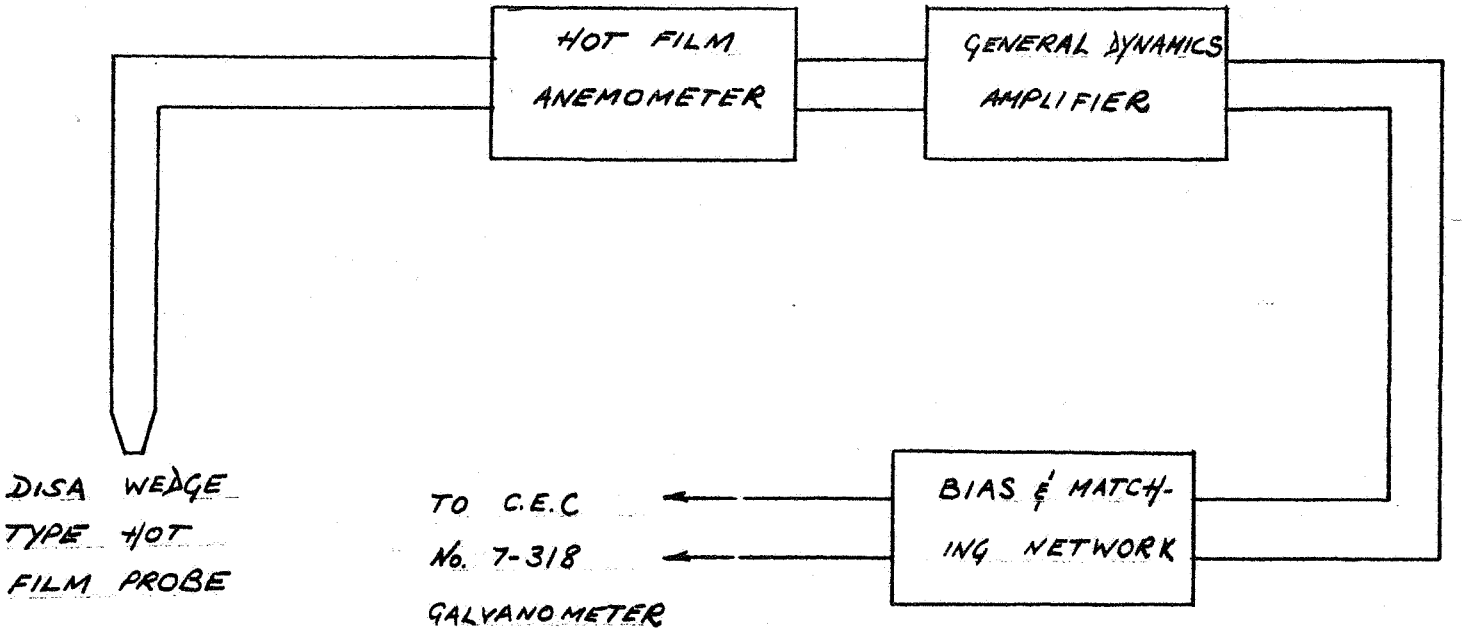
HOT FILM
ANEMOMETER
GENERAL DYNAMICS
AMPLIFIER
DISA WEDGE
TYPE HOT
FILM PROBE
TO C.E.C
No. 7-318
GALVANOMETER
BIAS & MATCH-
ING NETWORK

FIG. 8c

LARGE SCALE COPIES OF

FIGURES 9, 10, 11, 12, 13

ARE AVAILABLE UPON REQUEST

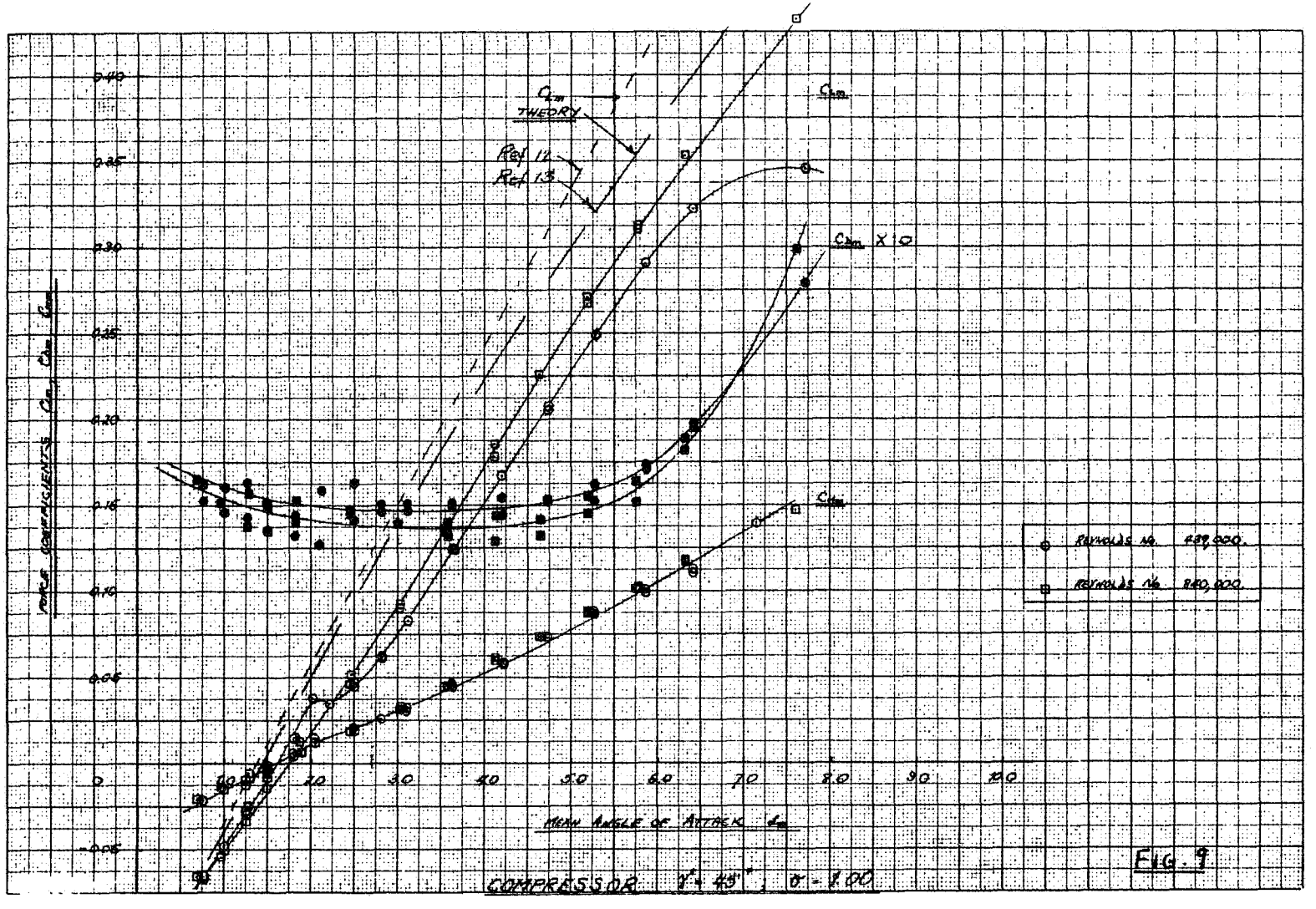
C_{Lm} THEORY
Ref 12
Ref 13
C_{Lm}
$C_{Dm} \times 10$
C_{Mm}
REYNOLDS NO. 439,000.
REYNOLDS NO. 880,000.
MEAN ANGLE OF ATTACK α_m
COMPRESSOR $\gamma = 49°$; $\sigma = 1.00$

FIG. 9

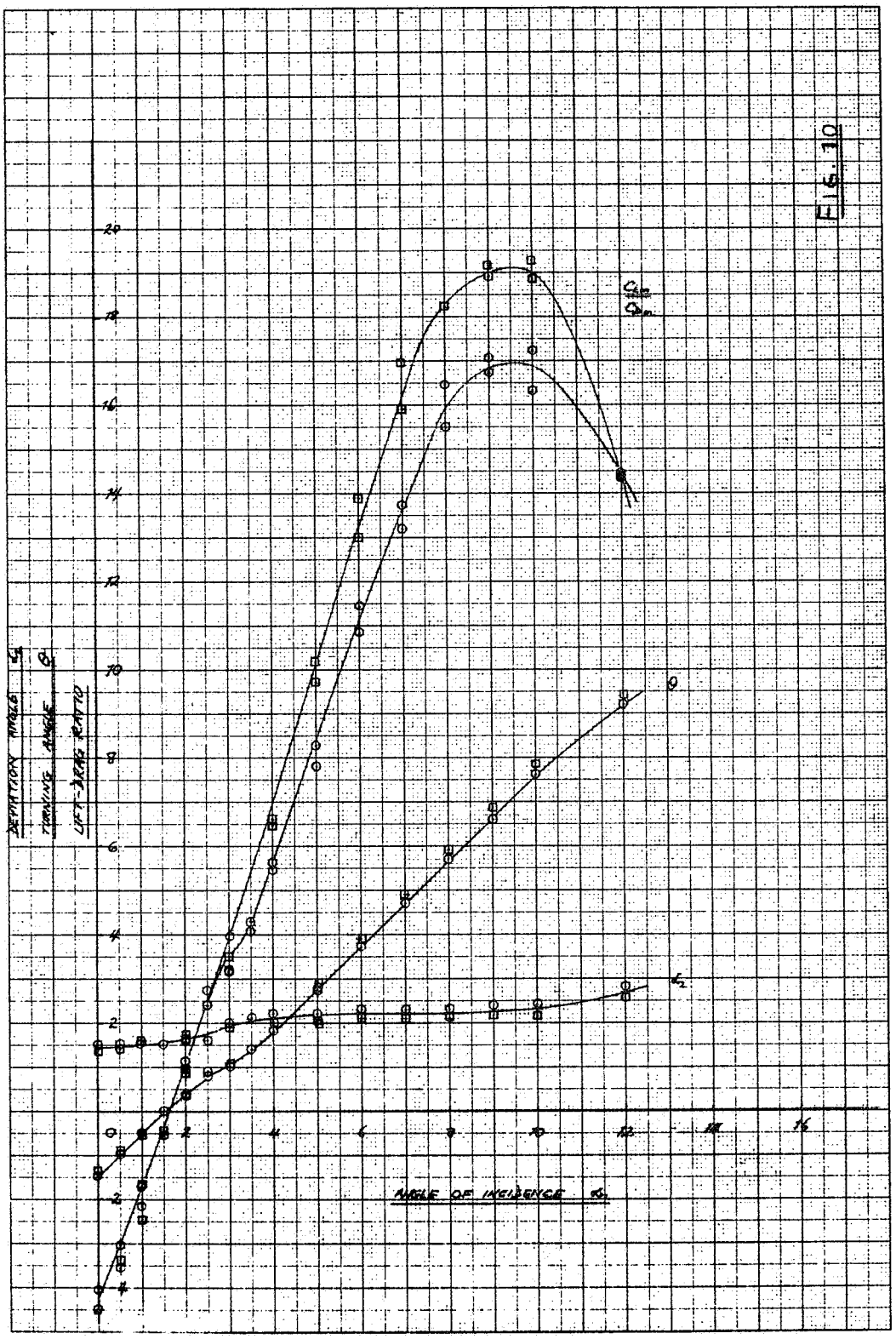
FIG. 10
DEFLECTION ANGLE ϵ_t
TURNING ANGLE θ
LIFT-DRAG RATIO
$\frac{C_{Lm}}{C_{Dm}}$
θ
ϵ_t
ANGLE OF INCIDENCE α_t
20
18
16
14
12
10
8
6
4
2
0
-2
-4
2
4
6
8
10
12
14
16

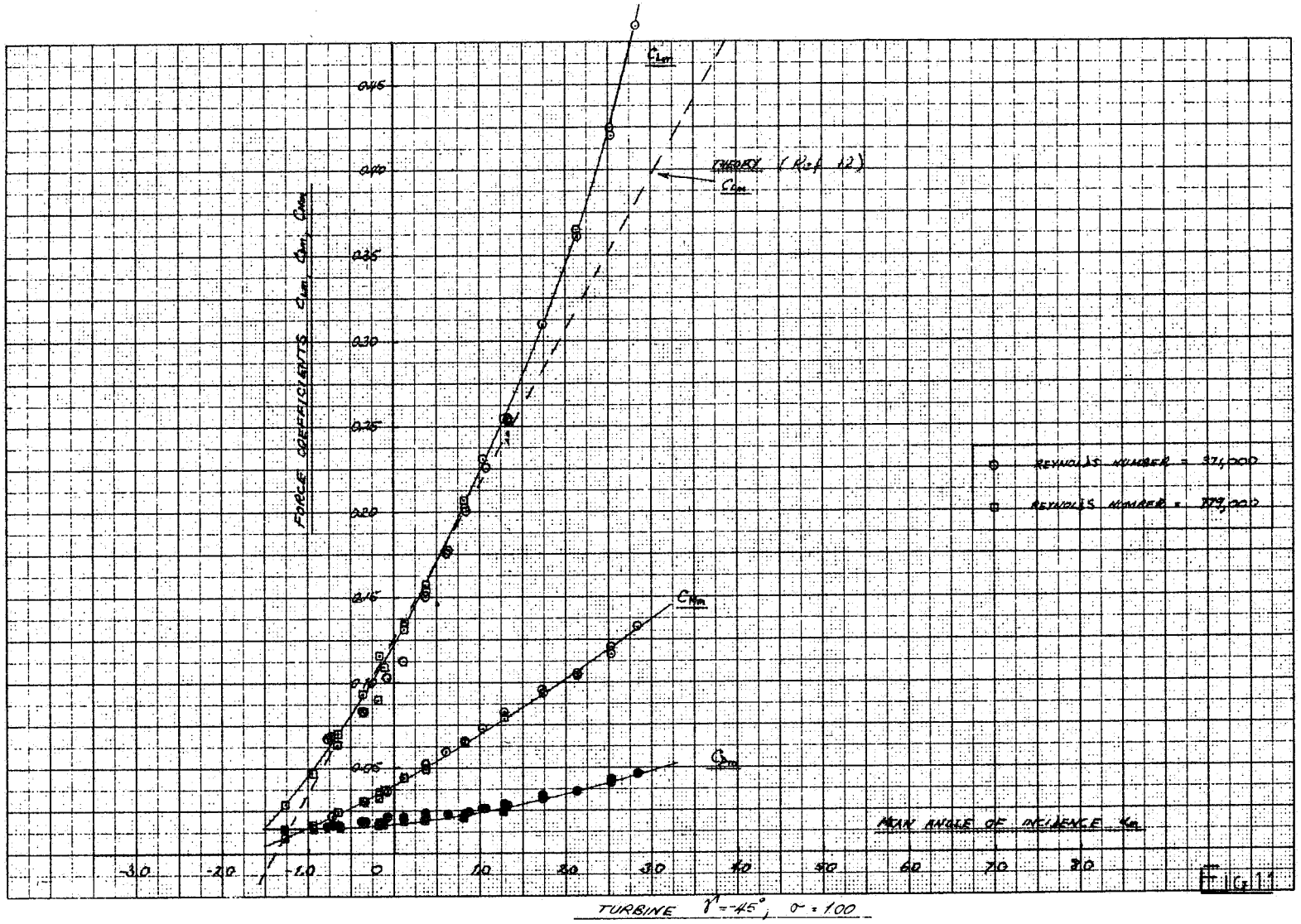
FORCE COEFFICIENTS C_{Lm}, C_{Dm}, C_{Nm}
C_{Lm}
THEORY ($R_e = \infty$)
C_{Dm}
C_{Nm}
C_{Dm}
REYNOLDS NUMBER = 371,000
REYNOLDS NUMBER = 379,000
MEAN ANGLE OF INCIDENCE α_m
0.45
0.40
0.35
0.30
0.25
0.20
0.15
0.10
0.05
-30
-20
-10
0
10
20
30
40
50
60
70
80
TURBINE $\gamma = -45°$, $\sigma = 1.00$
C.11

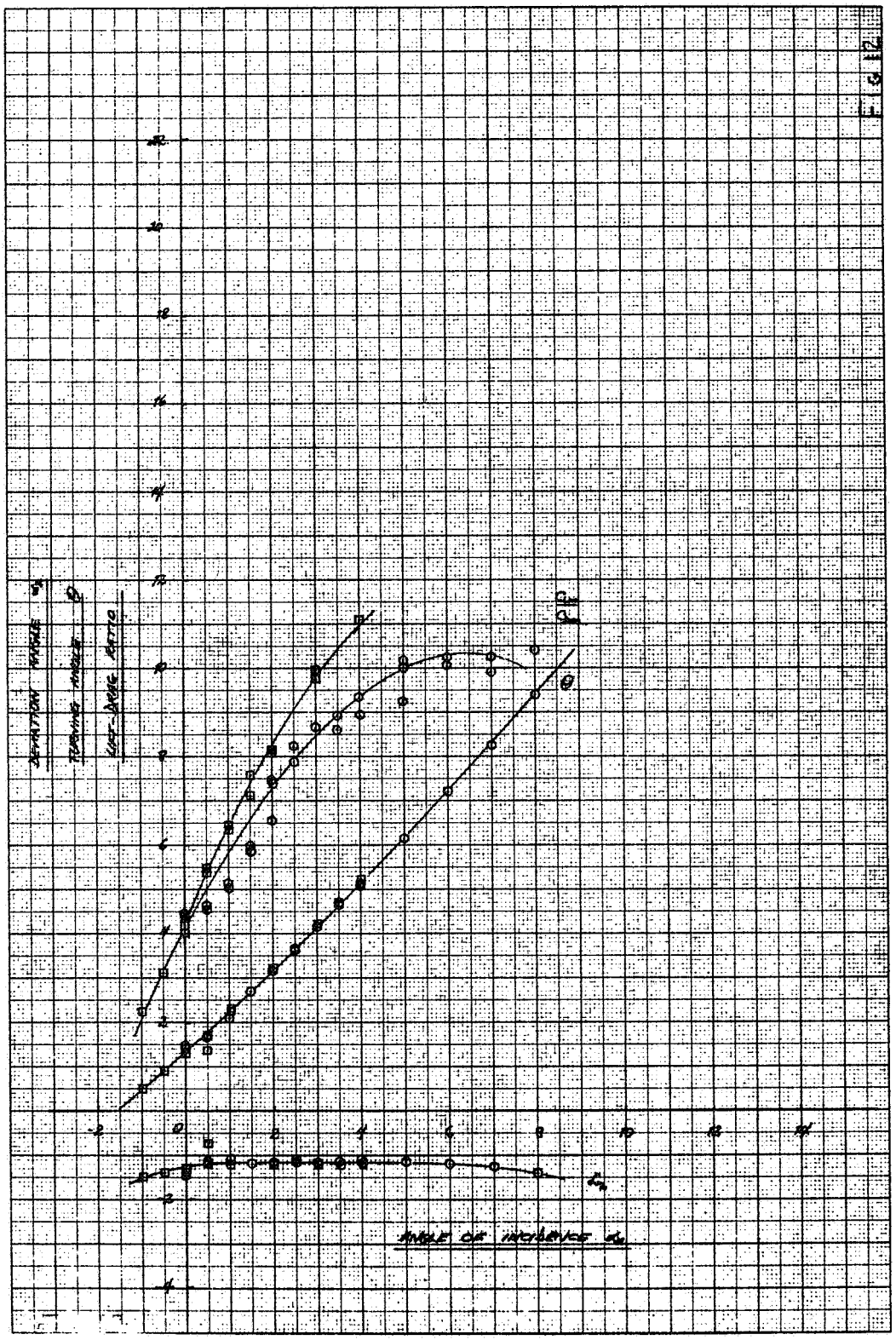
DEFLECTION ANGLE δ_e
TRAINING ANGLE θ
LIFT-DRAG RATIO
C_D
C_L
θ
ANGLE OF INCIDENCE α_w

FIG 12

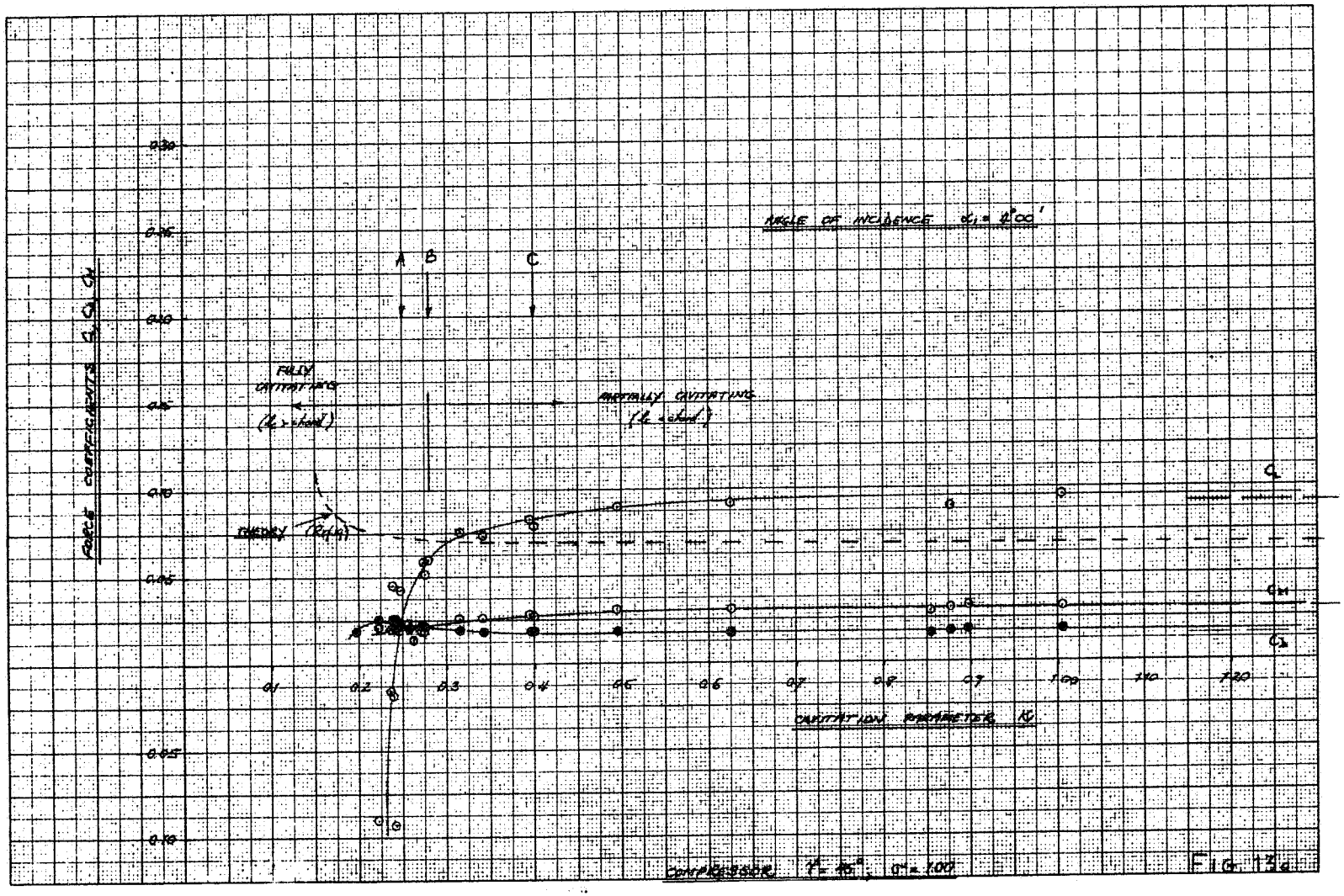
ANGLE OF INCIDENCE $\alpha_i = 12°00'$
B
C
FULLY CAVITATING ($\ell_c > \ell_{cav}$)
PARTIALLY CAVITATING ($\ell_c < \ell_{cav}$)
FORCE COEFFICIENTS C_L, C_D, C_M
C_L
C_M
C_D
0.30
0.15
0.10
0.05
0.025
0.10
0.1
0.2
0.3
0.4
0.5
0.6
0.7
0.8
0.9
1.00
1.10
1.20
CAVITATION PARAMETER σ_c
COMPRESSOR $\gamma = 45°$, $\sigma_T = 1.00$

FIG. 12a

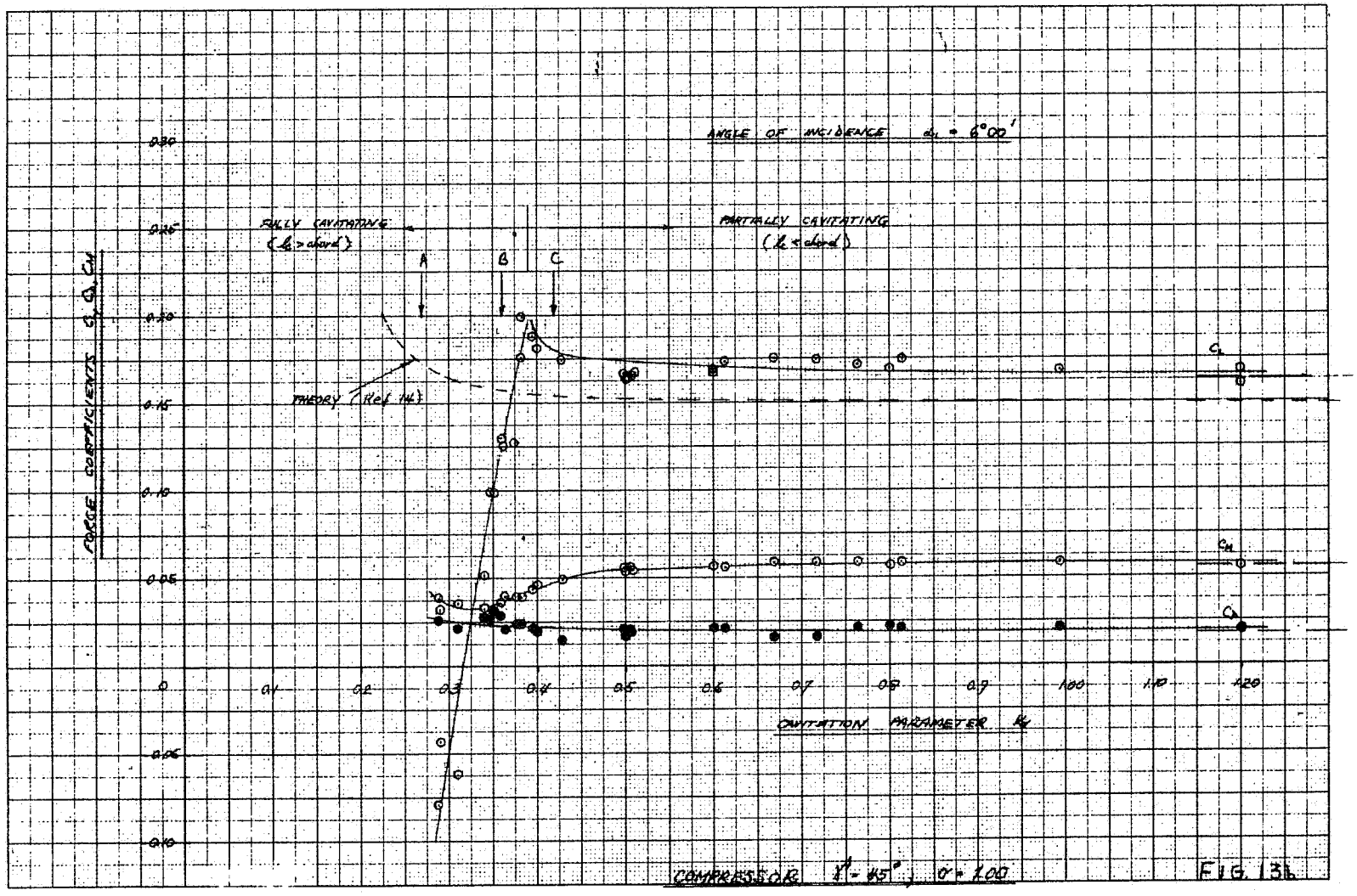
ANGLE OF INCIDENCE $\alpha_1 = 6°00'$
FULLY CAVITATING (ℓ_k > chord)
PARTIALLY CAVITATING (ℓ_k < chord)
A
B
C
THEORY (Ref 14)
FORCE COEFFICIENTS C_H, C_D, C_M
C_M
C_H
C_D
0.20
0.15
0.10
0.05
0
0.1
0.2
0.3
0.4
0.5
0.6
0.7
0.8
0.9
1.00
1.10
1.20
CAVITATION PARAMETER K_ℓ
COMPRESSOR $\gamma = 45°$, $\sigma = 1.00$

FIG. 13b

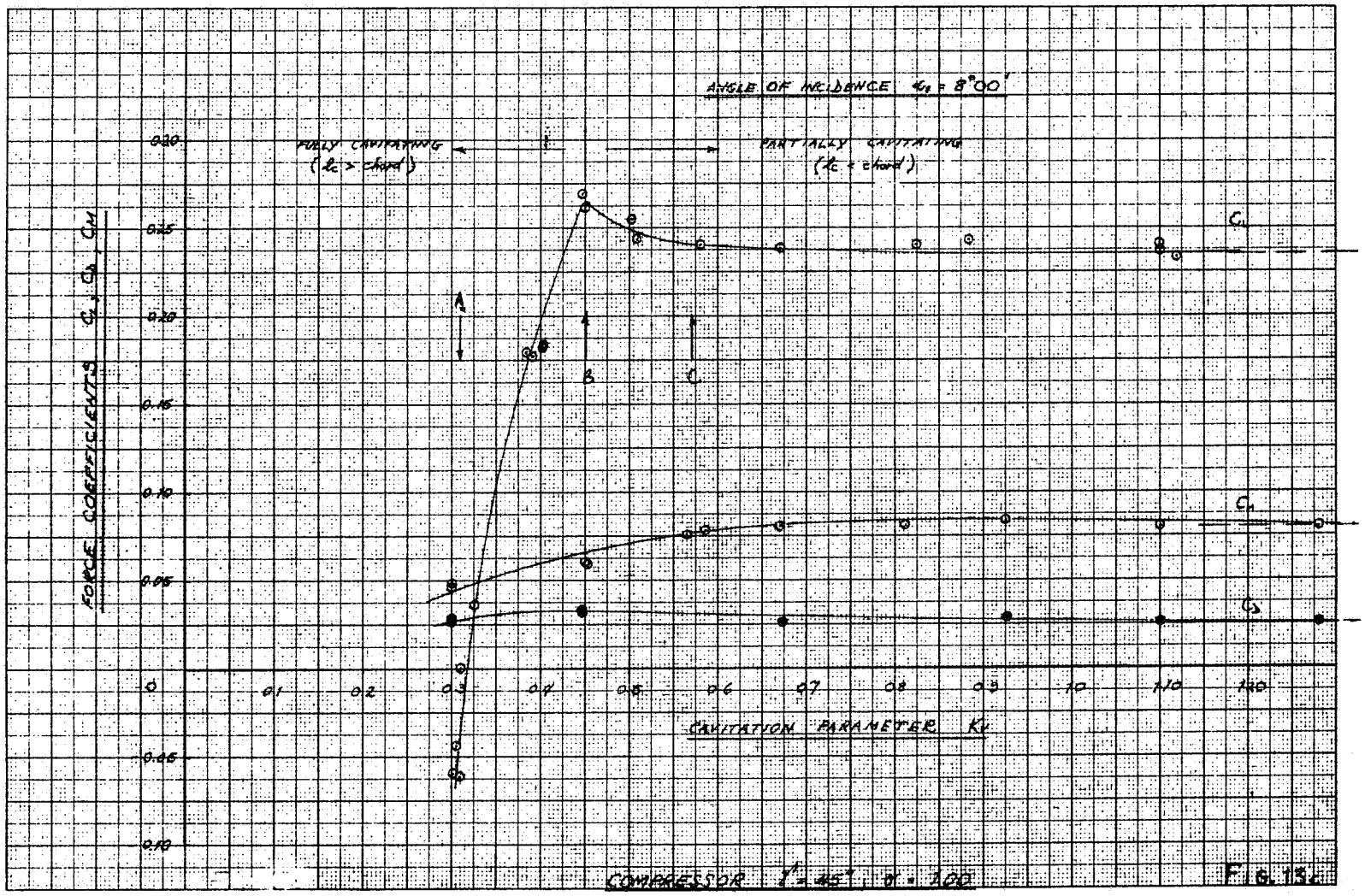
ANGLE OF INCIDENCE $\alpha_1 = 8°00'$
FULLY CAVITATING ($l_c >$ chord)
PARTIALLY CAVITATING ($l_c <$ chord)
FORCE COEFFICIENTS C_L, C_D, C_M
0.30
0.25
0.20
0.15
0.10
0.05
0
0.05
0.10
0.1
0.2
0.3
0.4
0.5
0.6
0.7
0.8
0.9
1.0
1.10
1.20
C_L
C_M
C_D
A
B
C
CAVITATION PARAMETER K_V
COMPRESSOR $\gamma' = 45°$, $\sigma = 1.00$

FIG. 15c

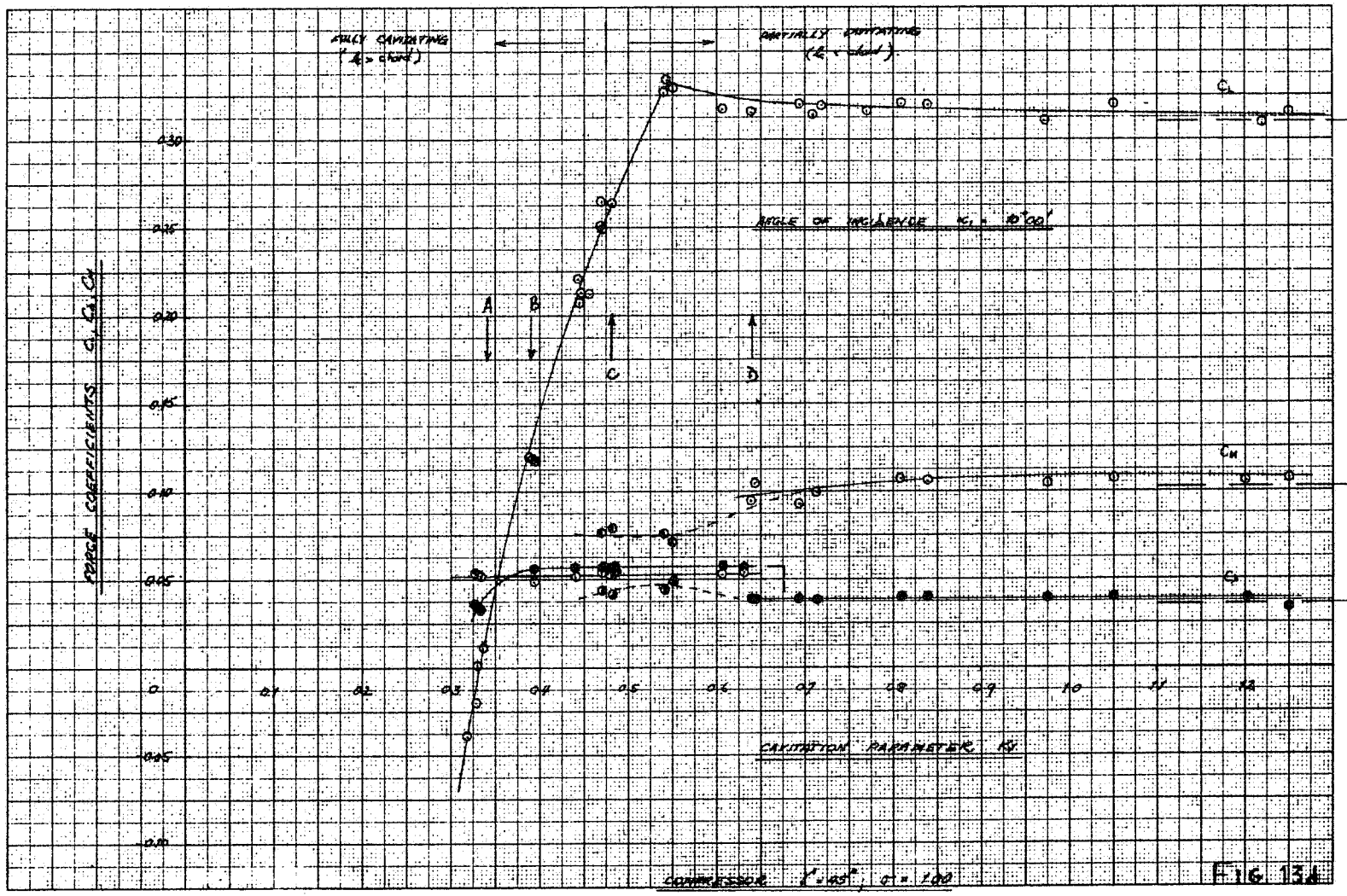
FULLY CAVITATING
PARTIALLY CAVITATING
FORCE COEFFICIENTS
ANGLE OF INCIDENCE
CAVITATION PARAMETER
A
B
C
D
0.30
0.25
0.20
0.15
0.10
0.05
0
-0.05
0.1
0.2
0.3
0.4
0.5
0.6
0.7
0.8
0.9
1.0
1.1
1.2

Fig. 13d

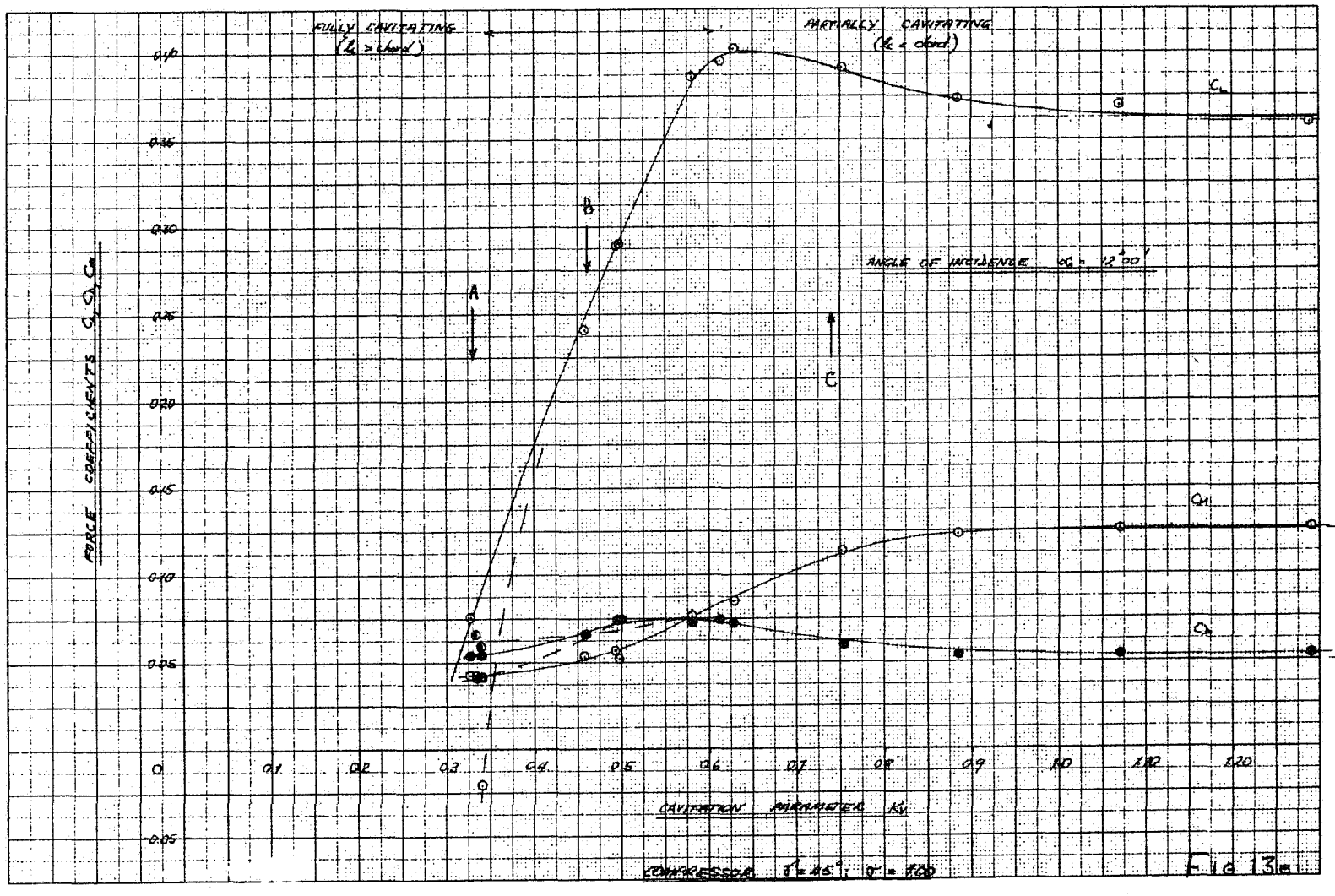
FULLY CAVITATING
(ℓc > chord)
PARTIALLY CAVITATING
(ℓc < chord)
FORCE COEFFICIENTS CL, CD, CM
ANGLE OF INCIDENCE α = 12°00'
A
B
C
CL
CD
CM
0.40
0.35
0.30
0.25
0.20
0.15
0.10
0.05
0
0.1
0.2
0.3
0.4
0.5
0.6
0.7
0.8
0.9
1.0
1.10
1.20
CAVITATION NUMBER Kv
CAMBERED δ = 45°; σ = 100

Fig 13a

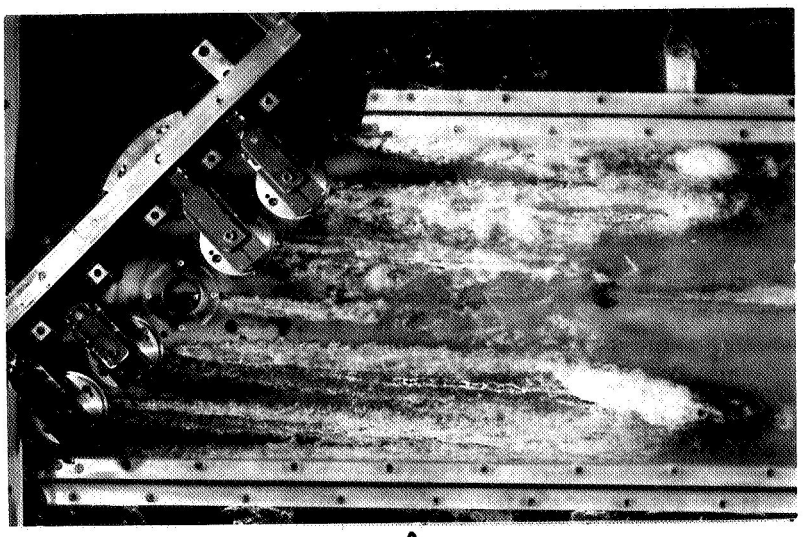

A

$\alpha = 4°$
V = 29 ft/sec
Kv = 0.25
$C_L = -0.03$

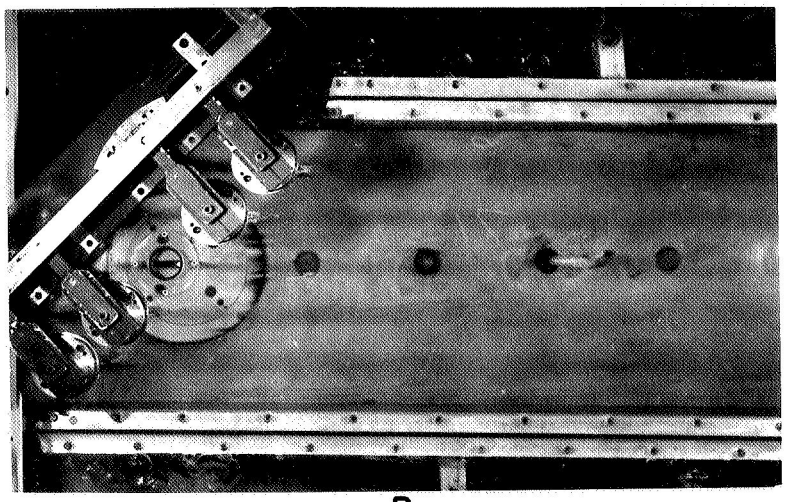

B

$\alpha = 4°$
V = 29 ft/sec
Kv = 0.28
$C_L = 0.06$

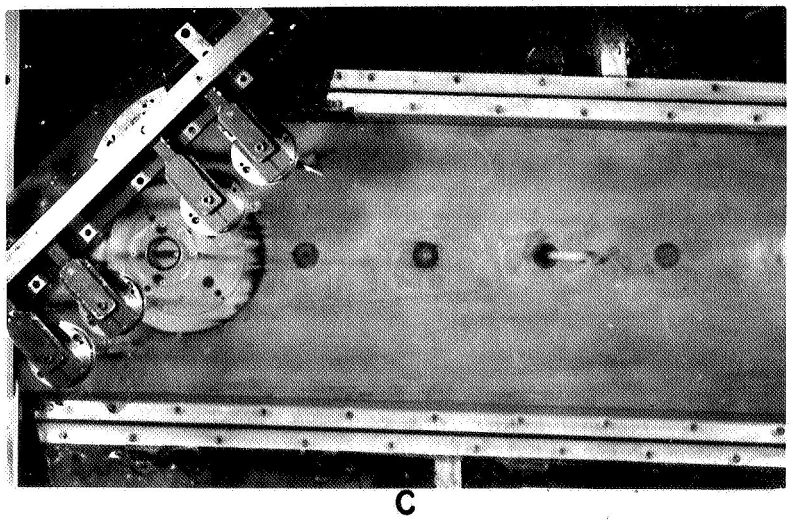

C

$\alpha = 4°$
V = 29 ft/sec
Kv = 0.40
$C_L = 0.08$

Fig. 14a

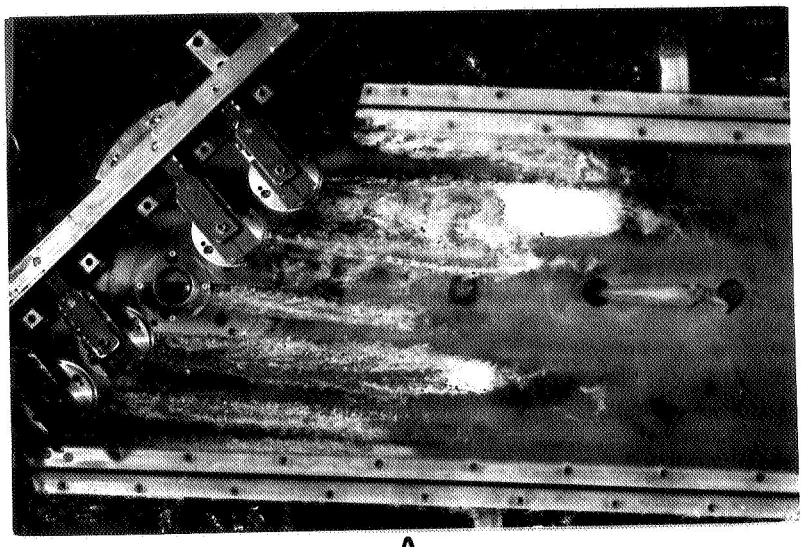

A

$\alpha = 6°$
V = 29ft/sec
Kv = 0.27
$C_L = -0.07$

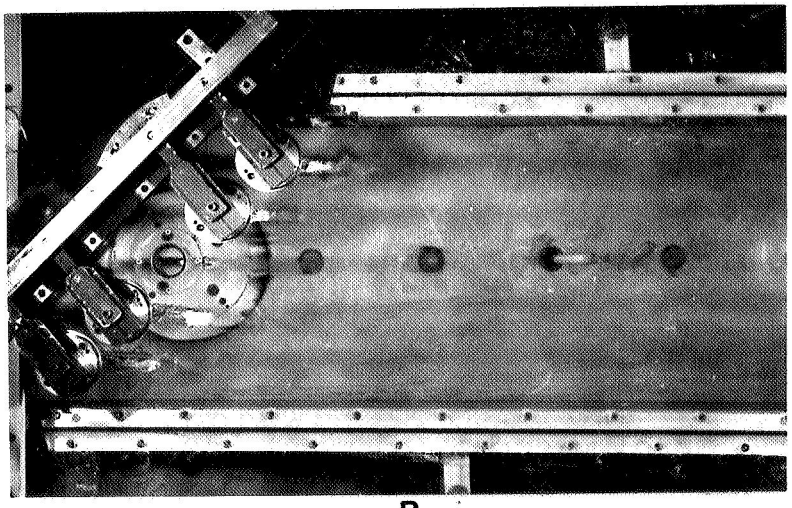

B

$\alpha = 6°$
V = 30ft/sec
Kv = 0.36
$C_L = 0.12$

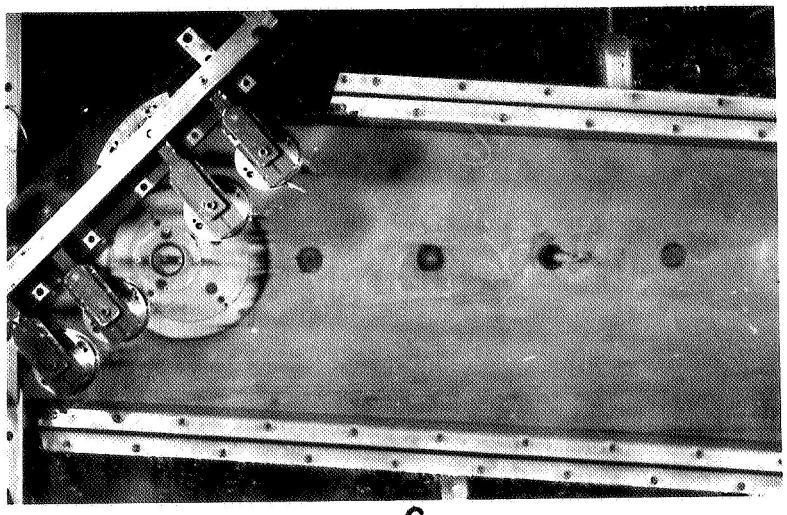

C

$\alpha = 6°$
V = 31ft/sec
Kv = 0.42
$C_L = 0.19$

Fig. 14b

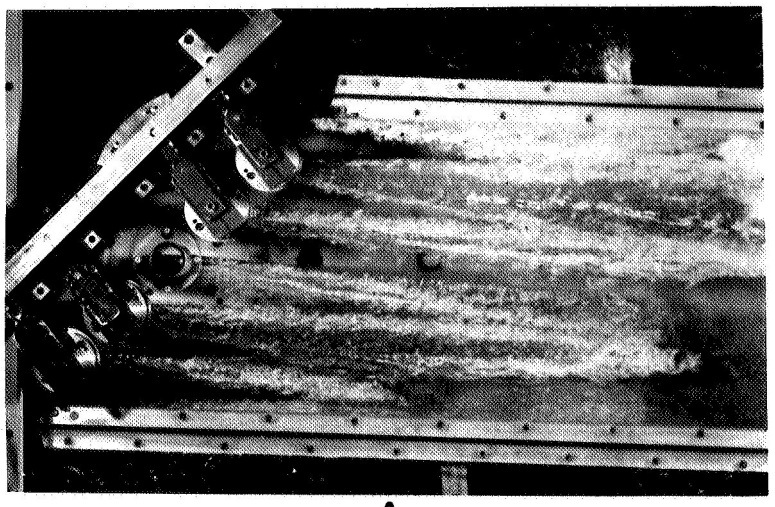

A

$\alpha = 8°$
V = 28ft/sec
Kv = 0.31
$C_L = 0.03$

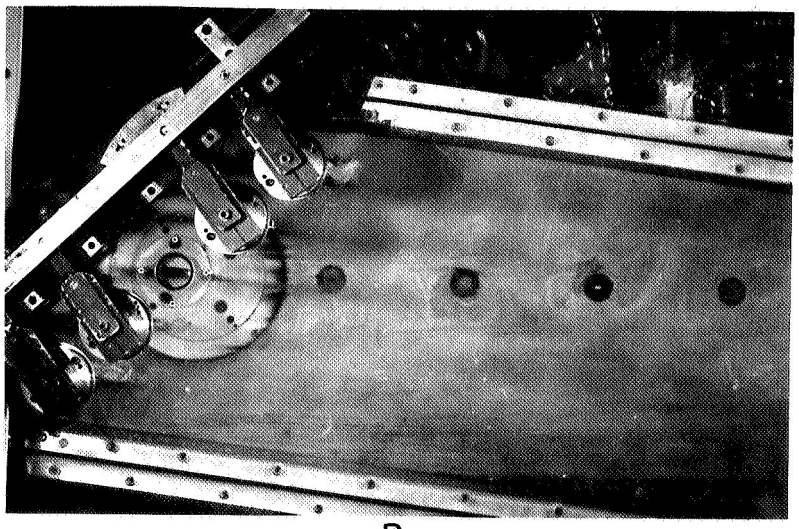

B

$\alpha = 8°$
V = 29ft/sec
Kv = 0.45
$C_L = 0.27$

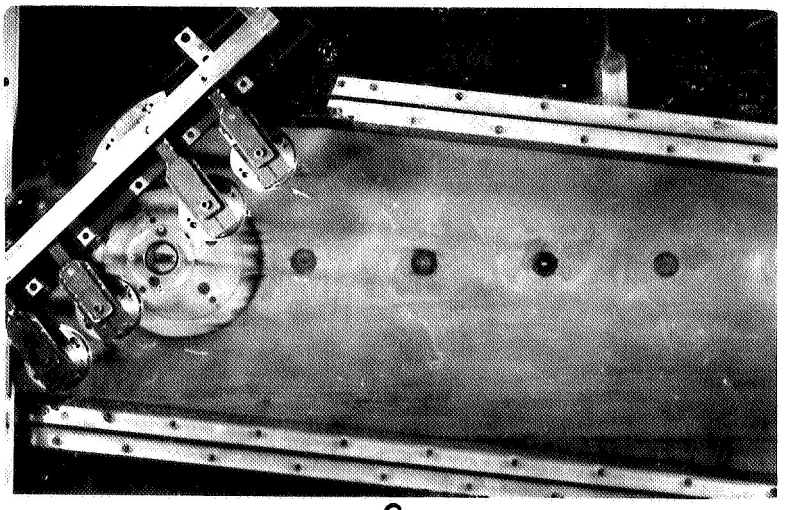

C

$\alpha = 8°$
V = 29ft/sec
Kv = 0.56
$C_L = 0.24$

Fig. 14c

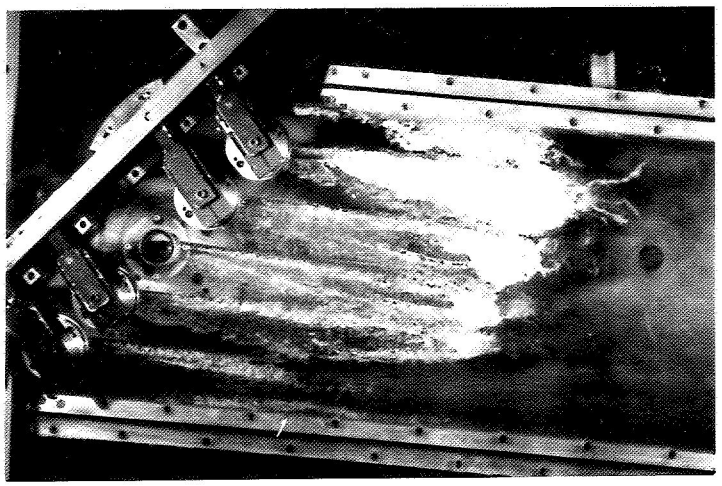

$\alpha = 10°$ $K_V = 0.34$

$V = 28$ ft/sec $C_L = -0.03$

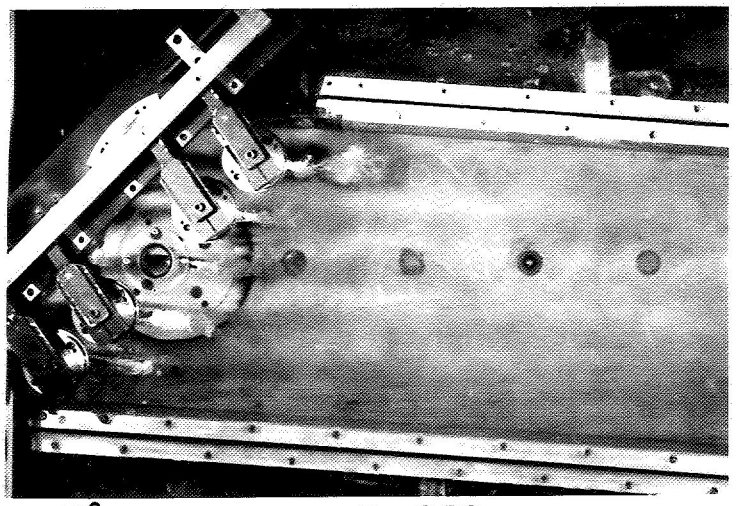

$\alpha = 10°$ $K_V = 0.39$

$V = 28$ ft/sec $C_L = 0.12$

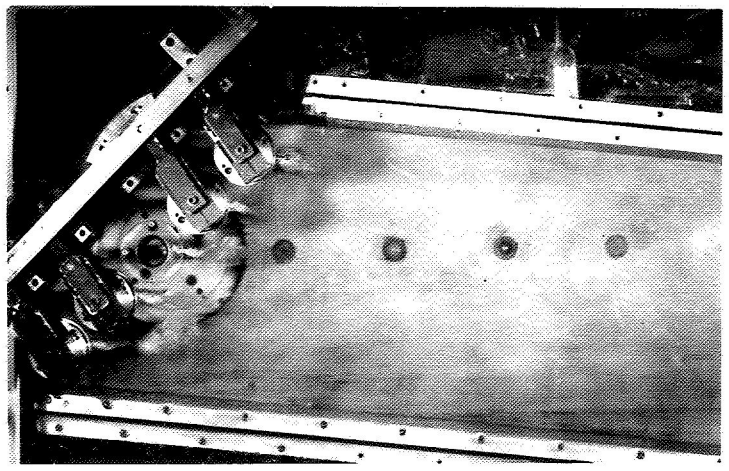

$\alpha = 10°$ $K_V = 0.48$

$V = 29$ ft/sec $C_L = 0.26$

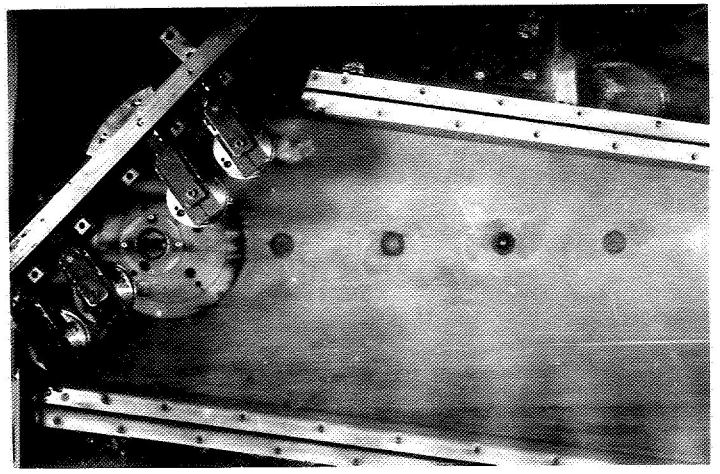

$\alpha = 10°$ $K_V = 0.64$

$V = 29$ ft/sec $C_L = 0.32$

Fig. 14d

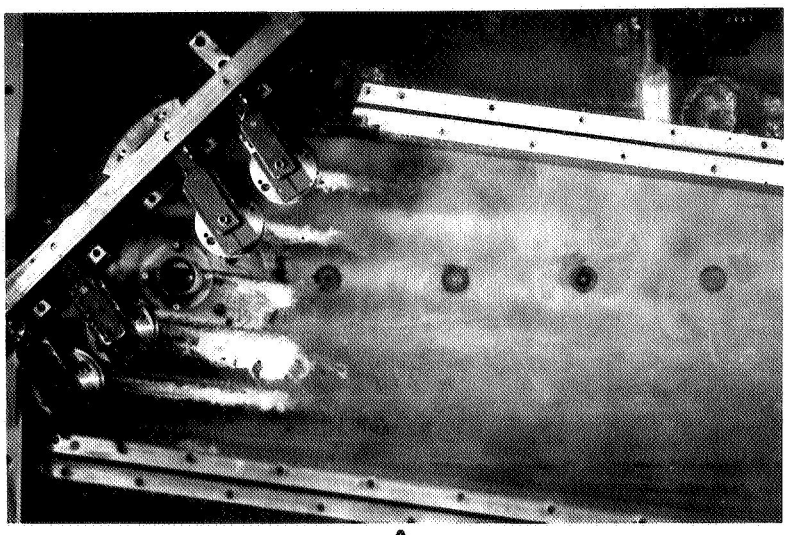

A

$\alpha = 12°$
V = 30 ft/sec
Kv = 0.33
$C_L = 0.04$

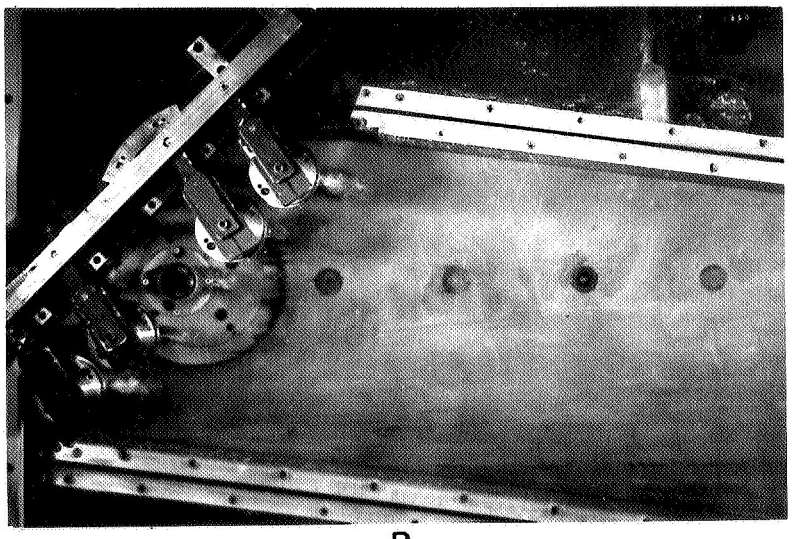

B

$\alpha = 12°$
V = 29 ft/sec
Kv = 0.46
$C_L = 0.23$

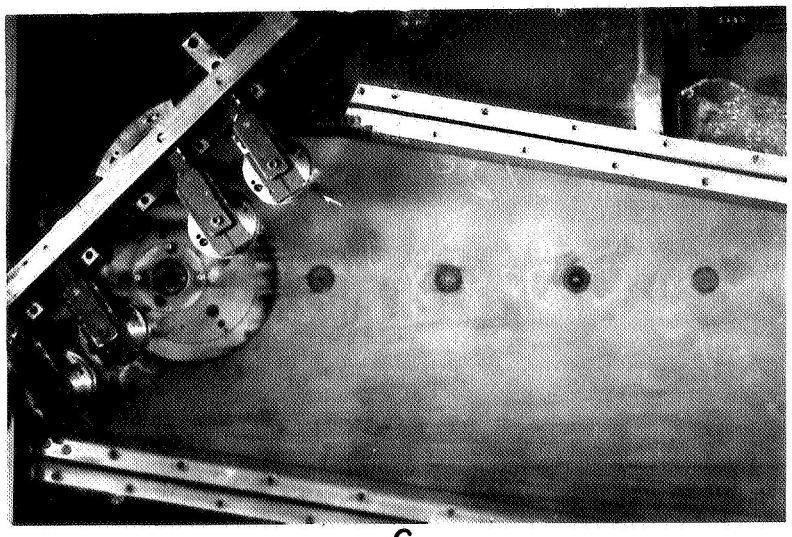

C

$\alpha = 12°$
V = 29 ft/sec
Kv = 0.74
$C_L = 0.38$

Fig. 14e

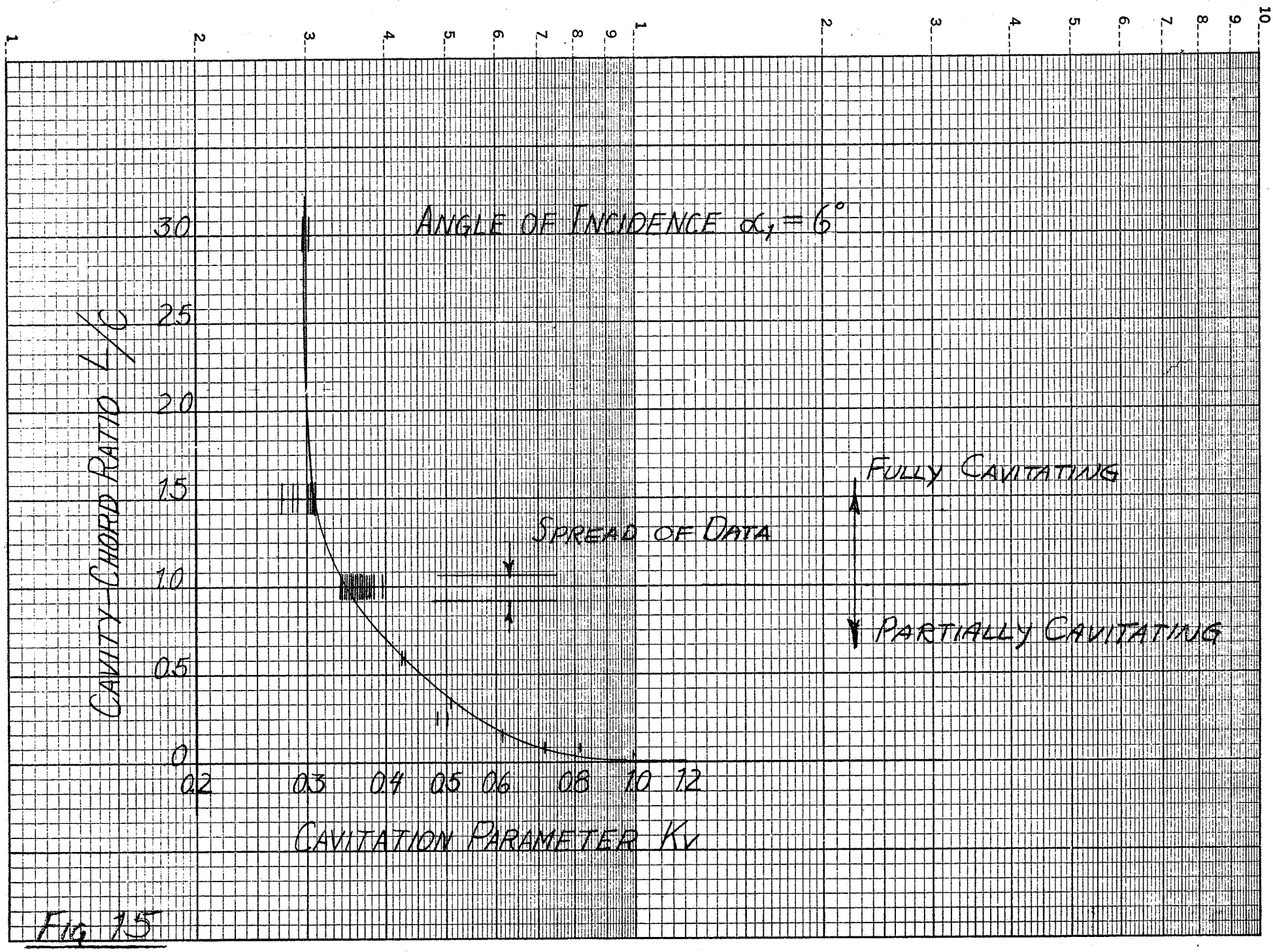
ANGLE OF INCIDENCE $\alpha_1 = 6°$
CAVITY-CHORD RATIO l/c
30
25
20
15
10
05
0
0.2
0.3
0.4
0.5
0.6
0.8
1.0
1.2
CAVITATION PARAMETER K_v
SPREAD OF DATA
FULLY CAVITATING
PARTIALLY CAVITATING

Fig. 15

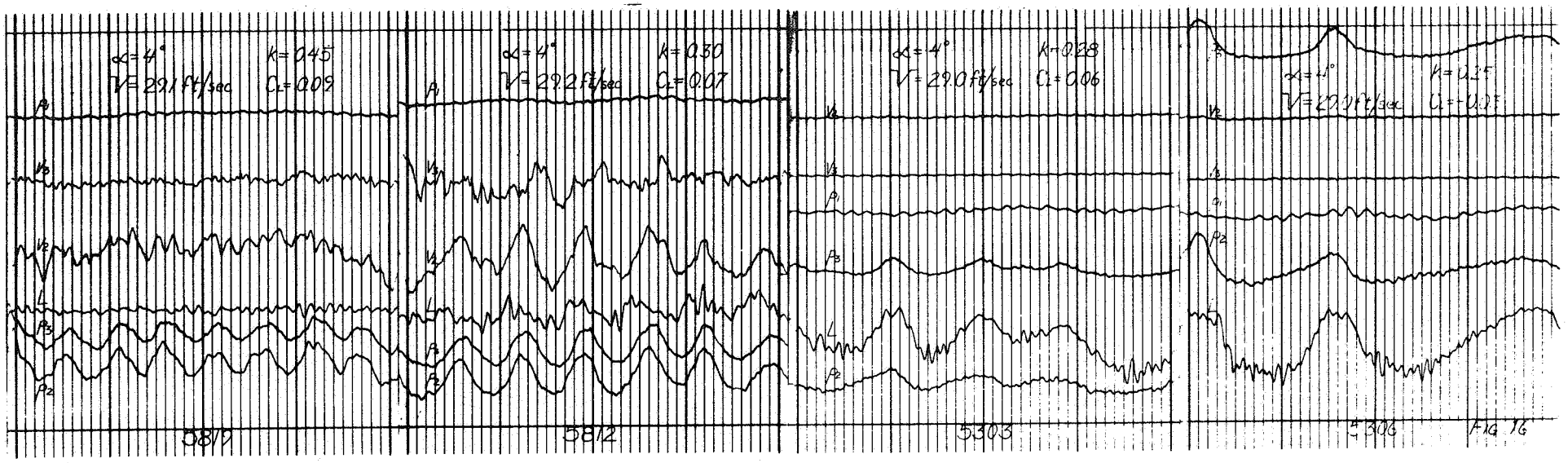
α = 4°
V = 29.1 ft/sec
k = 045
C_L = 0.09
α = 4°
V = 29.2 ft/sec
k = 0.30
C_L = 0.07
α = 4°
V = 29.0 ft/sec
k = 0.28
C_L = 0.06
α = 4°
V = 29.0 ft/sec
k = 0.25
C_L = 0.05
5809
5812
5303
± 30G

FIG 16

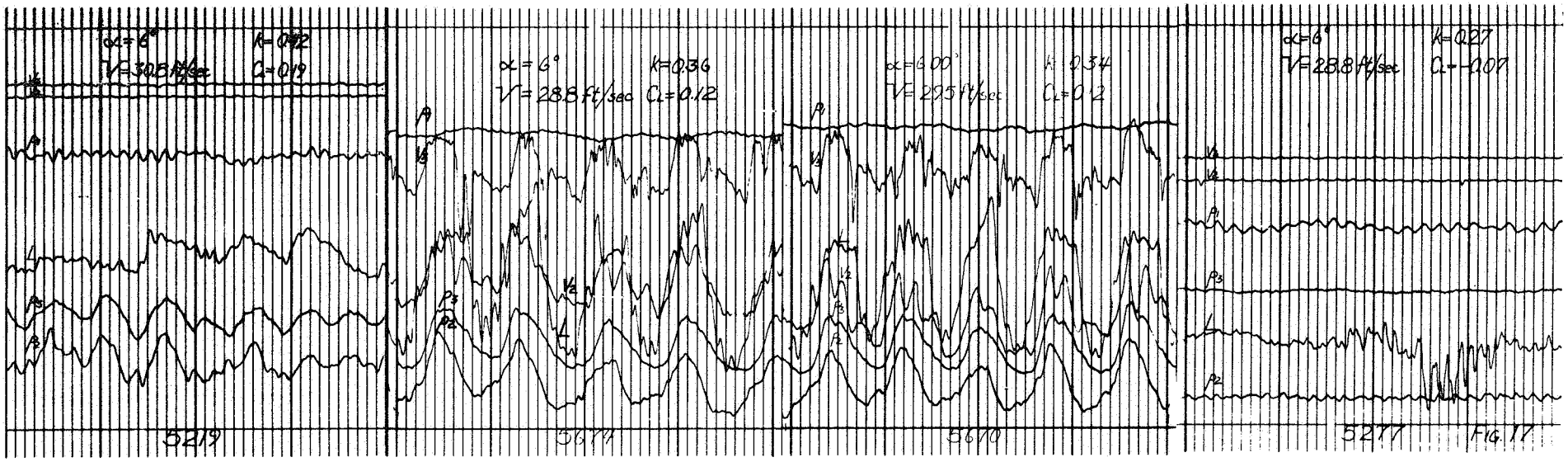
α=6°
V=30.8 ft/sec
k=0.42
CL=0.19
5219
α=6°
V=28.8 ft/sec
k=0.36
CL=0.12
5677
α=6.00°
V=29.5 ft/sec
k=0.34
CL=0.12
5670
α=6°
V=28.8 ft/sec
k=0.27
CL=0.07
5277

FIG. 17

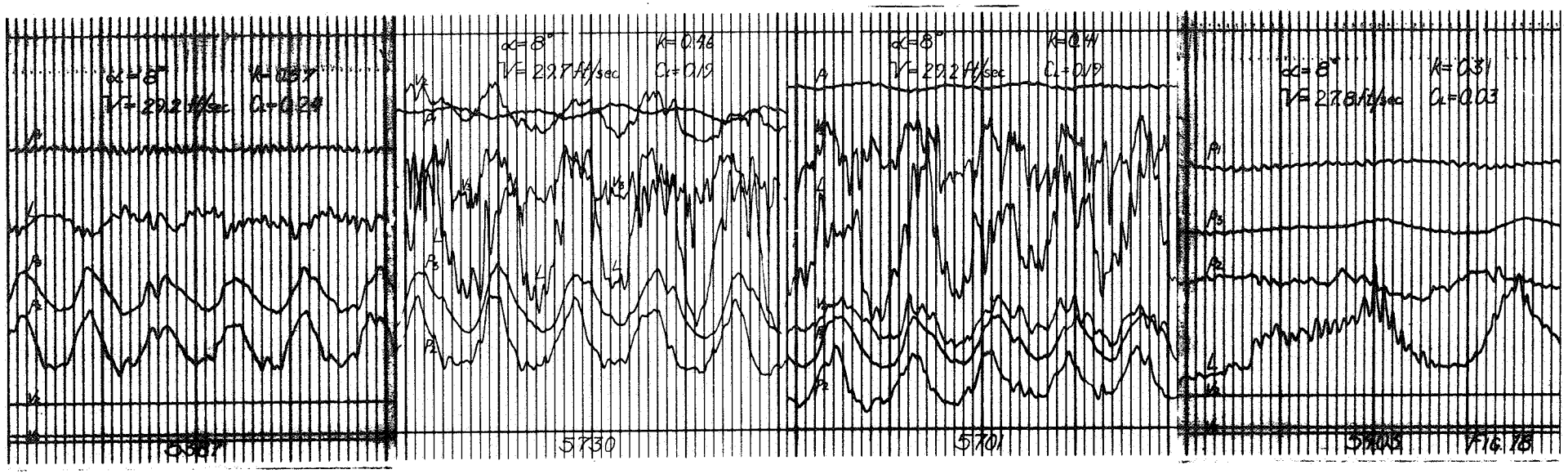
α=8°
V=292 ft/sec
K=0.96
C_L=0.19
α=8°
V=292 ft/sec
K=0.44
C_L=0.19
α=8°
V=278 ft/sec
K=0.34
C_L=0.03
5730
5701
5703

FIG. 7B

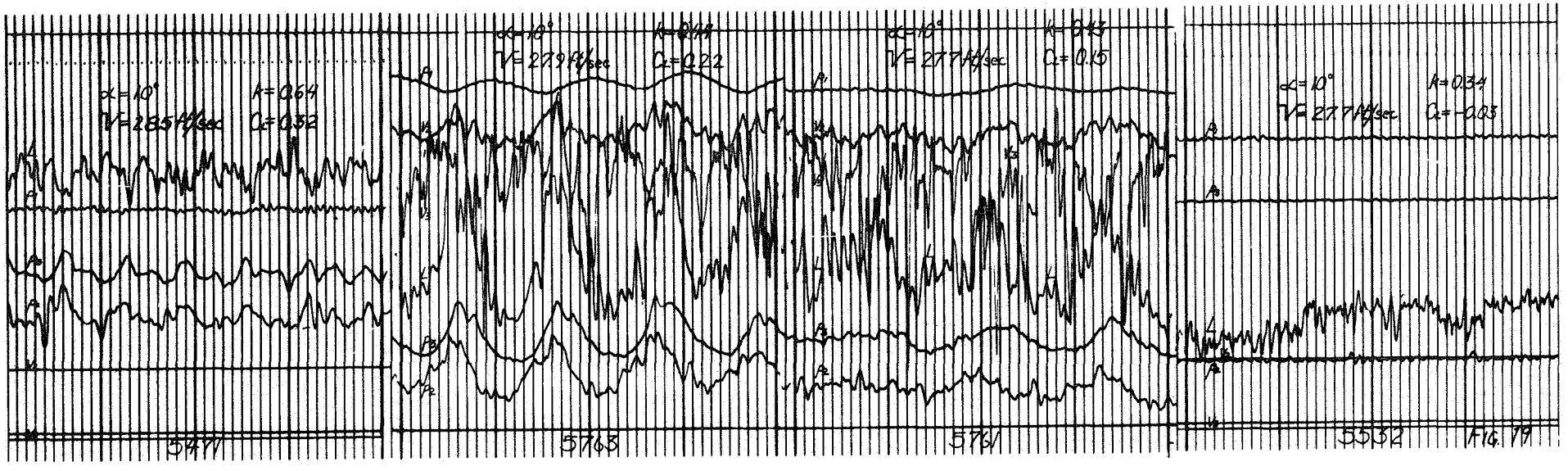
α = 10°
V = 285 ft/sec
k = 0.64
Cz = 0.32
5497
α = 10°
V = 279 ft/sec
k = 0.44
Cz = 0.22
5765
α = 10°
V = 277 ft/sec
k = 0.45
Cz = 0.15
5791
α = 10°
V = 277 ft/sec
k = 0.34
Cz = -0.03
5532

FIG. 19

FIG 20

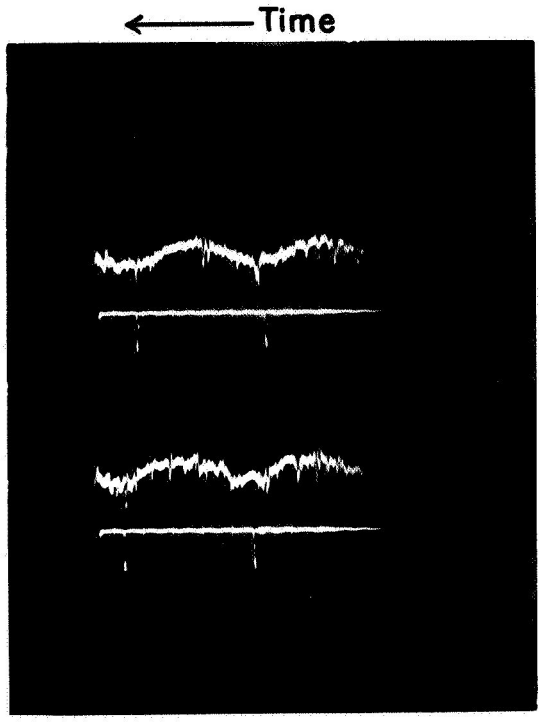

V = 22 ft/sec

Freq. = 10 cps

Overheat = 7.7%

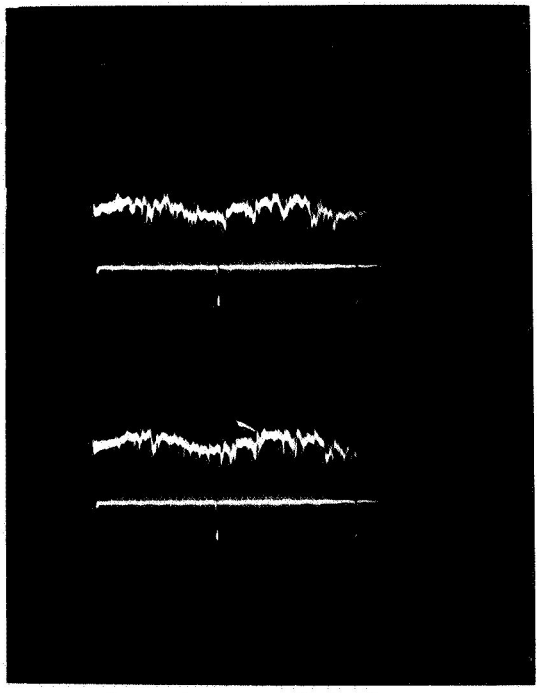

V = 22 ft/sec

Freq. = 10 cps

Overheat = 5.0%

Fig. 21

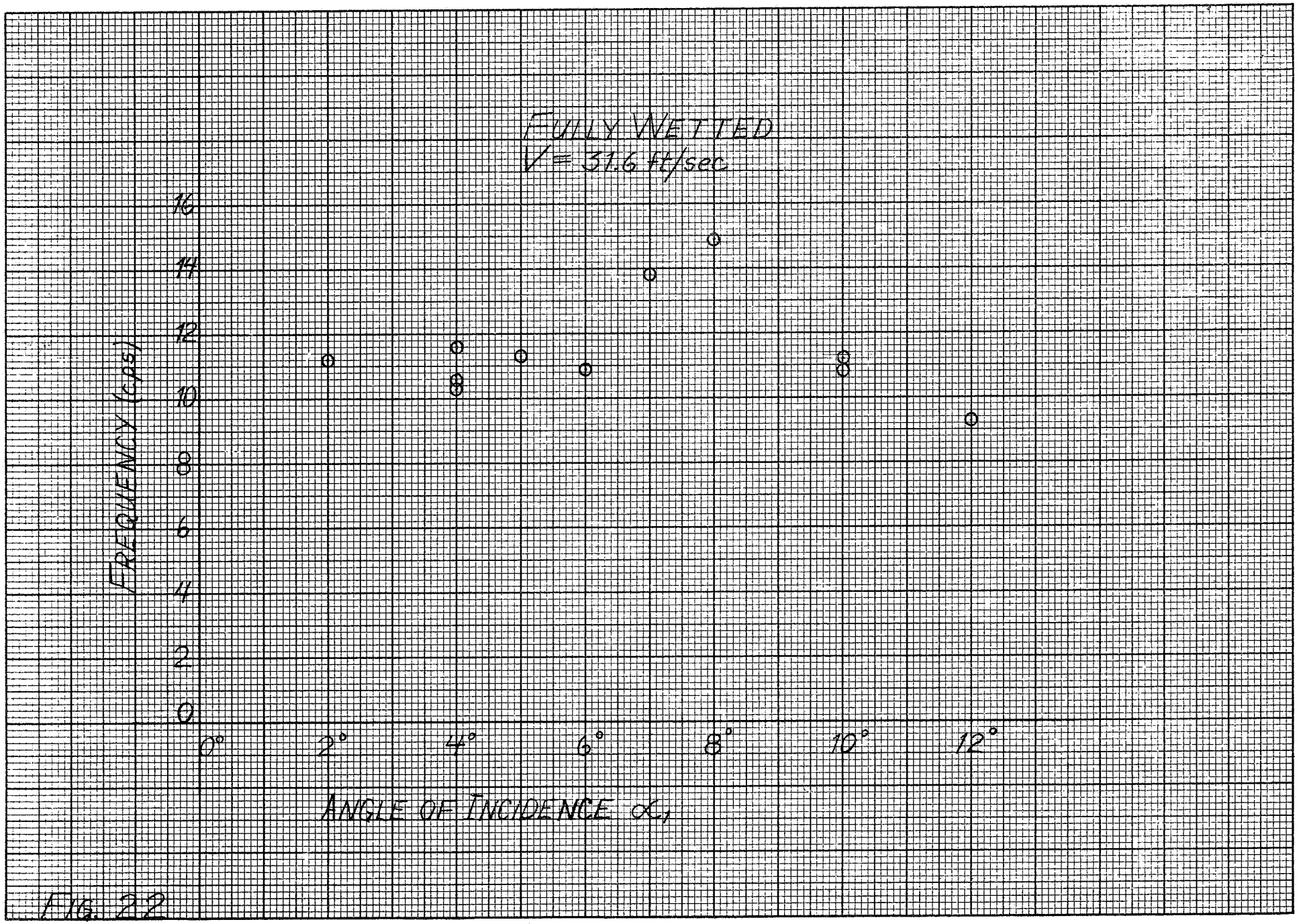
FULLY WETTED
V = 31.6 ft/sec
FREQUENCY (cps)
16
14
12
10
8
6
4
2
0
0°
2°
4°
6°
8°
10°
12°
ANGLE OF INCIDENCE α,

FIG. 22

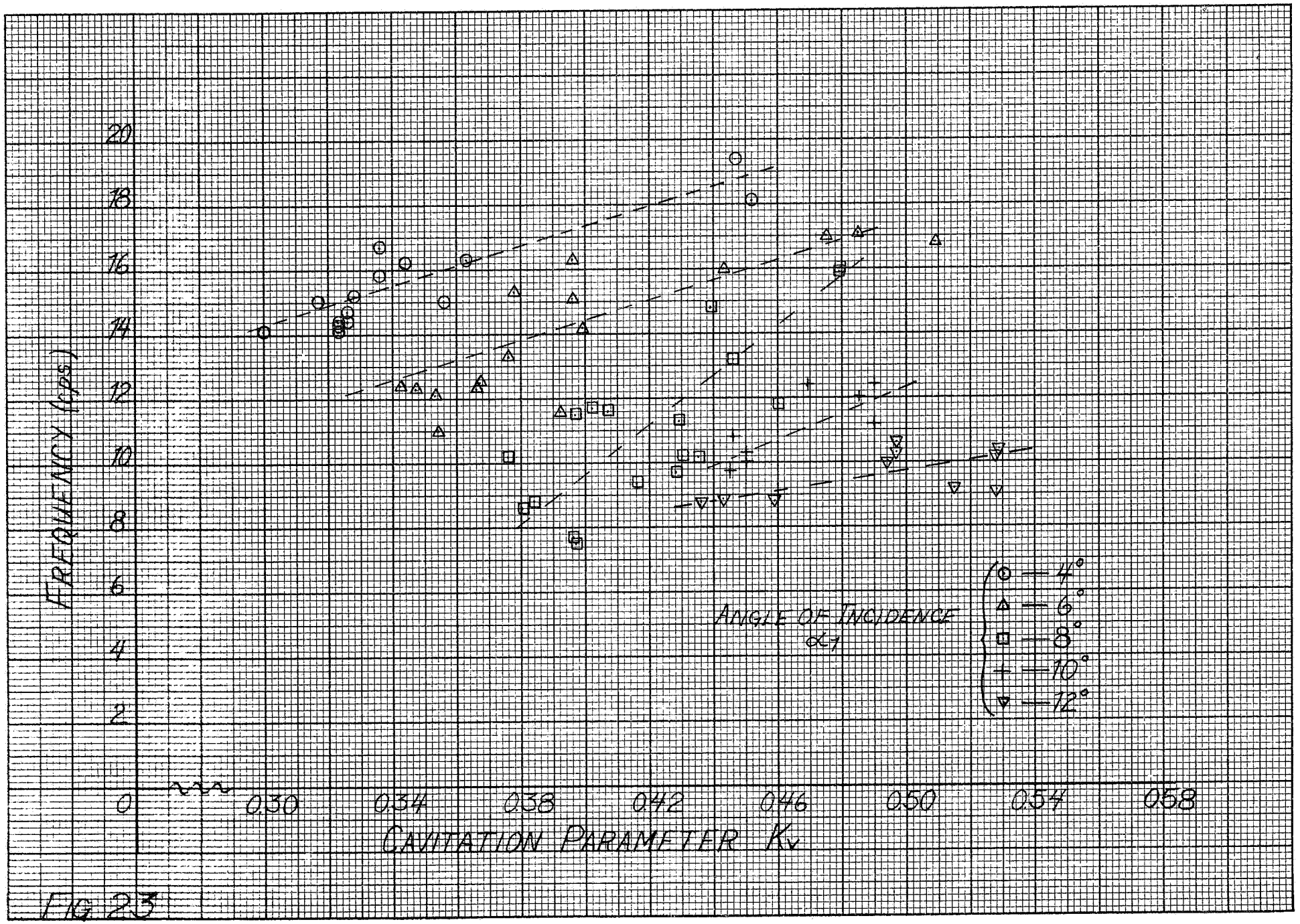
FREQUENCY (cps)
20
18
16
14
12
10
8
6
4
2
0
0.30
0.34
0.38
0.42
0.46
0.50
0.54
0.58
CAVITATION PARAMETER K_v
ANGLE OF INCIDENCE α_1
○ — 4°
△ — 6°
□ — 8°
+ — 10°
▽ — 12°

FIG 23

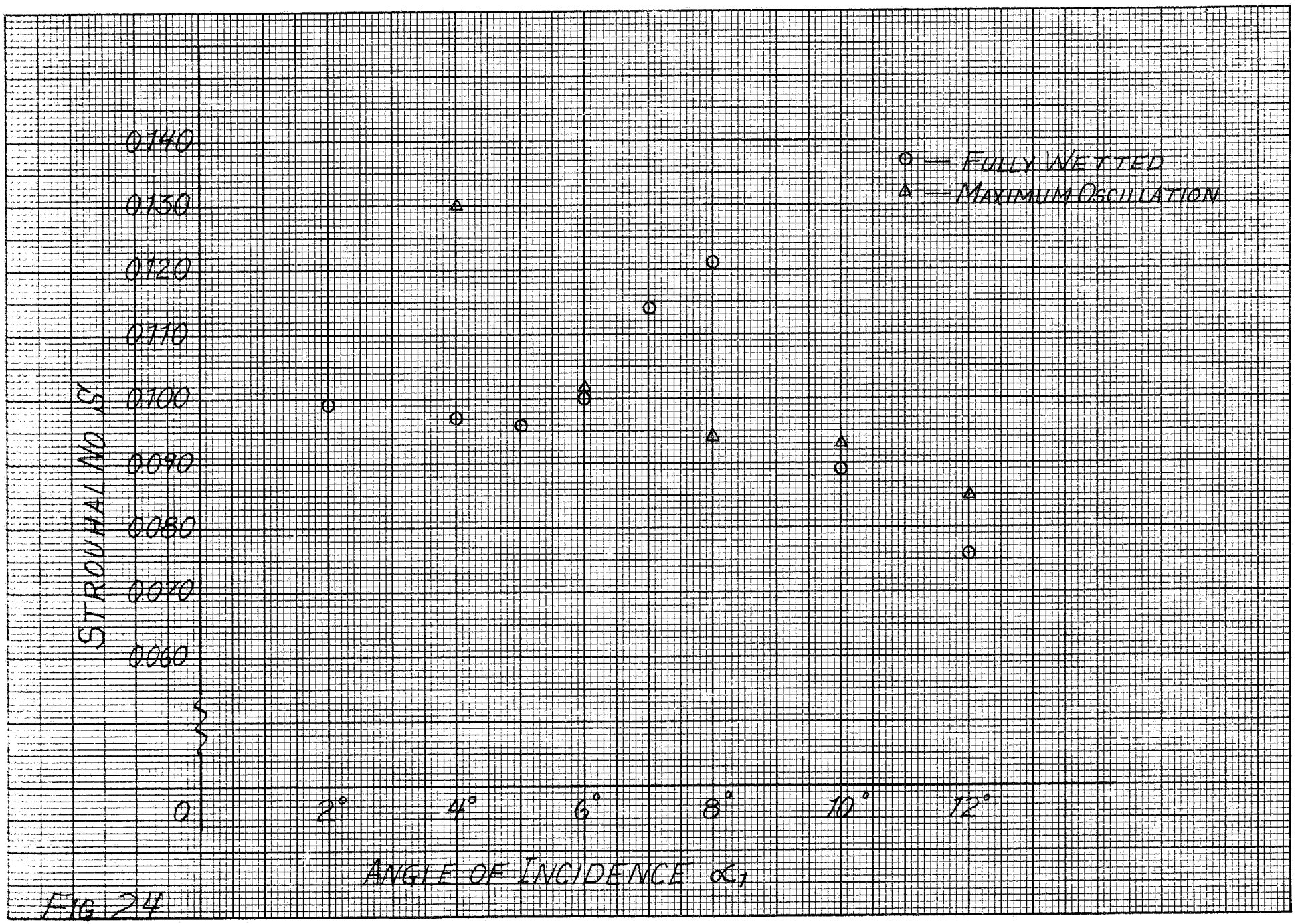
0·140
0·130
0·120
0·110
0·100
0·090
0·080
0·070
0·060
0
STROUHAL NO S
2°
4°
6°
8°
10°
12°
ANGLE OF INCIDENCE α_1
○ — FULLY WETTED
△ — MAXIMUM OSCILLATION

FIG 24

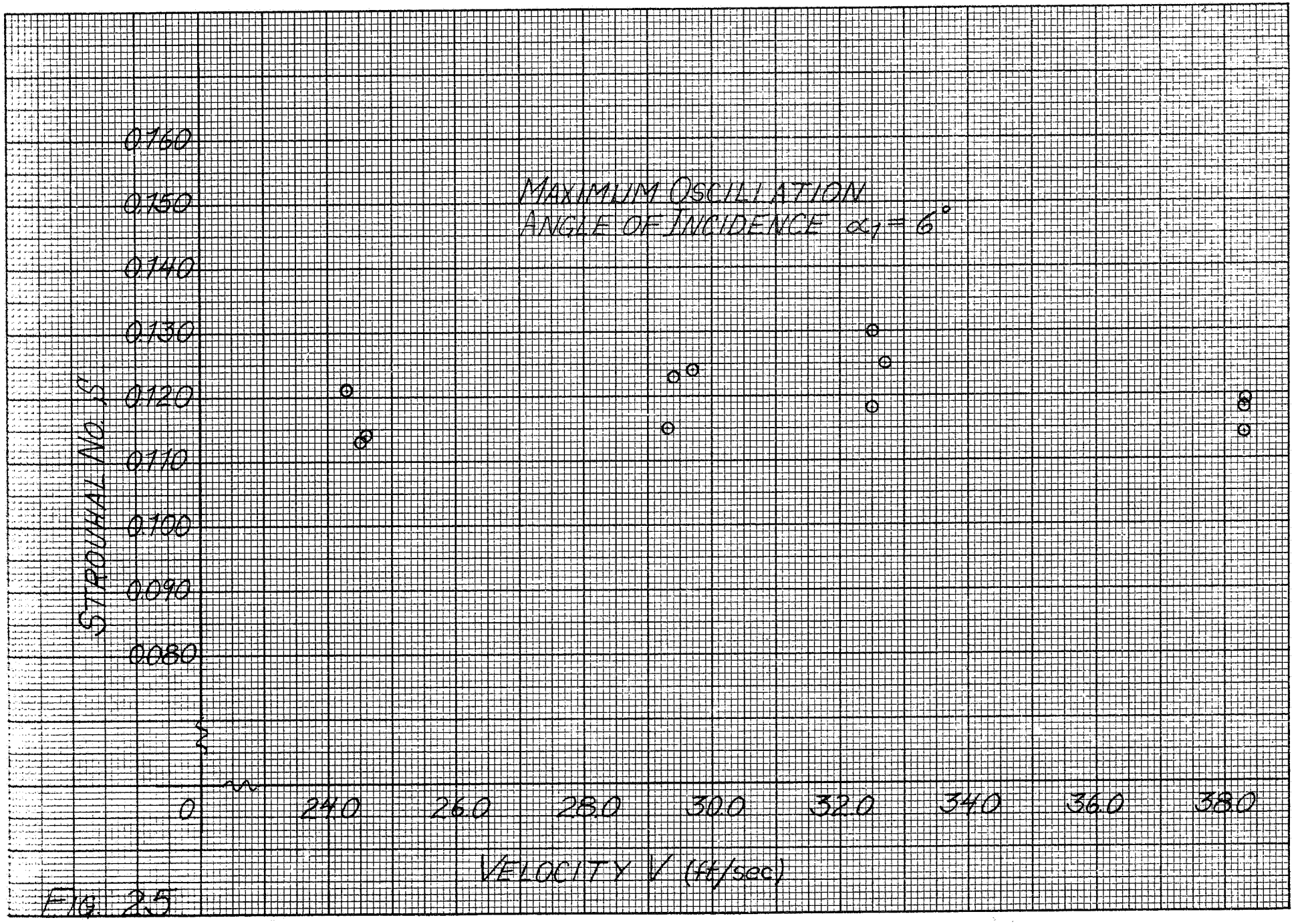
MAXIMUM OSCILLATION
ANGLE OF INCIDENCE $\alpha_1 = 6°$
0.160
0.150
0.140
0.130
0.120
0.110
0.100
0.090
0.080
0
24.0
26.0
28.0
30.0
32.0
34.0
36.0
38.0
STRAIGHTAWAY ζ_s
VELOCITY V (ft/sec)

Fig. 25

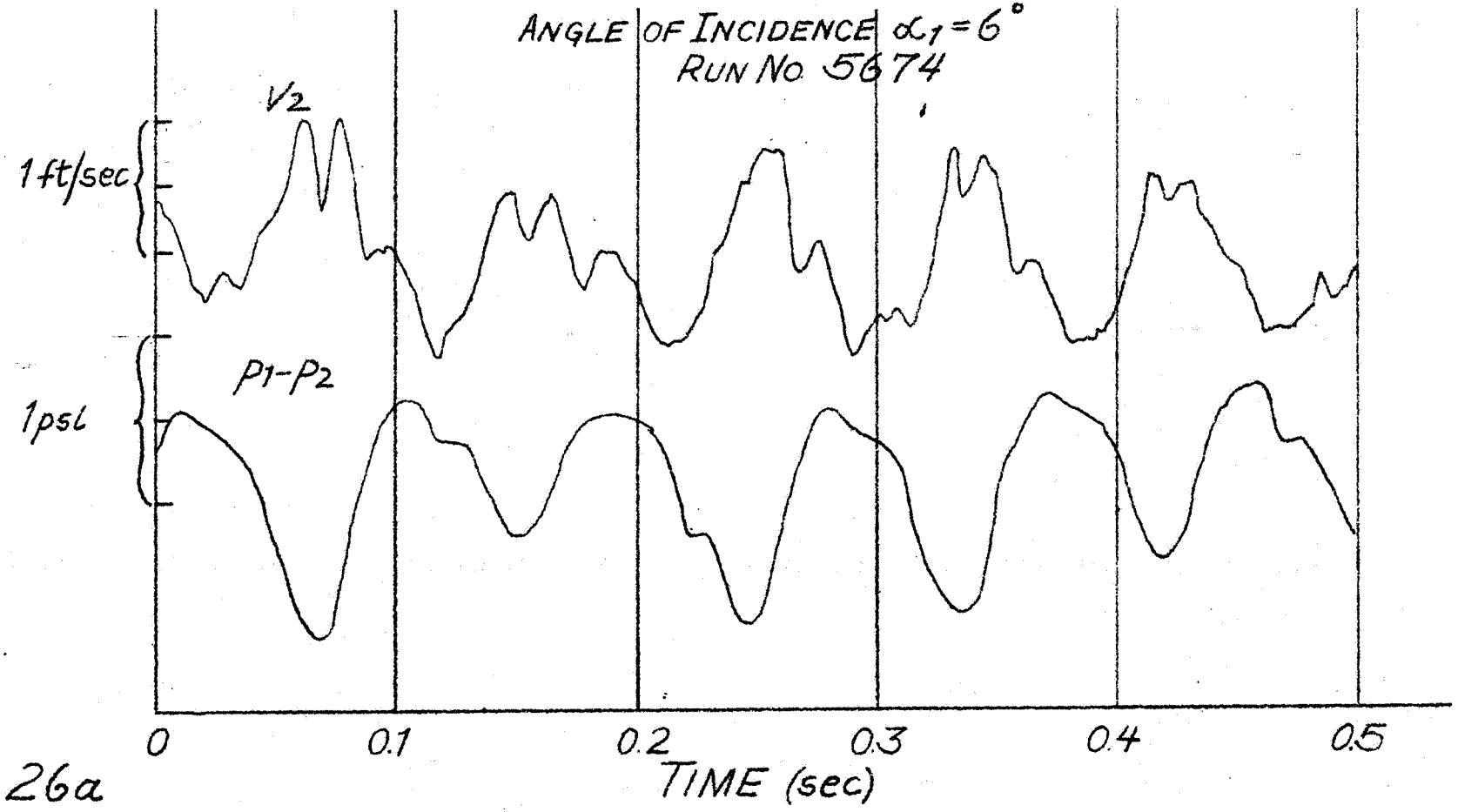
ANGLE OF INCIDENCE $\alpha_1 = 6°$
RUN NO. 5674
V_2
1 ft/sec
$P_1 - P_2$
1 psf
0
0.1
0.2
0.3
0.4
0.5
TIME (sec)

FIG. 26a

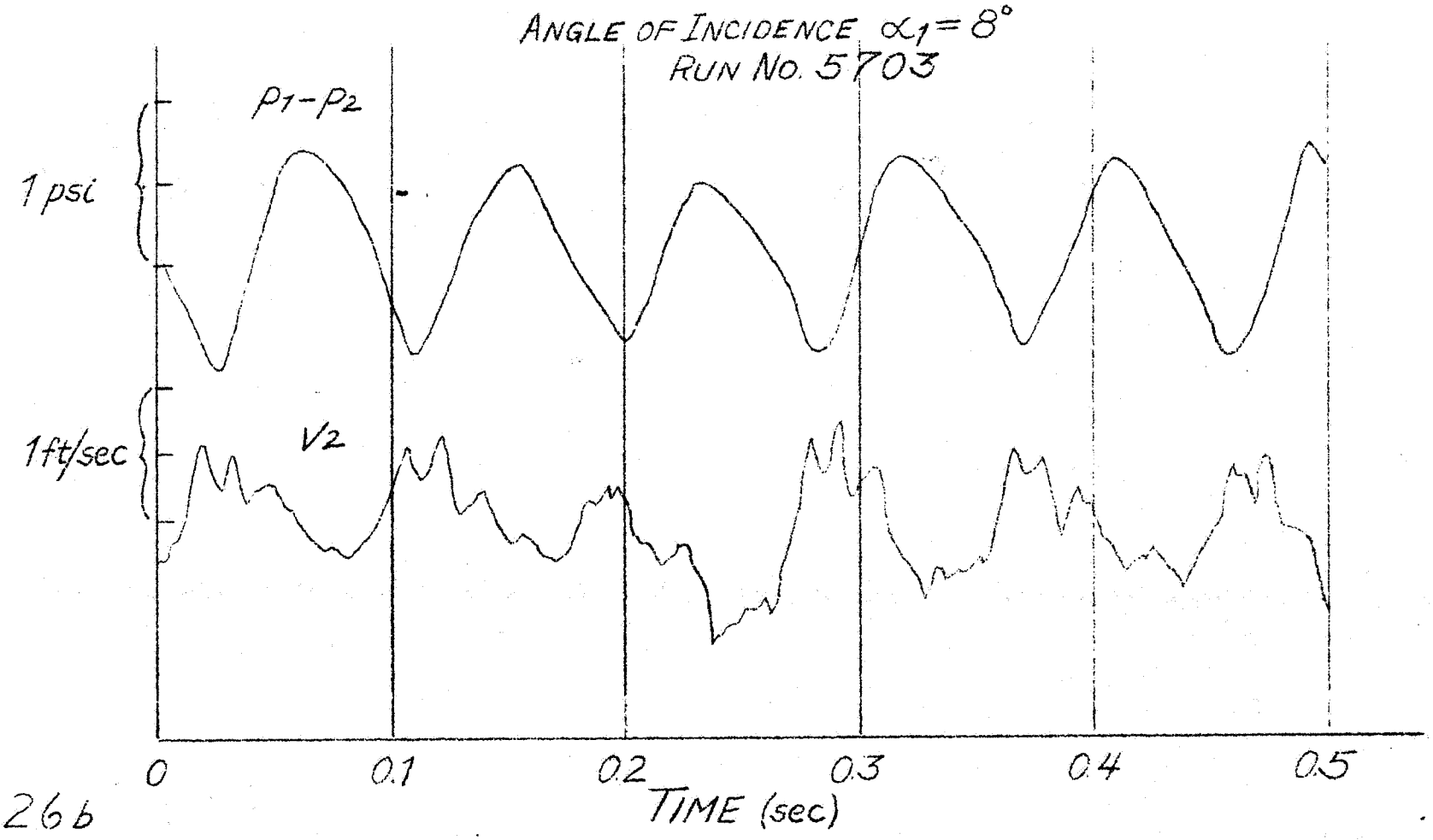
ANGLE OF INCIDENCE $\alpha_1 = 8°$
RUN NO. 5703
$p_1 - p_2$
1 psi
1 ft/sec
V_2
0
0.1
0.2
0.3
0.4
0.5
TIME (sec)

FIG 26b

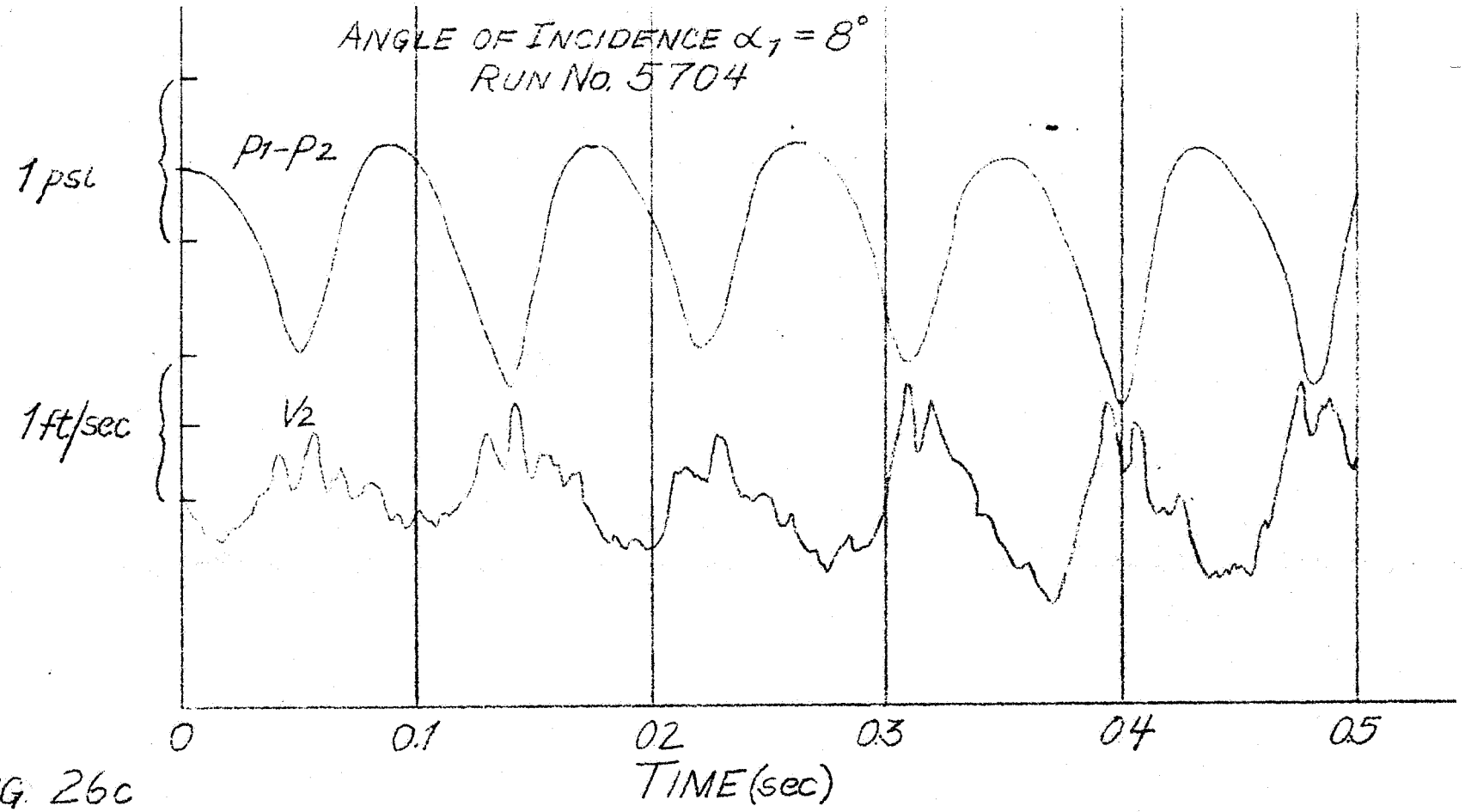
ANGLE OF INCIDENCE $\alpha_1 = 8°$
RUN No. 5704
$p_1 - p_2$
1 psi
V_2
1 ft/sec
0
0.1
02
03
04
05
TIME (sec)

FIG. 26c

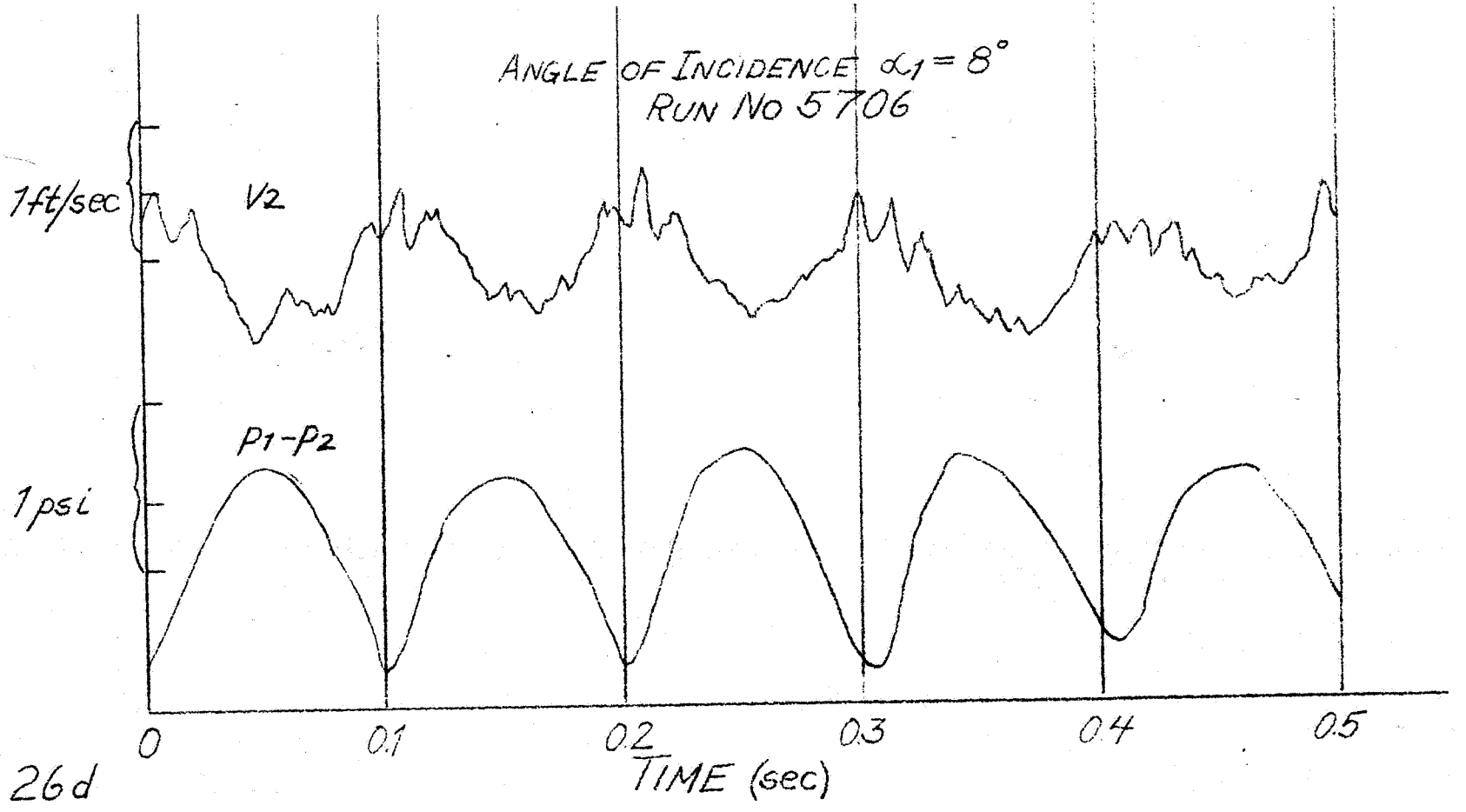
ANGLE OF INCIDENCE $\alpha_1 = 8°$
RUN NO 5706
1ft/sec
V2
P1-P2
1psi
0
0.1
0.2
0.3
0.4
0.5
TIME (sec)

FIG 26d

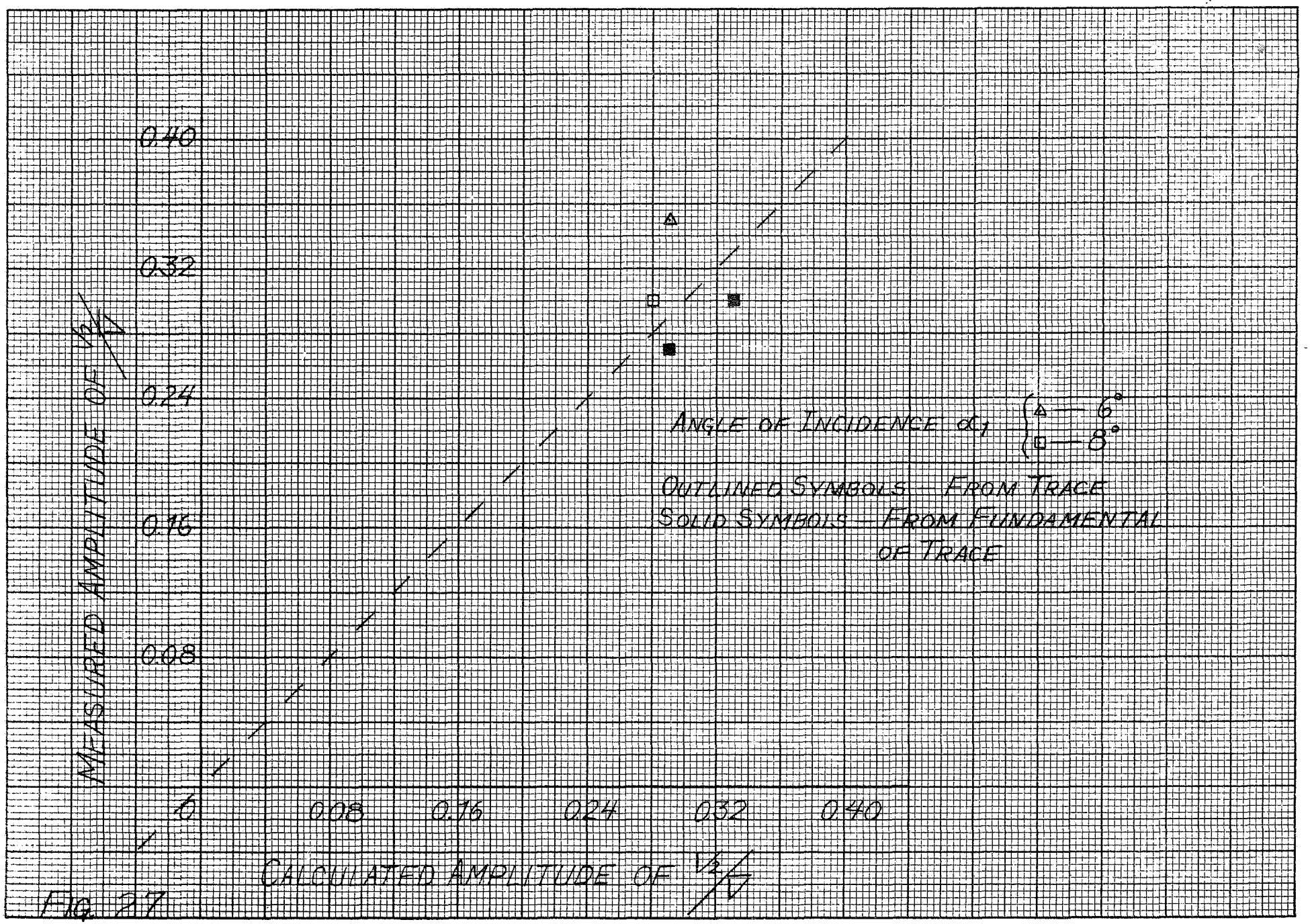
0.40
0.32
0.24
0.16
0.08
0
MEASURED AMPLITUDE OF
0.08
0.16
0.24
0.32
0.40
CALCULATED AMPLITUDE OF
ANGLE OF INCIDENCE α_1
6°
8°
OUTLINED SYMBOLS — FROM TRACE
SOLID SYMBOLS — FROM FUNDAMENTAL OF TRACE

FIG. 27

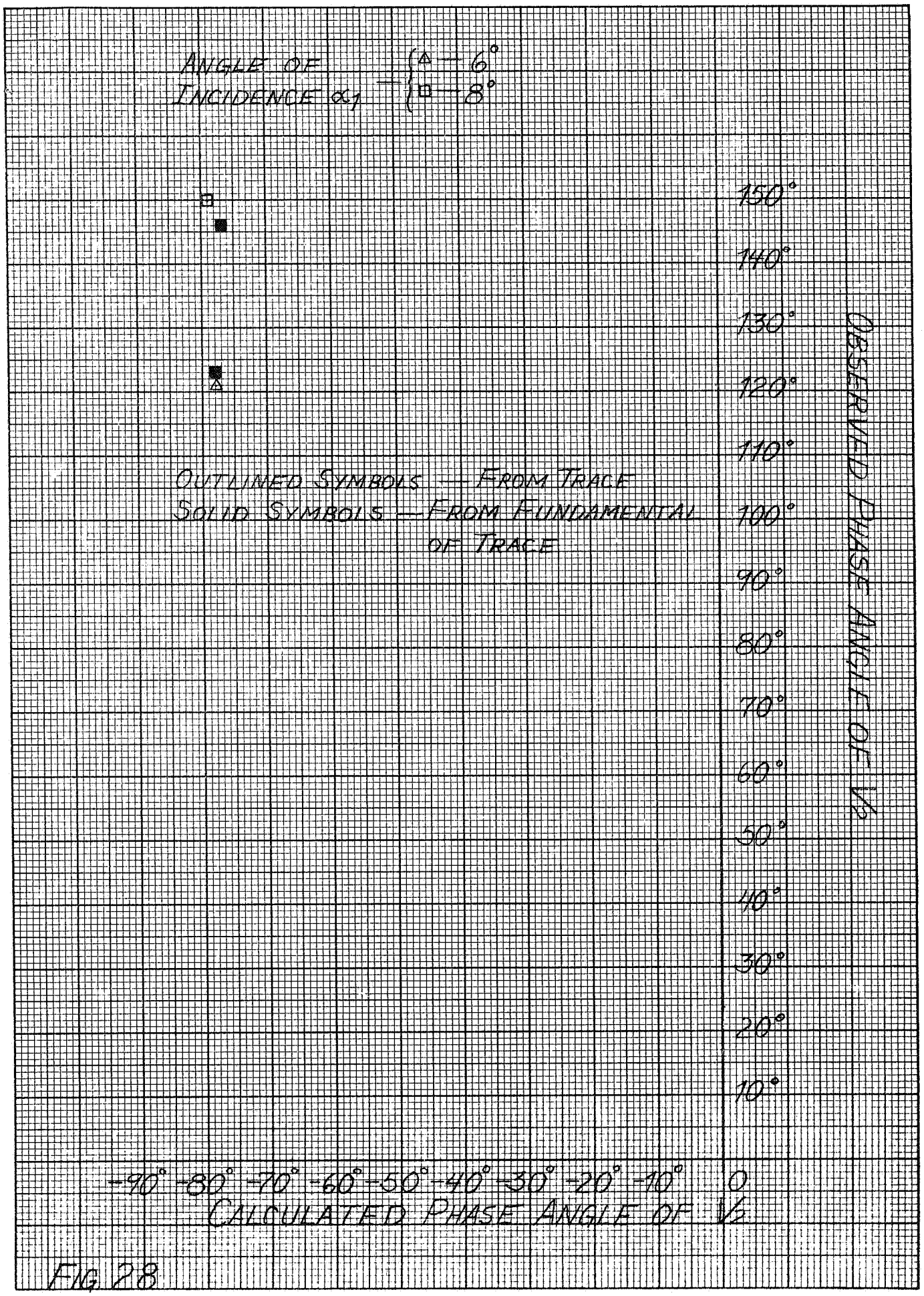
ANGLE OF INCIDENCE α_1 — △ — 6° □ — 8°
OUTLINED SYMBOLS — FROM TRACE
SOLID SYMBOLS — FROM FUNDAMENTAL OF TRACE
150°
140°
130°
120°
110°
100°
90°
80°
70°
60°
50°
40°
30°
20°
10°
0
OBSERVED PHASE ANGLE OF V_2
-90° -80° -70° -60° -50° -40° -30° -20° -10°
CALCULATED PHASE ANGLE OF V_2

FIG 28

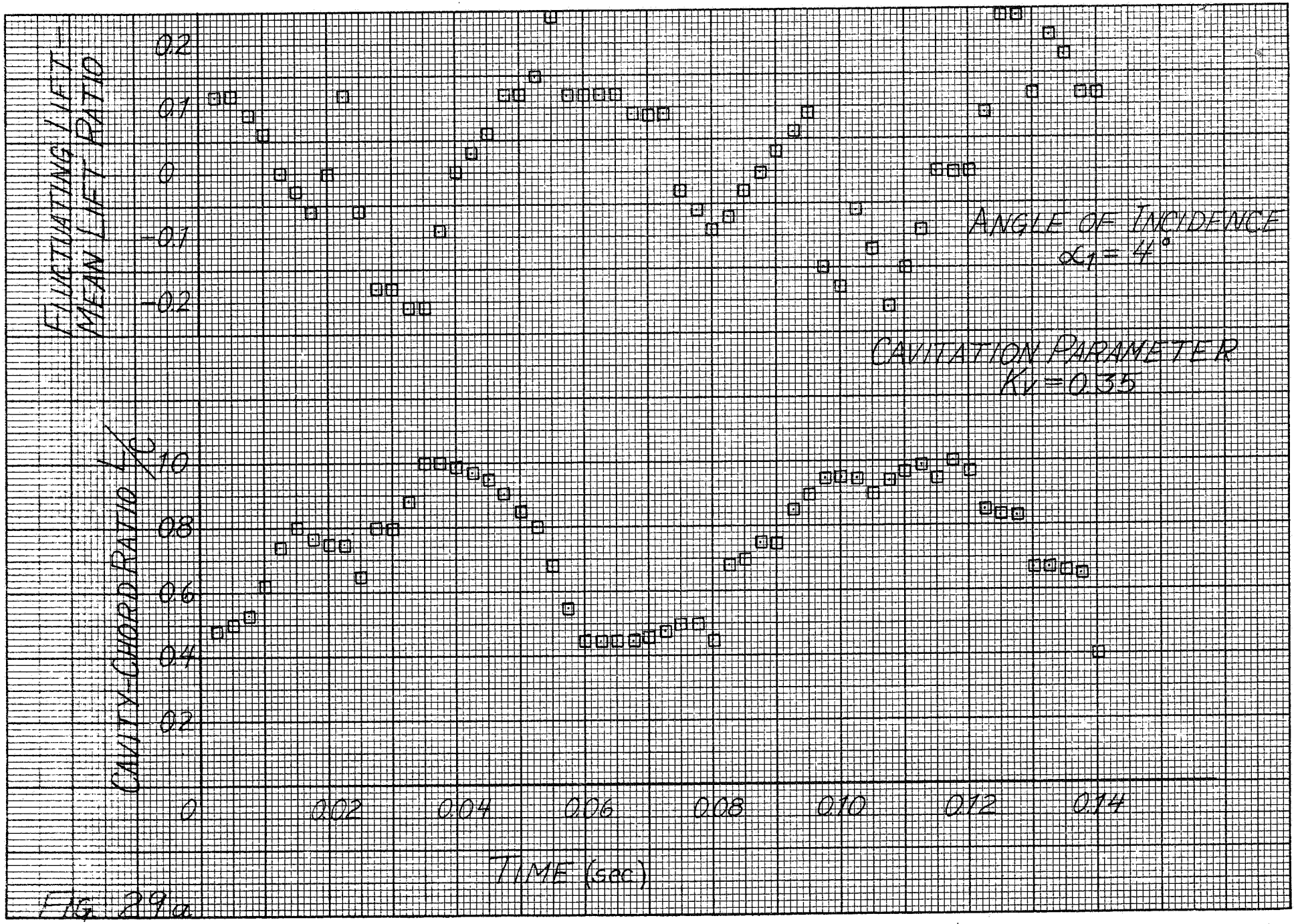
FLUCTUATING LIFT
MEAN LIFT RATIO
CAVITY-CHORD RATIO
l/c
0.2
0.1
0
-0.1
-0.2
1.0
0.8
0.6
0.4
0.2
0
0.02
0.04
0.06
0.08
0.10
0.12
0.14
TIME (sec)
ANGLE OF INCIDENCE
$\alpha_1 = 4°$
CAVITATION PARAMETER
$K_v = 0.35$

Fig. 29a

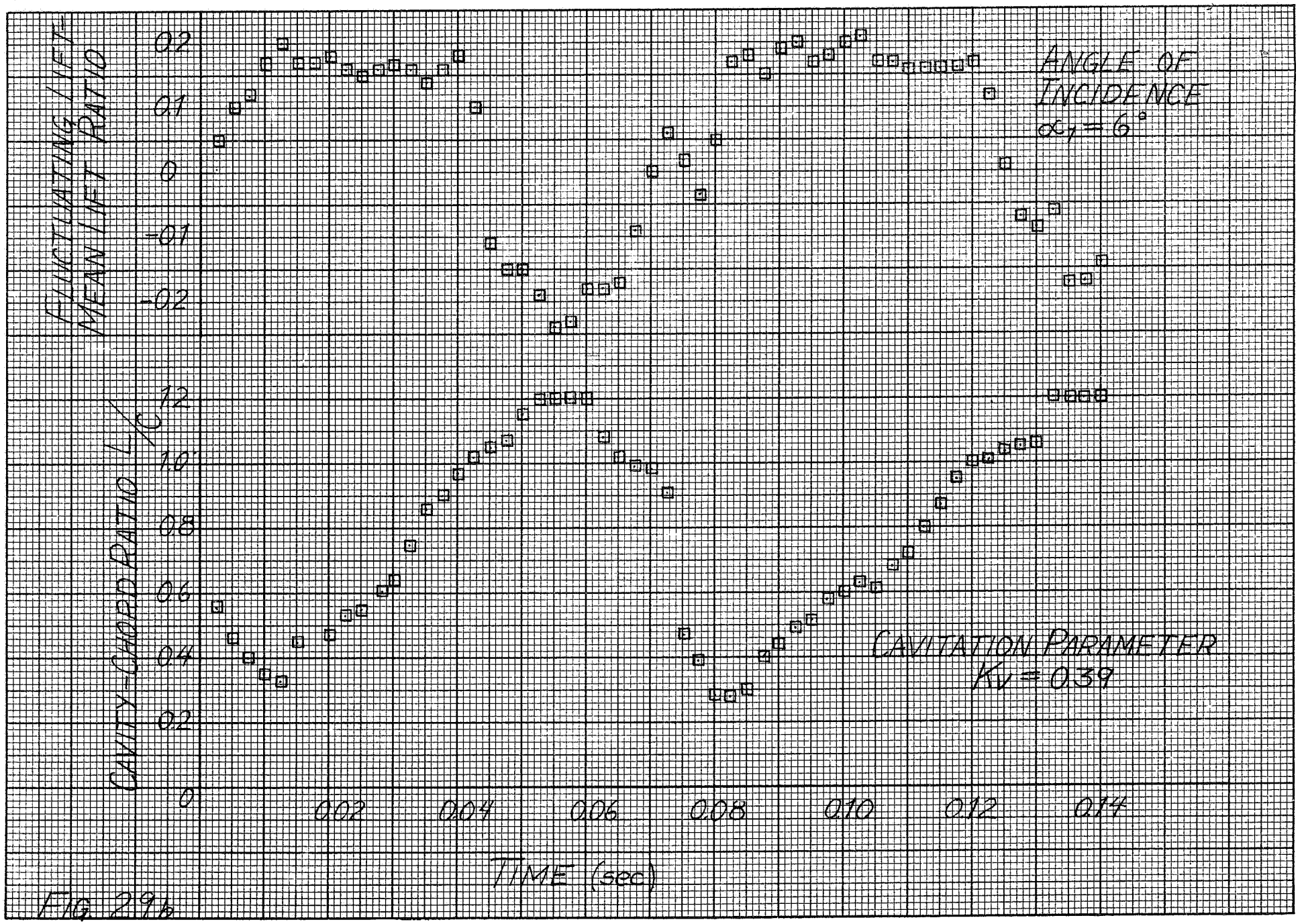
FLUCTUATING LIFT / MEAN LIFT RATIO
CAVITY-LIFT RATIO
02
01
0
-01
-02
12
10
08
06
04
02
0
002
004
006
008
010
012
014
TIME (sec)
ANGLE OF INCIDENCE
$\alpha_1 = 6°$
CAVITATION PARAMETER
$K_V = 039$

FIG. 29b

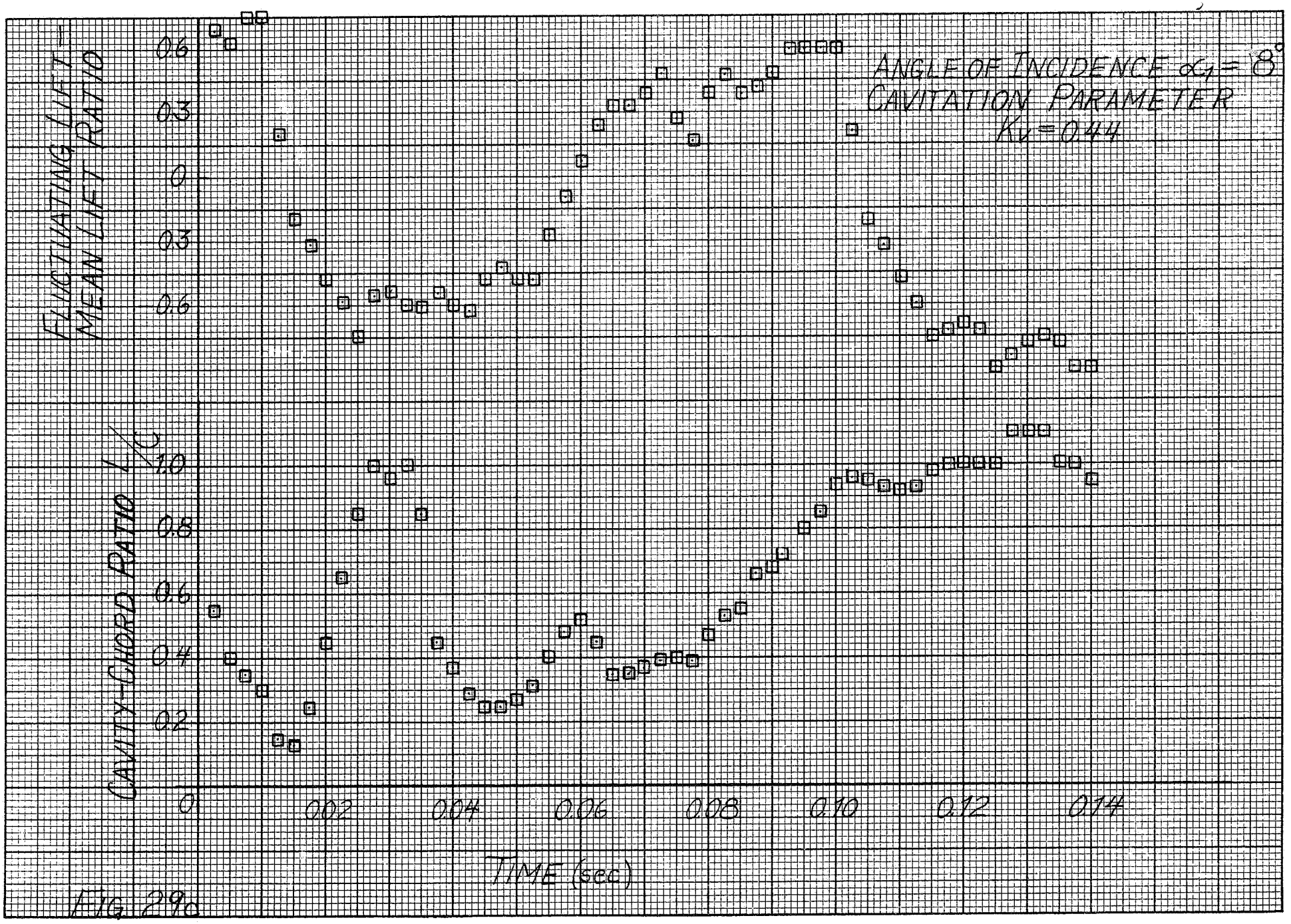

Fig. 29a

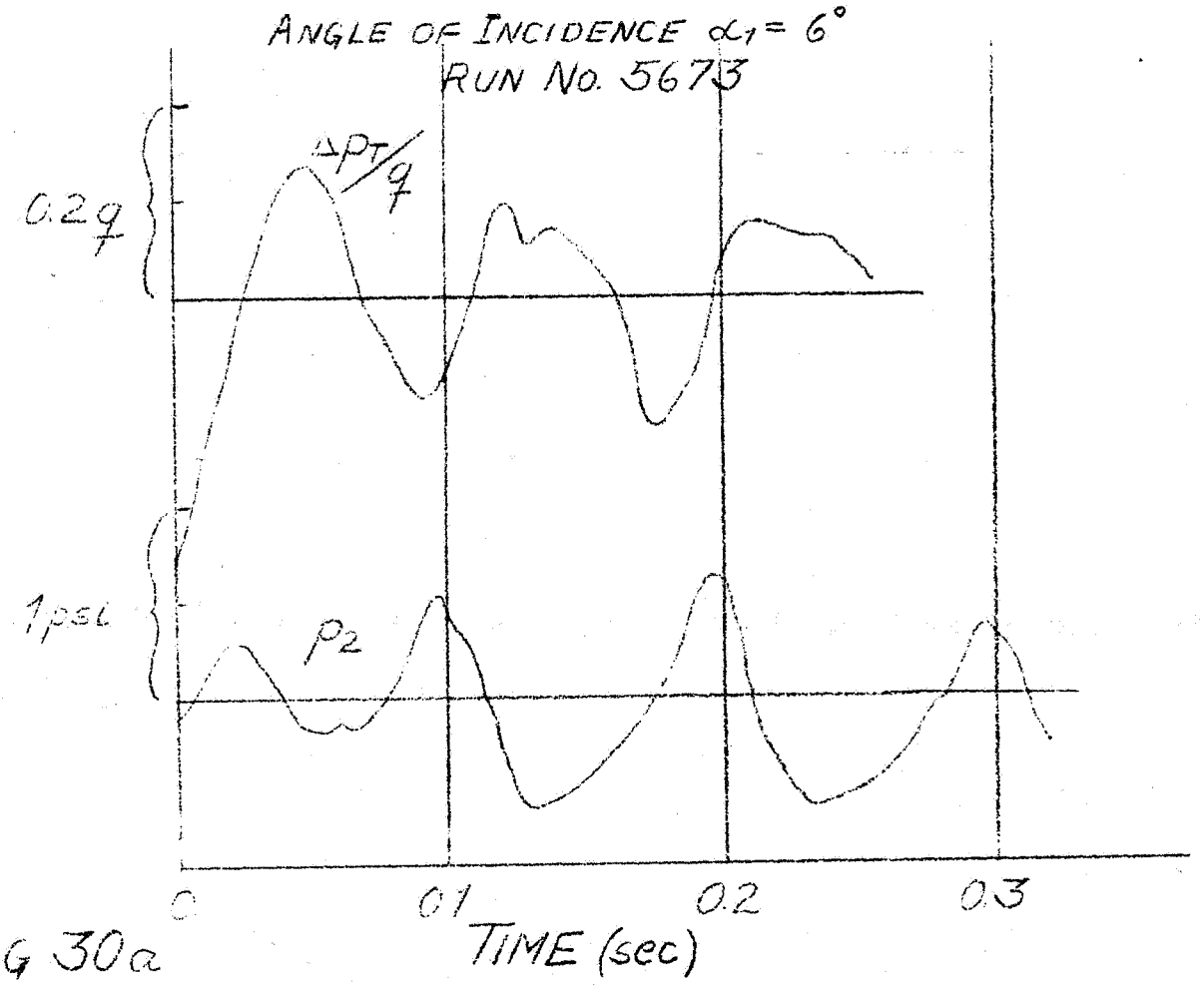
ANGLE OF INCIDENCE $\alpha_1 = 6°$
RUN No. 5673
$\Delta p_T/q$
0.2 q
1 psi
p_2
0
0.1
0.2
0.3
TIME (sec)

FIG 30a

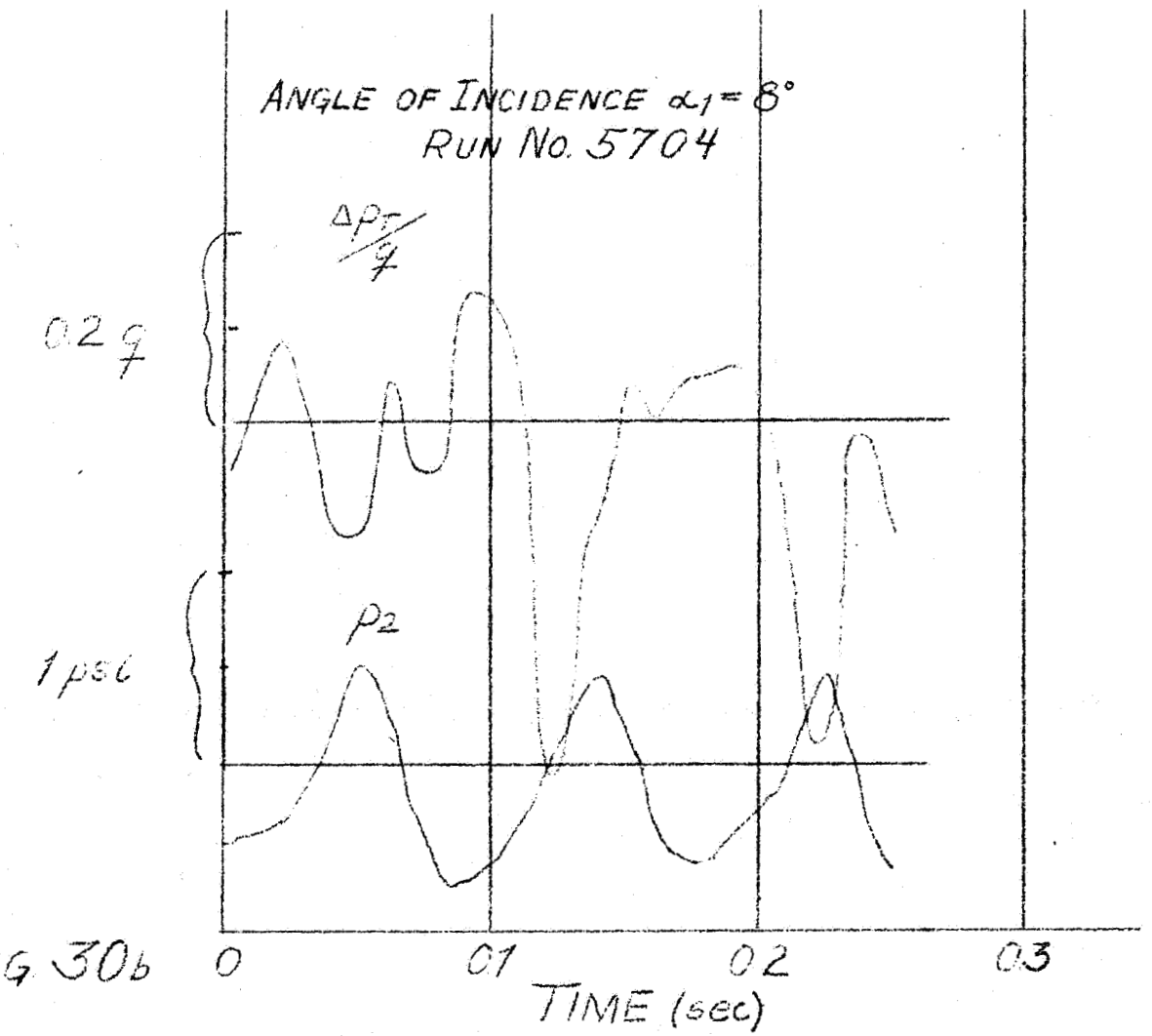
ANGLE OF INCIDENCE $\alpha_1 = 8°$
RUN No. 5704
$\frac{\Delta p_T}{q}$
0.2 q
p_2
1 psi
0
0.1
0.2
0.3
TIME (sec)

FIG 30b